THERMOMECHANICAL CHARACTERIZATION OF Ti-RICH TiNi SHAPE MEMORY ALLOYS

A THESIS SUBMITTED TO
THE GRADUATE SCHOOL OF NATURAL AND APPLIED SCIENCES
OF
MIDDLE EAST TECHNICAL UNIVERSITY

BY

FATİH YAŞAR

IN PARTIAL FULFILLMENT OF THE REQUIREMENTS
FOR
THE DEGREE OF MASTER OF SCIENCE
IN
METALLURGICAL AND MATERIALS ENGINEERING

DECEMBER 2006

Approval of the Graduate School of Natural and Applied Sciences.

Prof. Dr. Canan ÖZGEN
Director

I certify that this thesis satisfies all the requirements as a thesis for the degree of Master of Science.

Prof. Dr. Tayfur ÖZTÜRK
Head of Department

This is to certify that we have read this thesis and that in our opinion it is fully adequate, in scope and quality, as a thesis for the degree of Master of Science.

Prof. Dr. Şakir BOR
Supervisor

Examining Committee Members

Prof. Dr. Çiğdem ERÇELEBİ	(METU, PHYS)	————
Prof. Dr. Şakir BOR	(METU, METE)	————
Prof. Dr. Cevdet KAYNAK	(METU, METE)	————
Assoc. Prof. Dr. Kadri AYDINOL	(METU, METE)	————
Assist. Prof. Dr. Arcan DERİCİOĞLU	(METU, METE)	————

I hereby declare that all information in this document has been obtained and presented in accordance with academic rules and ethical conduct. I also declare that, as required by these rules and conduct, I have fully cited and referenced all material and results that are not original to this work.

Name, Last name: Fatih YAŞAR

Signature :

ABSTRACT

THERMOMECHANICAL CHARACTERIZATION OF Ti RICH TiNi SHAPE MEMORY ALLOYS

YAŞAR, Fatih
M.S., Department of Metallurgical and Materials Engineering
Supervisor: Prof. Dr. Şakir BOR

December 2006, 126 pages

Titanium-nickel is a unique class of material known as Shape Memory Alloy (SMA). A thermoelastic martensitic phase transformation is responsible for its extraordinary properties such as shape memory effect and superelasticity. The near equiatomic Ti-Ni alloys are the commercially most exploited SMAs because of the unique combination of these properties and superior ductility, strength, fatigue resistance and corrosion resistance. The properties of Ti-Ni SMAs are very sensitive to composition and the processing parameters. The properties of Ti-Ni SMAs can be modified to a great extent by choice of composition, mechanical working and heat treatment.

Thermo-mechanical treatments are required to strengthen the matrix and improve the shape memory characteristics. Plastic deformation and subsequent annealing is the common way to improve shape memory properties.

In the present study, Ti- 50 at% Ni wire specimens are produced and used for the investigation of the effect of different heat treatment and cold working processes on shape memory characteristics. To investigate the thermomechanical behavior of differently processed wire specimens, a fully computerized servo hydraulic thermomechanical testing machine was designed and constructed. Testing machine was capable to perform different types of tests that are selected by the user. It can both heat and cool the specimen automatically according to the testing sequence by applying DC current directly through the SMA wire or by sending liquid nitrogen into the cooling chamber. Temperature is measured by a K-type thermocouple directly mounted on the wire specimen with a glass tape. Force that is applied to the specimen is produced by hydraulic power unit with a double action cyclinder and it is controlled by a controller which takes the feedback from the loadcell and LVDT (Linear Variable Distance Transducer). During performig thermomechanical-tests all the data of loadcell, LVDT and thermocouple are collected by a data acqusition system integrated with a host computer that operates the program XPC Target.

Ti-Ni alloy with equiatomic composition is prepared in vacum induction furnace. Specimen cast in the form of rod was then hot swaged. Subsequent to swaging, cold wire drawing, intermediate annealing at 500 °C and water quenching was applied to obtain SMA wire with a diameter of 1.52 mm. Ti-Ni wires produced were subjected to four different processes. All the samples were initially solution heat treated at 925 °C for 30 minutes prior to water quenching. Some of the samples were further treated by an intermediate anneal at 500 °C. To see the effect of cold working; prior to intermediate annealing, 20 % or 40 % cold work was applied to another group of specimens.

To study the shape memory characteristics of specimens subjected to the above mentioned processes, four types of test, namely constant stress free recovery test,

constant strain free recovery test, constant stress constrained recovery test and constant strain constrained recovery test, were designed and applied cyclically.

The tests have shown that the stress plateau observed in the first cycle of the tests disappear upon cycling and the shape memory characteristics improve and stabilize with cycling. Once trained by cycling, fractional free recovery was observed to reach to 100 % and recovery stress to reach 120% of the applied stress if shape recovery is prevented.

Keywords: TiNi, SMA, Shape Memory Alloy, Titanium, Nickel, Thermomechanical Characterization.

ÖZ

Ti ZENGİN TiNi ŞEKİL BELLEKLİ ALAŞIMLARIN ISIL MEKANİK KARAKTERİZASYONU

YAŞAR, Fatih
Yüksek Lisans, Metalurji ve Malzeme Mühendisliği Bölümü
Tez Yöneticisi Prof. Dr. Şakir BOR

Aralık 2006, 126 sayfa

Şekil Bellekli Alaşım (ŞBA) olarak da bilinen Titanyum-Nikel alaşımlarındaki ısıl elastik martensit faz dönüşümü bu malzemenin alışılmadık şekil bellek etkisi ve süperelastik özelliğinin nedenidir. Bu özelliklerin eşsiz kombinasyonu, yüksek süneklik, dayanç, yorulma ve korozyon direnci eşit atomik orandaki TiNi alaşımınının ticari olarak en çok yararlanılan şekil bellekli alaşım olmasına yol açmıştır. TiNi şekil bellekli alaşımların özellikleri bileşimine ve işlem değişkenlerine çok hassas olduğundan bileşim seçimi,mekanik işlemler ve ısıl işlemlerle TiNi ŞBA'nın özellikleri büyük oranda değiştirilebilir.

Isıl mekanik işlemler alaşımın dayancını ve şekil bellek özelliklerini arttırmak için gereklidir. Plastik deformasyon sonrası uygulanan tavlama işlemi ise şekil bellek özelliğini geliştirmek için kullanılan genel bir yöntemdir.

Bu çalışmada Ti-50 at % Ni tel numuneler üretilerek değişik ısıl işlem ve soğuk hadde işlemlerinin şekil bellek özellikleri üzerine olan etkileri araştırılmıştır.

Değişik işlemler görmüş tel numunelerin ısıl mekanik davranışlarını araştırmak için bilgisayar kontrollü servo hidrolik bir ısıl mekanik test cihazı tasarlanmış ve üretilmiştir. Test cihazı kullanıcı tarafından seçilen çeşitli tiplerdeki testleri uygulayabilmektedir. Test cihazı test sırasına göre otomatik olarak numuneyi ısıtıp soğutabilmektedir. Isıtma doğrudan tel numune üzerinden DC akım geçirilmesiyle, soğutma ise soğutma kabinine sıvı azot gönderilmesiyle sağlanmış, numune sıcaklığı ise numune üzerine cam bantla yapıştırılan K tipi termokupl ile ölçülmüştür. Numuneye uygulanan kuvvet, çift yönlü silindire sahip bir hidrolik güç ünitesi kullanılarak üretilmiş, ve yük hücresi ve LVDT'den alınan geri besleme verilerini kullanan bir işlemci kullanılarak kontrol edilmiştir. Isıl mekanik testler sırasında yük hücresi, LVDT ve termokupl'dan gelen bütün veriler XPC Target programı kullanılarak bir bilgisayara monte edilmiş veri toplama kartı ile toplanmıştır.

Eşit atomik oranlı TiNi alaşımı vakumlu indüksiyon fırınında hazırlanmıştır. Çubuk şeklinde dökülen alaşıma sıcak şekillendirmeyi takiben soğuk tel çekme, 500 °C sıcaklıkta ara tavlama ve suya daldırma işlemleri uygulanarak 1.52 mm çapında şekil bellekli tel numuneler elde edildi. Üretilen Ti-Ni tele dört ayrı işlem uygulandı. Bütün numunelere 925 °C' de 30 dakika süreyle uygulanan çözelti ısıl işlemi sonunda su verildi. Bazı numunelere çözelti ısl işlemini takiben 500 °C'de ara tavlama uygulanırken, soğuk işlemin etkisini görmek için diğer bir gurup numune, ara tavlamadan önce % 20 veya %40 oranlarında soğuk haddelendi.

Yukarıda bahsedilen işlemler uygulanmış numunelerin şekil bellek özelliklerini belirlemek için sabit gerilim serbest geri dönüşüm, sabit gerinim serbest geri dönüşüm, sabit gerilim sınırlandırılmış geri dönüşüm ve sabit gerinim sınırlandırılmış geri dönüşüm olarak adlandırılan dört gurup test döngüsel olarak uygulandı.

Testler, ilk döngüde oluşan gerilim düzlüğünün test döngüleriyle birlikte kaybolduğunu ve şekil bellek özelliklerinin yine test dögüleriyle geliştiğini ve sabitlendiğini göstermiştir. Döngülerle birlikte eğitilen şekil bellekli numenin oransal serbest geri dönüşümün % 100' e, şekil geri kazanımının engellendiği durumda ise dönüşüm geriliminin % 120'e ulaştığı gözlendi.

Anahtar Kelimeler: TiNi, ŞBA, Şekil Bellekli Alaşım, Titanyum, Nikel, Isıl-mekanik Karakterizasyon.

To my parents, Hanife and Mustafa Yaşar.

ACKNOWLEDGEMENTS

First and foremost, I would like to express a great deal of thanks and gratitude to Prof. Dr. Şakir BOR for his encouragement, insight and close guidance. Prof. BOR far exceeded my expectations from an advisor and made my entire graduate experience unforgettable.

I would really like to thank Mrs. Gülay SANDIKCIOĞLU for being the initiator of the support of the TUBİTAK-SAGE for this thesis study. Special thanks need to be given to Dr. Yusuf Ziya KARABAY, he patiently encouraged me to start and finish this study. Moreover, I would like to thank Ahmet Nazım ÖZSOY for his valuable assistance with the electronic hardware setup and programming the testing software in this research.

I would also like to thank to all memebers of the Mechatronics Division in TÜBİTAK-SAGE who assisted to this work. In particular, I wish to thank Erdinç N. YILDIZ for providing useful comments and suggestions, Dr. Alper AKMEŞE for an invaluable insight on the testing machine controller design.

I would also take the opportunity to thank all my colleagues in TÜBİTAK-SAGE, Metallic and Ceramic Materials Division, for their help and invaluable discussing during my study.

Sincere thanks go to the following persons for their very helpful technical assistance, in particular to Ömer AKÇAY, Şaban SEYHAN and Osman ULUIŞIK.

TABLE OF CONTENTS

CHAPTER 1

INTRODUCTION

Shape memory alloys (SMAs) are a class of alloys that display the unique ability to undergo nonlinear deformations and return to their original shape when heat is applied or the stress causing the deformation is removed as a result of a martensitic phase-change, which can be temperature induced (shape memory effect) or stress induced (superelastic effect), respectively.

Martensitic transformations can be defined simply as a diffusionless lattice shearing deformation resulting in cooperative atomic movement. There is a 1-to-1 correspondence called “lattice correspondence” between the lattice points of parent and martensitic phases. Habit plane is a specific plane between the parent and martensitic phase along which the shear occurs during transformation. Since there is no strain and rotation in the habit plane through out the entire transformation, this type of shape deformation is called invariant plane homogeneous shear strain. Martensites with different habit planes are called variants. Martensitic phase transformation can be driven by temperature change, applied stress or magnetic field and the high temperature parent phase called austenite if FCC, beta if BCC transforms to low temperature and lower symmetry phase called martensite and vice versa.

When shape memory alloys cooled down under zero stress, parent phase transforms to martensite and 24 possible internally twinned martensite variants form self-accommodating structures to minimize the macroscopic volume

change. The applied stress biases the self accommodating structure and favors the growth of selected martensite variants among the others. When this biased structure is heated above A_f temperature, it recovers back to its original shape which is called shape memory effect (SME). If self-accommodated structure is permanently biased (generally by forming dislocations, internal stresses or applying force during transformation), large macroscopic strain will be induced with forward and back transformations which is called two-way shape memory effect (TWSME).

Stressing of austenite in the range of A_f to a certain temperature (M_d) results in stress induced transformation (SIM). Favored martensite variants form and during unloading, these martensite variants transform back to austenite recovering the deformation since they are not chemically stable at that temperature. This deformation behavior is called pseudoelasticity (PE) or superelasticity. Pseudoelasticity is a more generic term than superelasticity. As the temperature increases the stress needed for transformation also increases and at M_d exceeding the stress for dislocation slip deteriorates the pseudoelastic response.

Titanium Nickel (TiNi) shape memory alloys have been the focus of extensive research due to its unique characteristics such as high recoverable strain and ductility. However, thermo-mechanical treatments, such as deformation and the subsequent annealing are required to strengthen the matrix to prevent dislocation slip and improve the shape memory characteristics. Deformation magnitude, temperature, rate, mechanism, and annealing temperature and time are all important parameters for the final shape memory properties.

Many uses of SMAs have been developed, ranging from biomedical, to space structures. Of particular importance for these applications is an understanding of the generation of recovery stresses with respect to temperature, as well as the

stress and strain characteristics of the SMAs. For technological applications, mechanical response of the alloys must be predictable, reproducible and of appropriate magnitude. Shape Memory Alloys exhibit complex thermomechanical behavior when loaded mechanically or thermally due to the interaction of transformed martensite with the surrounding parent phase and among the transformed martensitic variants themselves

The thermomechanical response of SMAs undergoes significant changes with variation in the chemical composition, microstructure developed during processing and thermomechanical cycling. Slight changes in the chemical composition of the alloy are known to create large changes in the transformation temperature. Deformation in martensitic and austenitic phase introduces crystalline defects which can raise the critical stress for dislocation and improve SME, TWSME and PE.

The purpose of the present study can be summarized as:

1. To design and construct a thermomechanical testing machine which can perform free recovery, constrained recovery and work production tests special for shape memory alloys.
2. To investigate the effect of cold working and heat treatment on shape memory properties of Ti rich TiNi alloy during cyclic loading.

Theoretical background about shape memory alloys in general and TiNi shape memory alloys in specific are given in Chapter 2. The experimental technique and the details of the testing machine developed are discussed in Chapter 3. Results and discussion is presented in the Chapter 4 and finally conclusions drawn from the experiments are given in the Chapter 5.

CHAPTER 2

THEORETICAL FRAMEWORK

2.1. Martensitic Transformation

There are two types of solid state transformations: diffusional and displacive. During the diffusional transformations, formation of a new phase of a chemical composition different than the matrix from which it is formed, requires long range diffusion, which is strongly dependent upon both time and temperature [1]. Displacive transformations which do not involve chemical composition changes, on the other hand, do not require large atomic migration, but rather the atoms are rearranged into a new and a more stable atomic structure in a cooperative movement by shear displacement of atoms and individual atomic movements of less than one interatomic spacing. Since no atomic migration is involved in martensitic transformations, they progress in a time independent fashion, with the motion of the surface between the two phases being limited by only the speed of sound [1].

Martensitic transformation begins to form at a martensite start (M_s) temperature and additional transformation ceases when the material reaches a martensite finish (M_f) temperature. The M_s and M_f temperatures depend on the composition of the metal. Martensitic transformations are observed in many types of metallic and non-metallic crystals, minerals, and compounds [1-2].

The shear mechanism that controls the transformation produces two important characteristics of the martensite transformation: orientation relationships between parent and product phases and surface tilting around the martensite crystal. Due to the absence of diffusion in the transformation, the composition of the parent austenite and product martensite is the same [3]. Some characteristic features of martensitic transformation are shown in Figure 2.1.

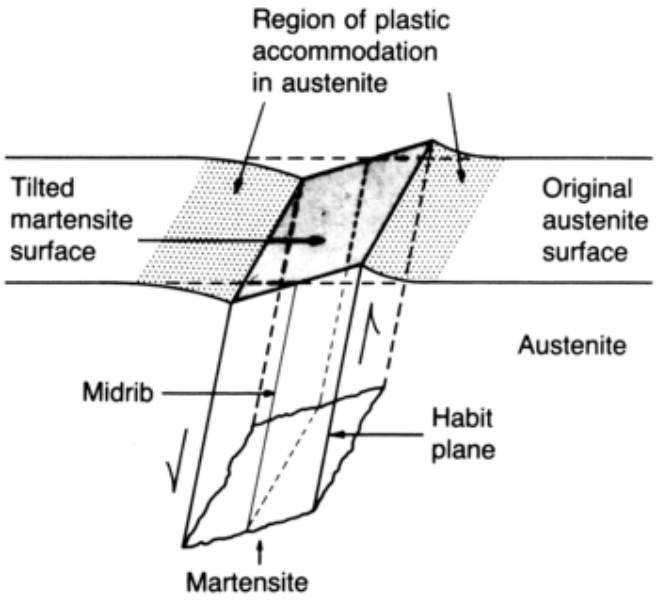

Figure 2.1 Diagram of martensite crystal, showing shear and surface tilting [3].

The shear mechanism in the martensite transformation given in Figure 2.2, showing the homogeneous shear, also known as the Bain strain, that generates the product lattice and two possible lattice invariant shear mechanisms, namely twining and slip, that produces the planar habit plane and preserves the macroscopic shape of the crystal [4].

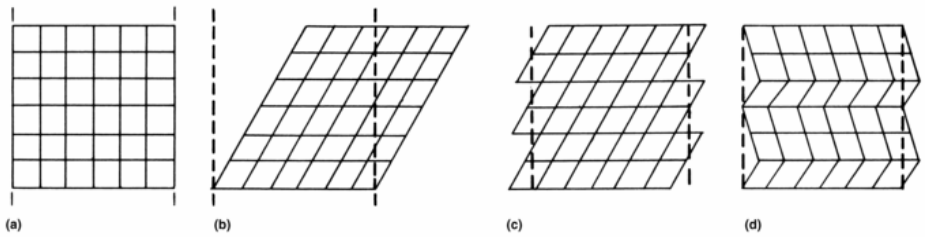

Figure 2.2 Diagram illustrating both deformations required for formation of martensite phase. (a) Parent crystal structure. (b) Lattice deformation caused by change in lattice type. (c) Slip type and (d) Twin type deformation required to keep habit plane undistorted. [4].

Figure 2.3 illustrates the progression of the transformation by homogeneous shear, which is the first part of a martensitic transformation. It is important to note that the interface progresses through each atomic layer; each atom is required to move by only a very small amount in a coordinated fashion. In real materials, Bain strain generally consists of several atomic shuffles in addition to the movement illustrated in Figure 2.3 [5].

The second part of a martensitic transformation, referred to as the lattice invariant shear, is shown in Figure 2.4. It is an accommodation step: the martensitic structure produced is of a different shape, and often volume, than the surrounding parent phase and must be altered to be accommodated in the available volume. There are two mechanisms by which this is possible: slip (Figure 2.4a) and twining (Figure 2.4b). In both cases, each individual cell, or parallelogram, has the new martensitic structure, but the overall shape is that of the original Austenite. While slip by dislocations is a permanent process twining can accommodate shape changes in a reversible way. For shape memory to occur to any significant extent, it is required that the accommodation be fully reversible

or, stated alternately, that twining be the dominant accommodation process. In Figure 2.4, only two directions or variants of shear are required to restore the original, overall shape of the matrix; in three-dimensions the situation can be complicated: Cu-Zn-Al Martensites for example, require four Martensite variants for full, three-dimensional accommodation, and Ni-Ti Martensites require three [5].

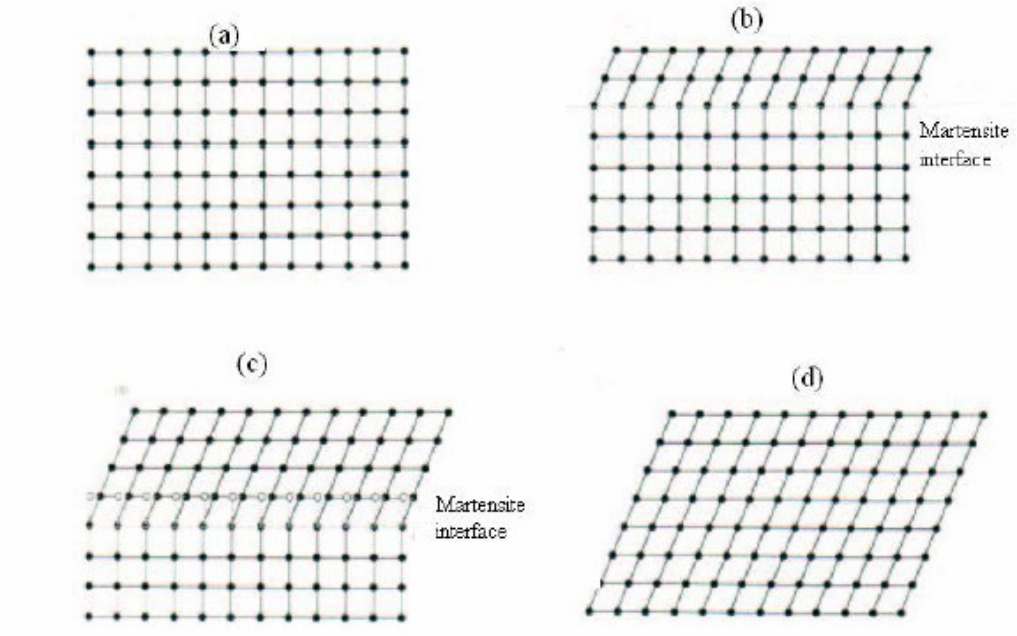

Figure 2.3 Transformation from Austenite to Martensite in two-dimensions (a) being completely austenitic and (d) being completely martensitic (c) the interface advances, each layer of atoms is displaced only by a small distance [1].

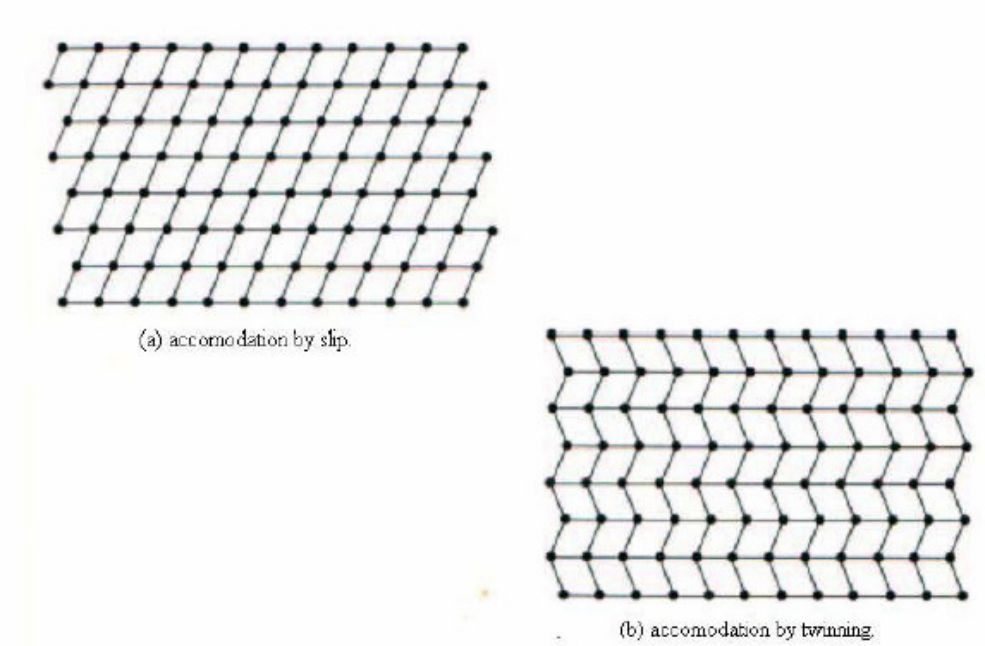

Figure 2.4 Two mechanisms of accommodating the shape change due to the atomic shear of a martensitic transformation [1].

The amount of transformation is generally independent of time (athermal). Mostly, whenever there is sufficient driving force to compensate the shape strain, nucleation is almost instantaneous and the growth velocity of the martensite is approximately one third of the velocity of sound. Sufficient driving force is attained only when the specimen is super cooled to a suitably low temperature below the equilibrium temperature T_E (where the chemical free energy of the M and P phase equal). A driving force is necessary for the reverse reaction also [6]. Application of stress promotes the transformation. The highest temperature at which martensite can form under stress is called "M_d "

2.2. Thermoelastic Martensitic Transformations

After the homogeneous shear to the martensite crystal structure, the lattice invariant displacement can not accommodate the shape deformation totally, and the resulting shape change has to be reset by the surrounding matrix. If the residual accommodation can be provided by elastic deformation of the surrounding parent phase then this will be thermoelastic transformation, however if it occurs by the plastic yielding of the parent phase is called non-thermoelastic transformation [7]. In a thermoelastic martensitic transformation the martensite plates form and grow continuously as the temperature is lowered and disappear by the exact reverse path as the temperature is raised, with a balance existing at all times between two opposing energy terms in the system [8], [9], [10]. In case of non-thermoelastic transformation, plastic yielding of the parent phase by dislocation generation results in immobilization of the martensite/parent interface and further transformation will require new nucleation.

To progress the parent to martensite phase transformation, difference between chemical free energies should be greater than the strain energy and interface energy. This can accomplished by super-cooling to M_s which is below TE [11]. For the reverse path, again, a driving force is needed and it is supplied by superheating to A_s above the equilibrium temperature. In Figure 2.5, A_s-M_s hysterisis of two different alloys is given. As seen on the graph, a wide hysterisis for Fe-Ni means that because of the large shape strain a large driving force is needed for the transformation causing it to be non-thermoelastic in contrast to the Au-Cd alloy with a narrow hysterisis.

In Fe-Ni alloy, once a martensite plate reaches a certain size its growth ceases because its interface is immobilized by the matrix dislocations [12]. Such martensite plates do not exhibit 'backwards' movement when a specimen is heated. Instead, the parent phase (austenite) is nucleated as platelets within the

martensite plates. Since several variants of the parent are usually nucleated within a single martensite plate, the martensite plate as a whole does not revert to its original austenite orientation. In this case, parent phase prefers to nucleate and grows within the martensite phase [13]. A substantial part of the strain energy paid for by the thermodynamic driving force is thereby dissipated and not elastically stored in the system to help to maintain a condition of reversibility [7].

In thermoelastic martensites, transformation proceeds by the continuous growth of plates and the nucleation of new plates upon cooling. If the cooling process is stopped growth and nucleation ceases, but if it is resumed growth and nucleation continue until the plates impinge with an obstacle such as a grain boundary or another plate. When the specimen is heated, the reverse transformation occurs by the 'backwards' movement of the martensite/parent interface. The martensite plates revert completely to the parent phase and to the original lattice orientation, i.e. complete crystallographic reversibility [14].

In brief, martensitic thermoelasticity is based on a balance of chemical free energy and elastic forces during the course of forward and reverse transformations. The transformational shape change is damped elastically in the system. The strain energy created during transformation opposes the chemical free energy change and growth of martensite plate is arrested. Once the equilibrium is reached, if the temperature of the specimen either is increased or decreased, or an external force is applied, the thermal equilibrium will be disrupted and the martensite plates start to either grow or shrink. The strain energy stored in the matrix during the transformation plays important role in reversing the shape change and motion of the interfaces [15].

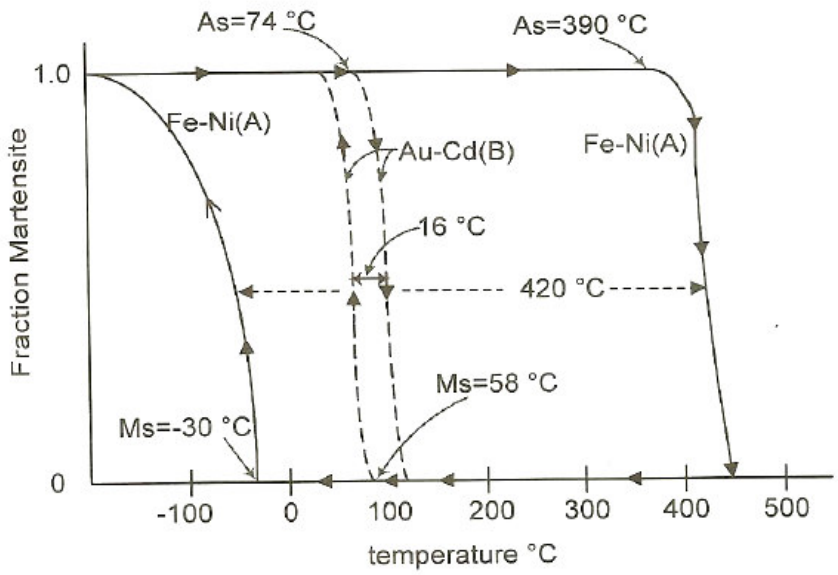

Figure 2.5 Hysterisis loops displayed in transformation curves for Fe-Ni and Au-Cd martensites [9].

2.3. Shape Memory Phenomenon

In shape memory alloys, the high temperature parent phase has a homogenous cubic crystal structure and relatively high modulus of elasticity, while martensite has a twinned monoclinic structure and lower modulus of elasticity [[16][17][18][19]. Although some sources mention an additional annealing phase and intermediary "R" phase, they concede that austenite and martensite are the principle constituents.

Martensite is generally of a lower symmetry phase than Austenite. Therefore, there are several ways by which Martensite can be formed out of Austenite.

However there is only one route by which the Martensite formed will revert back to Austenite. Shape memory effect can be explained in a very simple manner by a 2D geometrical concept depicted in Figure 2.6 upon cooling from Austenite Figure 2.6a), the self-accommodating variants of Martensite (Figure 2.6b) are formed. During the application of stress (deformation), the twin boundaries migrate and therefore result in a biased distribution of Martensite variants (Figure 2.6c). It is however important to note that no matter what the distribution of Martensite is, there is only one possible austenitic structure that these variants can revert back to. Therefore, the martensitic variants must return back to the original undeformed shape after reverting back to Austenite. Therefore, the shape accommodation due to a twin boundary movement can only be supported by a low symmetrical martensitic structure, and when the more symmetric Austenite structure is returned, the twining deformation must also disappear.

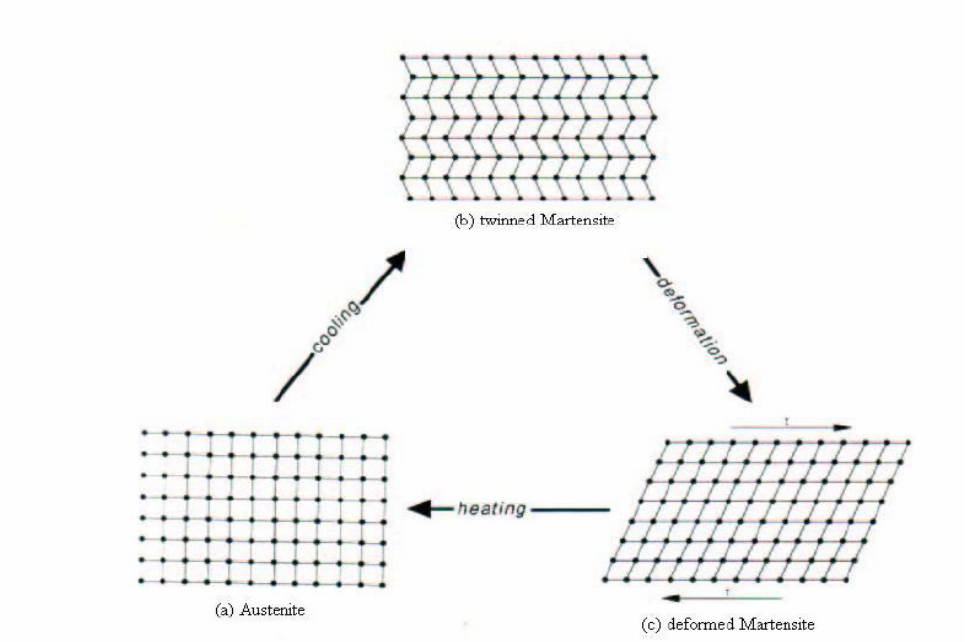

Figure 2.6 Shape memory shown microscopically: Austenite (a) is cooled to form twined Martensite (b) without undergoing a shape change, and then is deformed by moving twin boundaries (c). Heating either state (b) or (c) will return the originally austenitic structure and shape [1]

The shape memory effect can be described with reference to the cooling and heating curves, Figure 2.7. There is no change in the shape of the specimen cooled from above A_f to below M_f. When the specimen is deformed below M_f it remains so deformed until it is heated. The shape recovery begins at A_s and is completed at A_f. At the inflection point, between A_s and A_f, about 50% of the original shape is recovered.

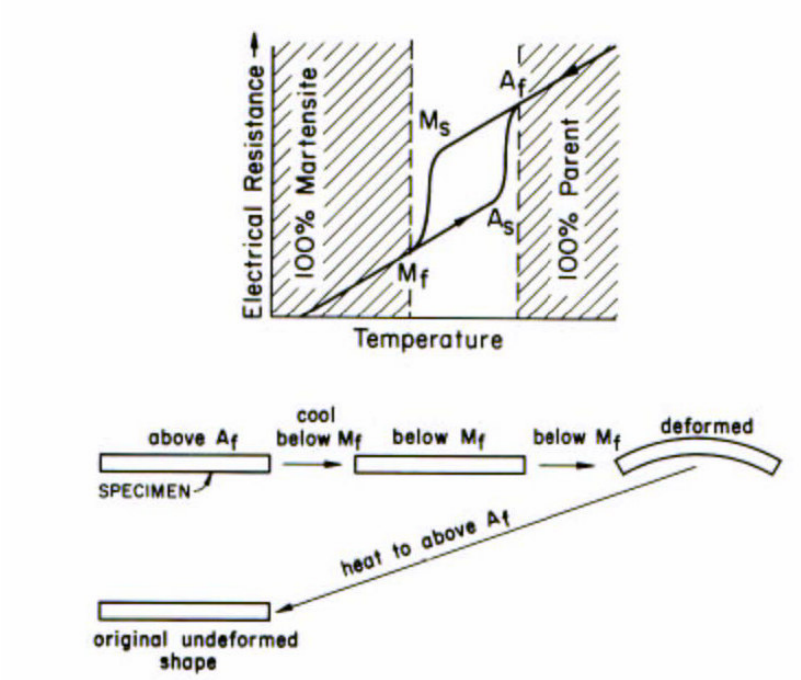

Figure 2.7 The shape memory effect as described with reference to a plot of electrical resistance versus temperature [25].

Once the shape has recovered at A_f there is no change in shape when the specimen is cooled to below M_f and the shape memory can be reactivated only by deforming the martensitic specimen again. In other words, the shape memory effect is a one time only occurrence and therefore it is frequently referred to as the one-way shape memory effect. Typical recoverable strains for TiNi SMAs are about 7%, while strains up to 10% are possible. Among the many alloys that exhibit SME, only the Cu-Zn-Al, Cu-Zn-Ni, and Ti-Ni alloys are presently of commercial importance.

Shape Memory Effect basically depends on ability to undergo thermoelastic martensitic transformations. Upon cooling a single crystal of the parent, typically

24 variants of martensite form, Figure 2.8. In a diamond-like morphology, they form in self-accommodating groups of four variants. As the martensite phase is deformed, some variants grow at the expense of others, and eventually only one variant persists. The surviving variant is that whose shape strain direction is most parallel to the tensile axis; thus permitting maximum elongation of the specimen. When this resultant single crystal of martensite is heated between A_s and A_f the original specimen shape and parent single crystal are regenerated [14].

Due to the crystallographic restrictions and to maintain the ordered structure, the single crystal of martensite has only one way to undergo the reverse transformation. In other words, there are numerous variants of the Bain strain during the forward transformation but only one during reversal. [14]

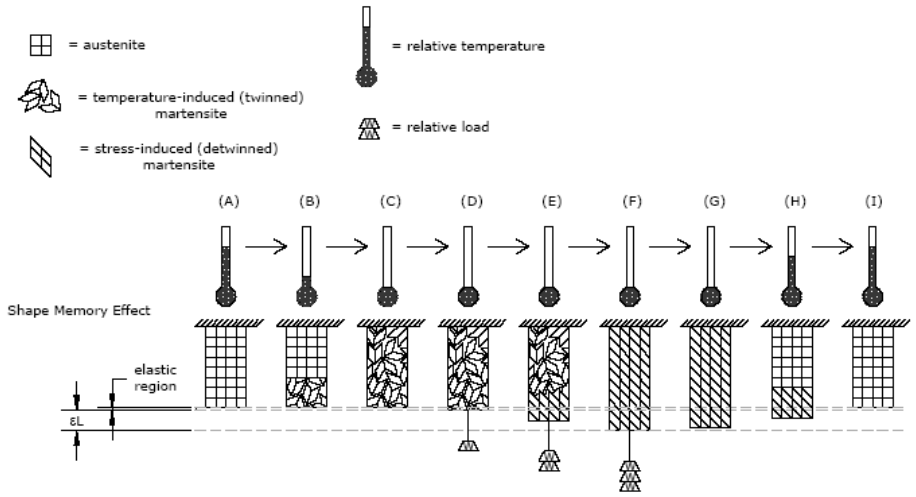

Figure 2.8 Illustration of shape memory effect with temperature-induced martensite formation.

2.3.2. Pseudoelasticity (Superelasticity)

When a SMA is in its austenite phase at a temperature not far from A_f, it exhibits a highly elastic behavior, i.e., deform up to 8% when loaded and then fully recover the strain by simply removing the load. This behavior is known as the pseudoelastic effect, pseudoelasticity or superelasticity, and is due to formation of martensite, which is called stress-induced martensite, as a result of the loading.

It is possible for stress to convert austenite to martensite without a change in temperature, as occurs in superelastic behavior [19]. Applying a force to austenitic material will put it in a linear elastic region governed by austenite's modulus of elasticity. When enough stress is present, the material transforms directly into detwinned martensite, also known as stress-induced martensite. The conversion proceeds in exactly the same manner as when transforming between temperature-induced (twinned) martensite and its stress-induced counterpart. That is, the specimen softens and exhibits large strains in response to small increases in stress. The only obvious difference is that the conversion from austenite to stress-induced martensite takes place at higher temperatures and stresses than the twinned to detwinned transformation. However, unlike its low temperature analog, martensite induced at high temperatures is not stable and will spontaneously revert to undeformed austenite when the stress is removed. Figure 2.9 illustrates superelasticity and Figure 2.10 shows the temperature-stress domain it is expected.

The critical stress to induce martensite increases linearly with temperature, and there is another temperature, M_d, above which martensite cannot be formed by stress; instead, the parent phase undergoes plastic deformation. It is to be noted that when stress-induced martensite forms, the stress is equivalent to a change in chemical free energy, the usual driving force for the martensitic transformation.

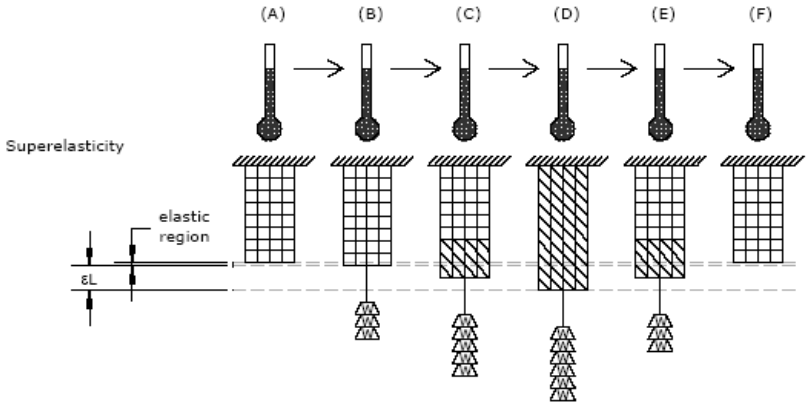

Figure 2.9 Illustration of the superelastic effect.

Superelasticity can be realized if the temperature of the material is below M_d and above A_s. If the temperature exceeds M_d the martensite can not be stress induced; if the temperature is below A_s the stress induced martensite will remain stable during unloading and shape recovery will not be observed. For full superelasticty, we require the application temperature to be above A_f [14].

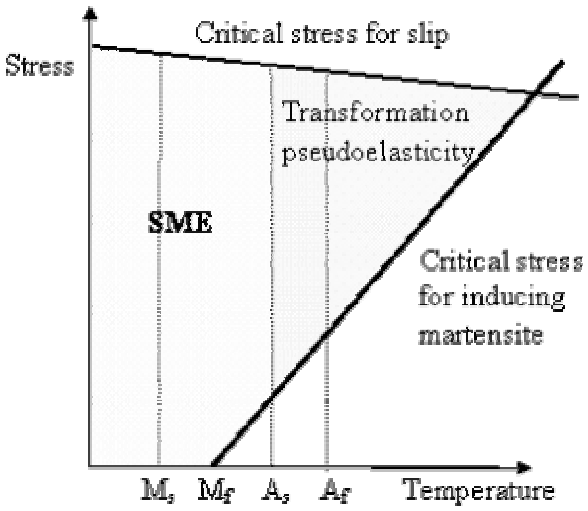

Figure 2.10 Schematic representation of the appearance of the SME and transformation plasticity [14]

2.3.3. Two Way Shape Memory Effect

In two-way shape memory, a properly processed sample can exhibit one shape when cold, change to a second shape when heated and return to its original shape when cooled again, all without mechanical intervention. Shape change occurs in two directions, during both heating and cooling, although no appreciable force is developed during the transition from a high to a low-temperature shape [20][21].

There are two methods of conditioning or 'training' to achieve two-way shape memory behavior, which involve: [22]

SME cycling: Cooling a specimen below M_f, deforming it to produce the preferred or 'surviving' variant, and then heating it to above the A_f temperature. These is the conventional shape memory treatment, and in such a case the

memory is perfectly provided as long as the deformation does not exceed some limiting value, say 7-8% [14].

SIM cycling: Deformation of a specimen above the M_s temperature to produce stress-induced martensite (SIM) and then reversal by release of the load. Provided that a certain strain is not exceeded complete superelastic loops in the stress-strain curves are obtained, and the original specimen dimensions are recovered completely when the applied stress is released [23].

The TWSM was observed after both SME and SIM cycling, and the results are termed SME training and SIM training. In both cases, the TWSM was observed to result from the preferential formation (and reversal) of a 'trained' variant of martensite. The training of a specimen to form a preferred variant on cooling to M_f can occur either by the prior deformation of thermal martensite or by superelastic stress cycling above M_s.

There are two mechanisms proposed for the TWSM. They are either based on residual stress fields or locally retained martensite. During cooling, due to training, some particular variants of martensite nucleate and grow; in contrast other variants do not appear. This leads to macroscopic shape change [24]. Dislocation structures are generated by training. TWSM are attributed to the microscopic residual stress field around those dislocation structures. Those residual stress fields favor the nucleation and the beginning of growth of some preferential variants, and the residual stresses are relaxed by the accompanying shape change. During cooling, those preferential variants grow without any assistance, thus causing the TWSM. The second mechanism is based on stabilization of martensite, retained above the original A_f temperature [25,26]. Growth of this locally stabilized preferential martensite is responsible for the TWSM. In any case, TWSM is not a natural feature of the alloy; it must be subjected to special thermomechanical treatment in order to display TWSM [8].

2.4 Ti - Ni Based Shape Memory Alloys

Shape memory alloys based on Nickel and Titanium has to date provided the best combination of material properties for most commercial applications. Rapid growth for shape memory alloys was initiated with the discovery of shape memory properties in TiNi system in the 1960's.

2.4.1 Metallurgy of Ti - Ni Alloys

TiNi SMAs are ordered intermetallic compounds based on the equiatomic composition. According to the phase diagram of TiNi, Figure 2.11, the TiNi phase exists as the stable phase down to room temperature. At low temperatures, the stoichiometric range of TiNi is very narrow and therefore the alloys often contain precipitates of a second intermetallic phase. The microstructure is thus primarily single phase, with small amounts of other phases mixed in the matrix. In the molten state, Titanium is very reactive and this results in some oxygen being present in the matrix. Oxygen decreases the stoichiometric range of the TiNi compound and can unexpectedly result in compositions within a three phase field. Ni_3Ti can be present for example in a Titanium rich alloy. Furthermore, the oxide Ti_4Ni_2O is isostructural with the intermetallic Ti_2Ni, which can make unique phase identification difficult. If the composition of the alloy deviates from stoichiometry, then larger precipitates are present, as seen for Ti-rich alloy. These larger second phase particles can have a marked effect on the hot workability of TiNi, particularly on the Titanium rich side where they are brittle and often result in cracking [25]

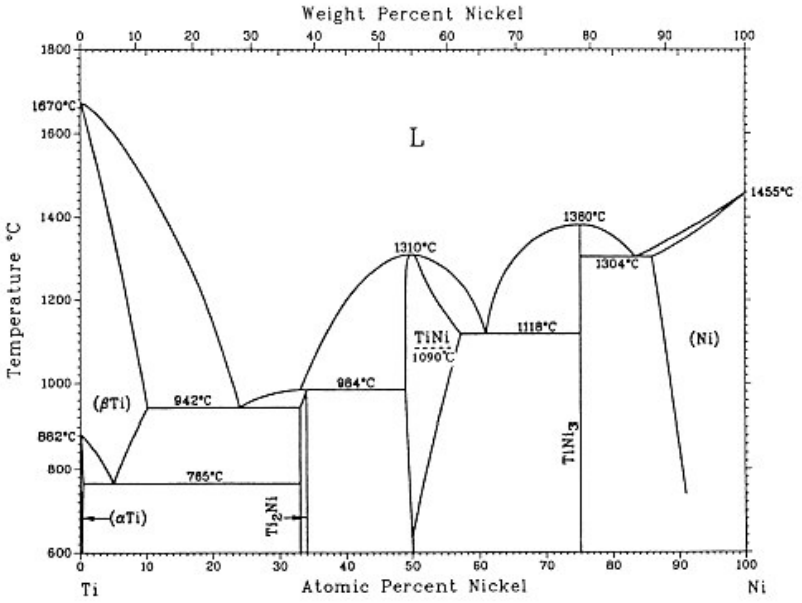

Figure 2.11 TiNi Phase diagram [27].

The central part of the phase diagram of TiNi, Figure 2.11, where TiNi transforms to B19' martensitic phase is important. On the nickel rich side Ti_3Ni_4, Ti_2Ni_2 and $TiNi_3$ precipitation has been reported and resulted in confusion for a while, whether there is a eutectoid reaction or not. But it is understood that the Ti_3Ni_4 and Ti_2Ni_3 phases are metastable intermediate phases and they transform to equilibrium $TiNi_3$ phase with longer aging time [1]. On the Ti rich side the equilibrium phase is Ti_2Ni but Ti is so active that it easily combines with oxygen and carbon at high temperatures. The order-disorder transition temperature of TiNi is at 1090°C as indicated by dotted line on the phase diagram [27].

As it can be deduced from the phase diagram, the composition range for ordered TiNi phase with B2 crystal structure is from 49 to 57 at % Ni at 1090°C. The

phase diagram of TiNi has been used to improve the shape memory characteristics by formation of precipitates. As it will be discussed later, precipitates change the transformation temperatures, strength and PE substantially.

2.4.2 Mechanical Properties

Like most SMAs, TiNi alloys show marked differences in mechanical behavior depending upon whether they are tested in the martensitic or austenitic state. The martensitic stress-strain curve can be divided into three well defined regions, Figure 2.12. An initial low plateau results from the stress induced growth of one martensitic orientation at the expense of the adjacent. At higher stresses, there is a second region that is linear, although not purely elastic. The deformation mechanism in this state is a mixture of elastic deformation on the detwinned martensite, together with the formation of new orientations of martensite, which intersect those already present and which provide additional heat recoverable strain. The transition to the third region is a result of the onset of irreversible plastic deformation, as in the case of yielding of all conventional metals. Therefore, the maximum amount of heat recoverable, or memory strain, is obtained by initially deforming the sample to the end of the second stage. If larger deformation strains are used, then the reversible martensitic deformation processes and the dislocations resulting from plastic flow interact and the memory strain will decrease. The length of the martensitic plateau in the stress-strain curve extends typically to around 5%-6%. However, depending on the details of the alloy and its prior thermomechanical history, the plateau can vary from a continuous curve with an inflection point to a clear horizontal plateau with a sharp yield point [23].

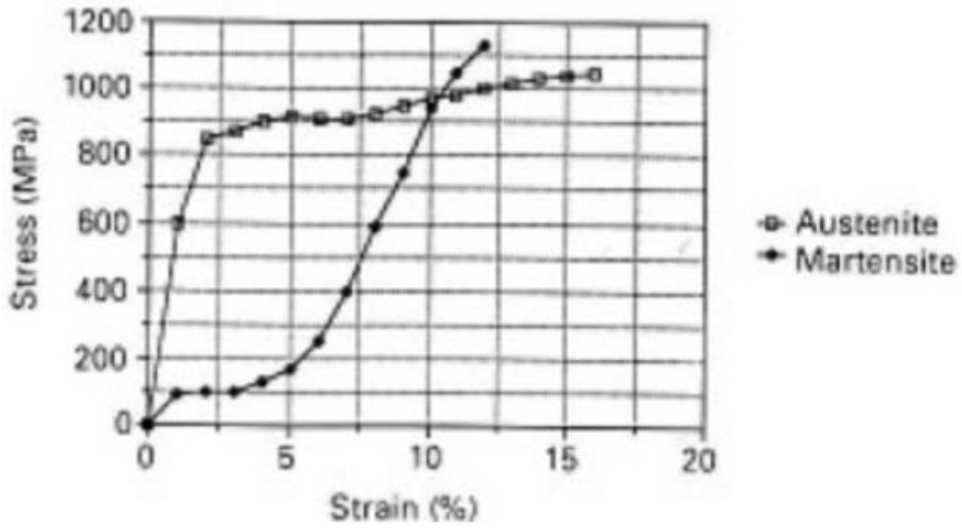

Figure 2.12 Stress-strain curve for a Ti-Ni-10% Cu alloy in the austenitic and martensitic conditions [1]

2.5 Thermo-mechanical Behavior of Shape Memory Alloys

Many uses of SMAs have been developed, ranging from biomedical, [28,29,30], to space structures. Of particular importance for these applications is an understanding of the generation of recovery strain and stresses with temperature, are how the alloy is to be activated as well as the stress and strain characteristics of the SMAs. But due in part to the lack of experimental data available on the subject there is a lack of understanding on how the generation of stresses in SMAs is related to the transformational behavior and why there is a change in the thermomechanical paths experienced by cycling [31].

A number of unique thermomechanical parameters must be introduced to describe shape memory behavior: most importantly the flow stress $\sigma_{P \rightarrow M}$

required to stress induce martensite; the amount ε_R of strain reversion; the strain limit ε_L for complete strain recovery; the internal stress which develops on heating a deformed but constrained sample, known as the "reversion stress" σ_R. In order to develop shape memory alloys for technological applications, parameters such as these must be predictable, reproducible and of appropriate magnitude. Some of these parameters defined schematically in Figure 2.13 are described in more detail below [32]:

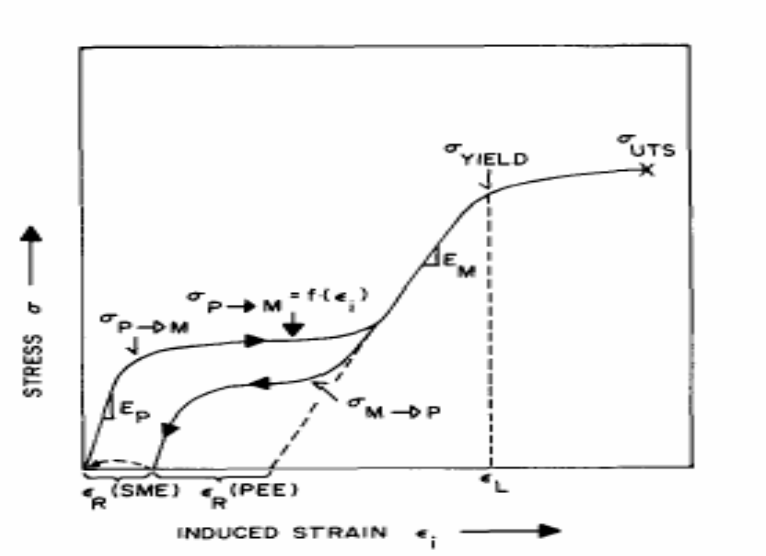

Figure 2.13 A schematic stress-strain curve for a shape memory alloy for M_s and $P_s < T_d < P_f$ and M_d, showing definitions of $\sigma_{P\rightarrow M}$, $\sigma_{M\rightarrow P}$, ε_i, ε_R and ε_L (SME is shape memory effect; PEE is pseudoelastic effect) [32].

The stress $\sigma_{P\rightarrow M}$ to induce martensite: Figure 2.14 illustrates the typical temperature dependence of $\sigma_{P\rightarrow M}$, between M_s and M_d. Because of the effective equivalence of temperature and stress with respect to thermoelastic martensitic

transformations, $\sigma_{M \rightarrow P}$ decreases from a maximum near M_d to a minimum near M_s. In other words, since the stability of the martensitic phase is enhanced by applied stress, the transformations temperatures shift to higher values [33,34]. This relationship can be expressed by a modified form of the Clausius - Clapeyron equation [32]:

$$\frac{d\sigma_{p \rightarrow m}}{dT} = \frac{\rho V G_c}{\varepsilon_L T_0} \tag{2.1}$$

VG_c = Chemical free energy difference

$$T_0 = T_0 = \frac{M_s + A_f}{2} \tag{2.2}$$

ρ = Density of material

ε_L = Maximum macroscopic strain crystallographically possible.

Reversion Strain (shape recovery) ε_R: Shape memory alloys have the ability of recovering of large amount of induced strains (%5-%8) by heating, which is called reversion strain ε_R. If the deformation temperature is above A_f then the ε_R will be equal to ε_{PE} (Pseudoelastic strain). If deformation temperature below A_s then ε_R will be equal to ε_{SME}. ε_R will be combination of ε_{PE} and ε_{SME} when the temperature is between A_s and A_f [32].

Strain Limit ε_L: There is for each shape memory alloy a strain limit ε_L which if exceeded leads to true plastic deformation. This is a critical value and of the order of 5% - 10%. Thus, if a strain greater than ε_L is induced, the shape memory behavior deteriorates and there is a decrease in ε_R, σ_R and useful work output. The basic prerequisite for shape memory behavior is that no true plastic deformation by dislocations occurs, in either the martensite or the parent phases [32].

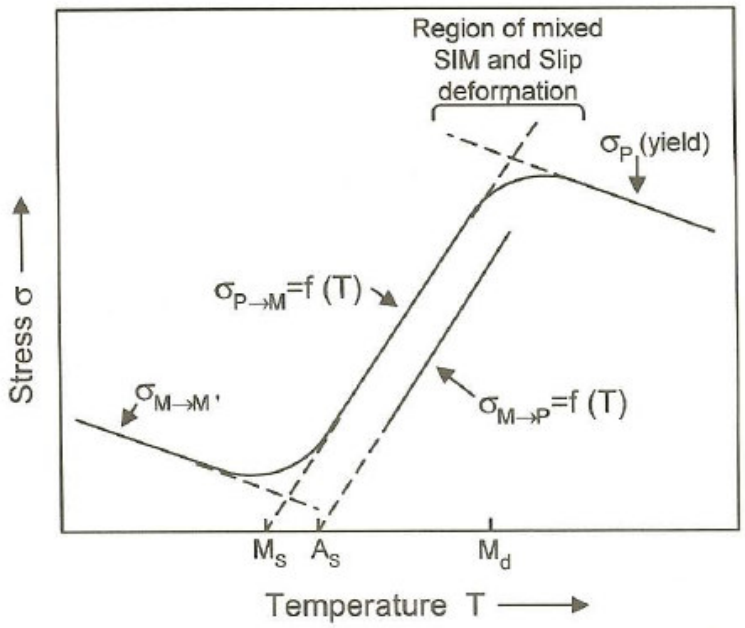

Figure 2.14 A schematic representation of the temperature dependences of $\sigma_{P\rightarrow M}$ and the flow stresses of the parent and martensite phases near the transformation range for a constant value of e ε_i [34].

The Reversion Stress σ_R: If the induced strain is held constant in the sample as it is heated through the reversion temperature range A_s to A_f (by constraining the sample against the tendency for shape recovery), an internal (reversion) stress will develop. This stress increases in sigmoidal fashion over the A_s to A_f range. The A_f temperature is shifted upward by the internal stress developed, while A_s is not (since there is no stress yet developed at A_s). Due to the shifts in transformations temperatures, the normal reversion temperature range is widened. The maximum level of reversion stress obtained on heating, which is achieved near A_f, is a direct function of the initial induced strain. It has been shown that σ_R (max) can be increased by increasing the induced strain, to a limit near ε_L the

strain limit. If an initial strain greater than ε_L is introduced, the potentials to developed reversion stress decreases. In addition, if a proportion of the initial strain is allowed to recover freely prior to constraint of the remaining strain, the sample will have a correspondingly lower value of reversion stress at A_f. In all, the value of σ_R (max) depends on the amount of reversible strain constrained in the sample as it is heated to A_f [32].

The fact that, during constrained recovery, the stress σ_R (max) developed may be substantially greater than the stress $\sigma_{P\rightarrow M}$ required to induce the martensite from the parent at some lower temperature has led to the utilization of shape memory alloys in energy conversion devices.

The main difference of the SMA from the conventional structural materials is the strong dependence of their deformation behavior to the testing temperature, i.e., strain ε is a sensitive function of temperature T as well as the stress σ, $\varepsilon = f(\sigma, T)$. The description of the thermomechanical behavior of SMA in the form of an exact mathematical function is not possible because of its complexity. Therefore, it appears to be reasonable to investigate some certain ranges of temperature, in which the SMA show characteristic stress-strain curves, Figure 2.15. These characteristic sorts of behavior are:

- One Way Shape Memory Effect
- Pseudoelasticity
- Two Way Shape Memory Effect

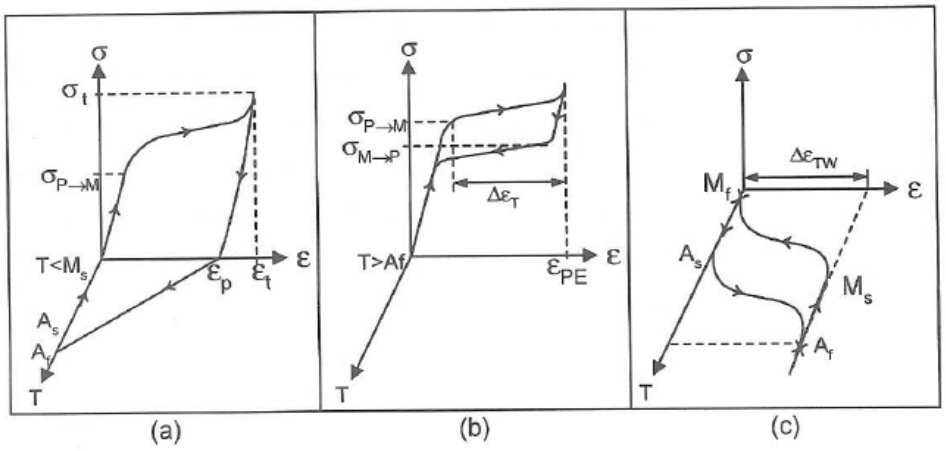

Figure 2.15 σ-ε-T curve of (a) SME, (b) σ-ε path of PEE, (c) ε-T path of TWSME.

2.6 Thermo-mechanical Characterization of Shape Memory Alloys

Shape memory alloys are capable of producing large forces when recovering the strain. The SME or reverse transformations refer to a **free recovery** (under zero load). If the strain recovery is forced to be under load, the SMA performs work and is termed a **restrained recovery**. If the SMA is prevented from recovering the strain, it generates stress when heated above the transformation temperature and is termed **constrained recovery**.

1. Free Recovery :

If a SMA is deformed in fully martensitic state all or some portion of the strain will recover upon heating. Free recovery is the name of this event against no applied load and is illustrated in Figure 2.16.

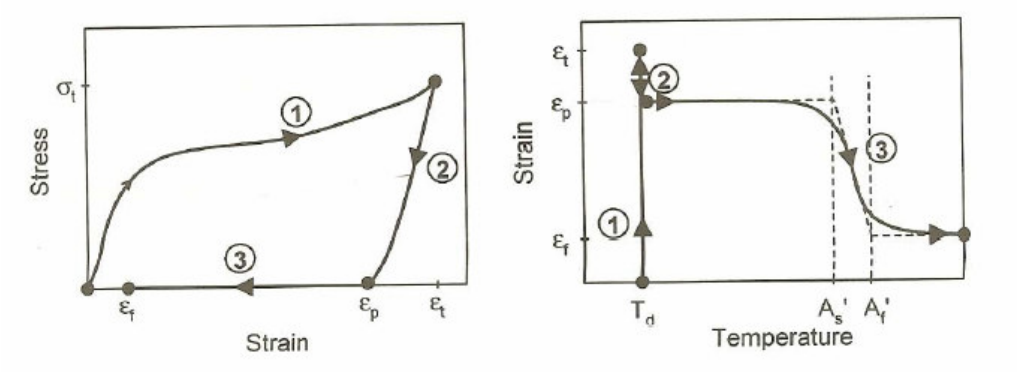

(a) (b)

Figure 2.16 a) Stress-Strain behavior of SMA and b) Strain-Temperature behavior of SMA [35].

In the stress-strain curve, along path 1 a strain is induced to the SMA until ε_t while it is in the martensitic state. Unloading will result in an elastic recovery shown as path 2 resulting in the permanent plastic deformation ε_p. With applied heat, SMA recovers all or part of the applied strain, path 3. Strain-Temperature curve shows the SMA behavior with temperature more clearly. T_d is the deformation temperature and is less than the martensite start temperature. Free recovery behavior of SMA can be characterized by inducing various ε_t and looking at the influence of it on ε_r an on A_f.

2. Constrained Recovery :

The most common applications of shape memory alloys involve an external dimensional constrain preventing the alloy from returning to its original shape when heated, and as a result high recovery forces are generated, Figure 2.17[35].

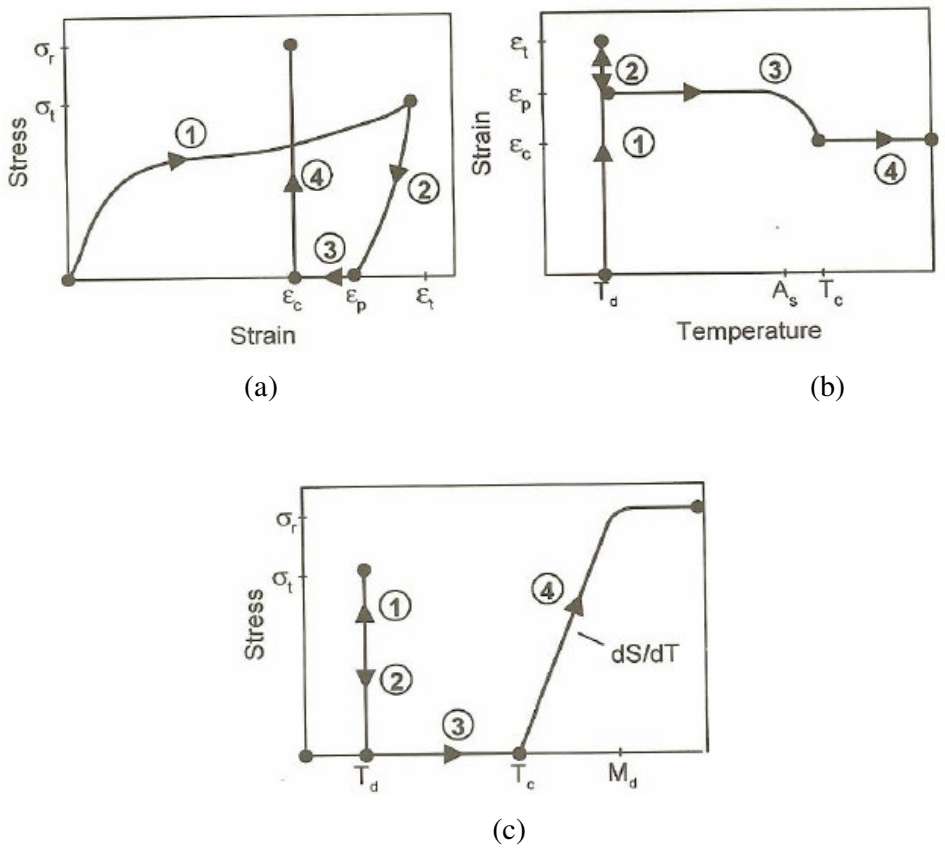

Figure 2.17 Constrained recovery (a) Stress-Strain, (b) Strain-Temperature and (c) Stress-Temperature graphs [35].

As can be seen from the stress-strain curve, after a given deformation (ε_t), elastic stress relaxation occurs and reversible plastic strain remains on the shape memory alloy (ε_p). Heating will result in recovery to the constrained point ε_c and from that point on, with increasing temperature, stress starts to increase and reach to σ_r. Same path is seen on the Strain-Temperature curve in Figure 2.17 (b). At the deformation temperature T_d strain increases to ε_t and by unloading reaches to ε_p. By heating, it follows the paths 2 and 3. In the stress-temperature curve at T_d stress increases to σ_r and reverts back to zero upon unloading. Stress again starts

to increase by heating at the contact point. The σ_r will reach its maximum at the point of M_d. The rate of change in stress with temperature can also be obtained from the stress-temperature curve.

Characterization of an alloy, which will be used in constrained recovery application, includes the determination of $\sigma_{r,}$ ε_c and $\varepsilon_{t.}$ Total deformation strain influence the recovery stress. There is an optimum deformation strain to achieve maximum response from the alloy.

3. Restrained Recovery or Work Production :

Work production applications include recovery against an applied stress. A shape memory wire lifting a weight as the wire is heated and lowering it when cooled is a typical example. If the stress applied by the weight (σ_0) is less than the recovery stress of the alloy, the amount of work done is $\sigma_0 \Delta\varepsilon$. This describes the work production during heating. If the applied stress is higher than the martensitic yield strength than the wire will be restretched during cooling.

During heating a shape memory alloy does work and during cooling work is done on the shape memory alloy when the application is done under constant stress. Therefore, the net work output is zero. In many applications, work that is done during heating is desired. This means that the applied load during heating is greater than the load during cooling. This concept is shown in Figure 2.18 with σ_H being the stress resisting recovery and σ_L is the stress for resetting.

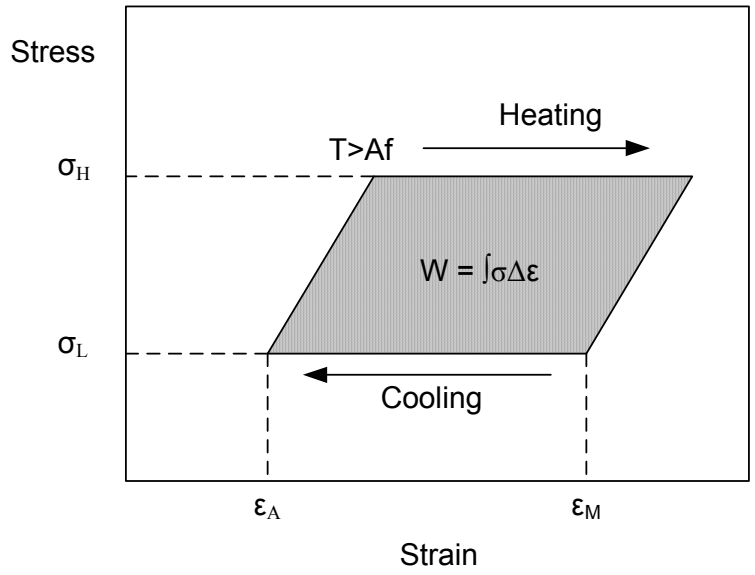

Figure 2.18 A typical actuator recovers against a higher load than is applied during cooling. Work output is the shaded area.

2.7 Effect of Thermo-mechanical Treatments on Shape Memory

Thermo-mechanical treatments have drastic effects on shape memory characteristics of materials. The thermomechanical response of SMAs undergoes significant changes with variation in the chemical composition, material processing and thermomechanical cycling. Slight changes in the chemical composition of the alloy are known to create large changes in the transformation temperatures [36]. The addition of a ternary element also has been shown to influence the martensitic transformation and the thermomechanical response of TiNi SMAs.

Deformations in martensitic and austenitic phase introduce defects to the structure. These defects can raise the critical stress for dislocation slip, which can improve SME, TWSME and PE. Also, these defects are possible nucleation sites for martensitic transformations which can lead to a change in transformation temperatures. On the other hand, complex dislocation structures and other internal defects can behave like barriers to martensitic transformations as well. As a result, plastic deformation in SMAs can strengthen the matrix which can result in higher stress for SIM transformation, longer fatigue life by suppressing irreversible dislocation slip and alter transformation temperatures [37].

Heat treatment is another effective method to change shape memory characteristics. Coherent or incoherent precipitates form with different heat treatment temperatures and time in appropriate compositions. Coherent precipitates form an internal stress field around them and this can help or oppose the martensitic transformation depending on the applied stress direction. If there is no applied stress, they increase the M_s temperature due to the internal stress field around them. Another effect of precipitates is that they change the composition of matrix because precipitates are either Ni-rich or Ti-rich depending on the initial composition. Composition effect is dominant for overaged precipitates where the sizes of precipitates are larger than the peakaged precipitates [38]. When the annealing temperature is higher than the recrystallization temperature, formation of new grains and grain growth will take place. Heat treatments after deformation can be performed to utilize the mechanical characteristics by rearrangement of dislocation structures, formation of precipitates and grains.

2.8 Effect of Cyclic Deformation on Shape Memory Effect

2.8.1 Thermal Cycling

In solutionized materials dislocations will be introduced by thermal cycling and their density will increase with the number of cycling. This will result in decrease in M_s temperature. The decrease of M_s could be prevented by increasing the strength of the material by cold working or precipitation hardening to prevent the formation of dislocations during repeated phase transformation [39].

2.8.2 Stress Cycling

Generally, with increased number of cycles the residual strain will increase, critical stress to induce martensite (σ_{SIM}) and stress hysterisis will decrease [39]. The increase of residual strain is due to the formation of dislocations during phase transformation and deformation of matrix. Sometimes, dislocations can also prevent the reverse transformation of martensite. Internal stress fields around the dislocations or residual martensites will assist the formation of stress-induced martensites, which means hysterisis. After certain number of cycling the steady state condition is obtained. This is due to the fact that work hardening suppresses the formation of new dislocations.

CHAPTER 3

EXPERIMENTAL TECHNIQUE

3.1 Thermo-mechanical Testing Machine

The results of tensile tests are used in selecting materials for engineering applications. Tensile properties frequently are included in material specifications to ensure quality. Tensile properties often are measured during development of new materials and processes, so that different materials and processes can be compared. Finally, tensile properties often are used to predict the behavior of a material under loading other than uniaxial tension.

Testing machines are either electromechanical or hydraulic. The principal difference is the method by which the load is applied. Hydraulic testing machines are based on either a single or dual-acting piston that moves the crosshead up or down. However, most static hydraulic testing machines have a single acting piston or ram. In a manually operated machine, the operator adjusts the orifice of a pressure-compensated needle valve to control the rate of loading. In a closed-loop hydraulic servo system, the needle valve is replaced by an electrically operated servo valve for precise control.

A number of unique thermo-mechanical parameters must be introduced to describe shape memory behavior: most importantly the flow stress required to stress induce martensite. $\sigma_{P\rightarrow M}$, the amount of strain reversion, ε_R, the strain limit for complete strain recovery, ε_L, the internal stress which develops on heating a

deformed but constrained sample, known as the "reversion stress" σ_R. In order to develop shape memory alloys for technological applications, parameters such as these must be predictable, reproducible and of appropriate magnitude. To apply various types of thermo-mechanical tests for determining the parameters mentioned above a testing machine is designed.

3.1.1 Testing Bench

A schematic drawing of the testing bench is given in Figure 3.1 Testing bench is set up by using two 30 mm ST-52 steel plate and extruded 6063 aluminum frames. Plates are chosen thick enough to prevent the bending and affecting the test results.

Grips shown in Figure 3.2 are machined from AISI 4140 steel and heat treated. Hardness after heat treatment is 55 HRC. By using a screw system on the grips specimen is mechanically squeezed between jaws. When the test begins it becomes more squeezed with the force on the specimen in the direction of tension.

Cooling chamber, Figure 3.3 is constructed from polycarbonate and polyamide. Main reason of this chamber construction is to cool the specimen homogenously by spraying liquid nitrogen and to prevent the air circulation around specimen during heating. Cooling chamber consisting of two coaxial cylinders each attached to one of the self gripping jaws has a structure that permits the tension test while preserving the specimen from outside effects and therefore works as a closed chamber.

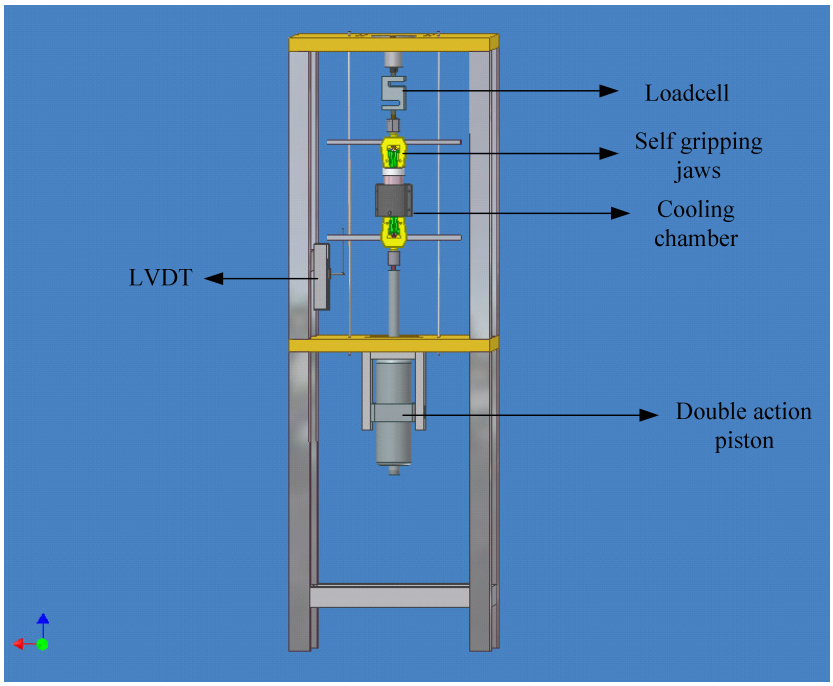

Figure 3.1 Testing bench solid model view.

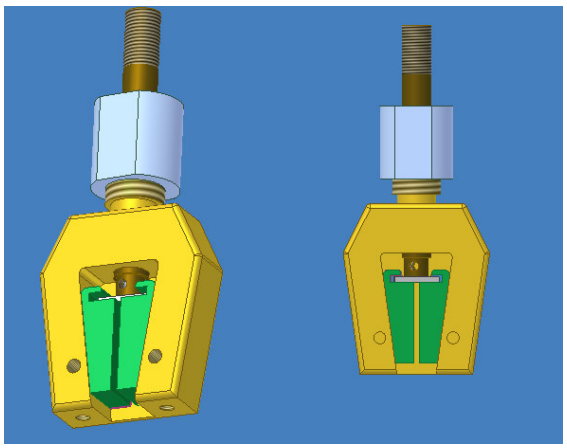

Figure 3.2 Self gripping jaw.

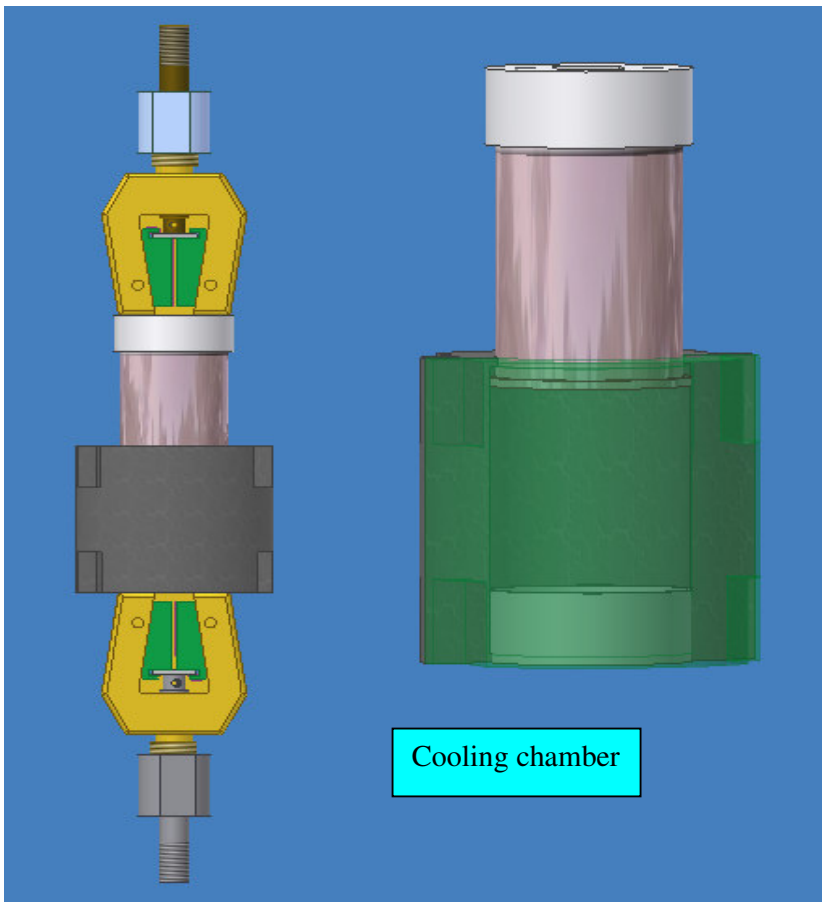

Figure 3.3 Self Gripping Jaws and Cooling Unit

3.1.2 Hydraulics

As a power unit a hydraulic system with a high frequency (200 Hz) servo valve which is controlled directly from a computer is used. Servo valves are known as high speed two directional valves. Controller takes the data from sensors and uses them in the calculations. At the end of those calculations, controller converts the necessary load or strain response into voltage and sends it as a command to the

servo valve. It regulates the hydraulic fluid flow to the upper or lover part of the piston and creates the necessary response for executing the order.

3.1.3 Sensors

Loadcell: Loadcells are transducers, which convert weight to electrical signals to be used by the indicator. For measuring the load on the specimen a strain gauge based loadcell, ESIT TCS S-type, with a capacity of 5 kN and suitable for handling both tension and compression forces is used loadcells. With its stainless steel cover, the TCS load cells are protected to IP68 standards meaning that they are fully immersable. To increase the weak electrical signals generated under load, an electrical voltage amplifier is used.

Load cell output is 2mV/V, i.e., at full capacity load cell gives 2mV for each volt of the power supply. Resolution of the load-cell can be adjusted by changing its supply voltage. In the present case, load-cell is fed by 6 V with a DC Power Supply. The output of the load-cell at 500 kg is expected to be 2 mV/V x 6 V = 12 mV. This output voltage is amplified 500 times, corresponding to 10 V at maximum load. By dividing 500 kg to 10 V, calibration constant is obtained as 50. During load reading, signals are multiplied by 50 X 9.81 to obtain it in units of Newton, i.e.

$$signal x 50 \frac{kg}{V} x 9.81 \frac{N}{kg} = F \tag{3.1}$$

Figure 3.4 S type TCS load-cell.

Linear Variable Displacement Transducer (LVDT)**:** The Linear Variable Differential Transformer is a non-strain-based displacement measuring instrument. The LVDT measurement principle is based on magnetic field variations upon displacement, which means that the resolution of LVDT may be very high. The smallest fraction of movement can be detected by suitable signal conditioning electronics. The external housing of the LVDT is fabricated of material having a high-magnetic permeability, which is desensitizing the device from the effects of external magnetic fields.

With the present testing machine, a 0-50 mm measuring capacity high accuracy LVDT is used. It gives -10 V / 10 V linear analog outputs which can be read by data acquisition system directly without an amplifier.

Figure 3.5 LVDT (Linear Variable Displacement Transducer)

Thermocouple: A thermoelectric device, thermocouple, consisting of two dissimilar metals joined so that a potential difference generated between the points of contact is a measure of the temperature difference between the points is used to measure temperatures accurately. Chromel-Alumel thermocouple with a temperature range of -200°C to 1200°C is used. Since thermocouples give very low voltages, to measure temperature, an amplifier factory calibrated between -40°C and 260°C is used.

Current Sensor: The device consists of a precision, low-offset linear Hall sensor circuit with a copper conduction path. Applied current flowing through this copper conduction path generates a magnetic field which is sensed by the integrated Hall IC and converted into a proportional voltage.

3.1.4 Heating

To heat the specimen joule heating or ohmic heating, which refers to the increase in temperature of a conductor as a result of resistance to an electrical current flowing through it, is used. A 5 volts and 350 watts power supply is used as the power. A DC electronic load is used for the controlling of current on the specimen. According to thermocouple feedback, control software sends voltage signal to electronic load. It applies current on the specimen proportionally with

the incoming signal. Control software sends voltage increments in an adjustable manner up to 10 volts. Electronic loads converts the incoming signals linearly to between 0 -50 Amps.

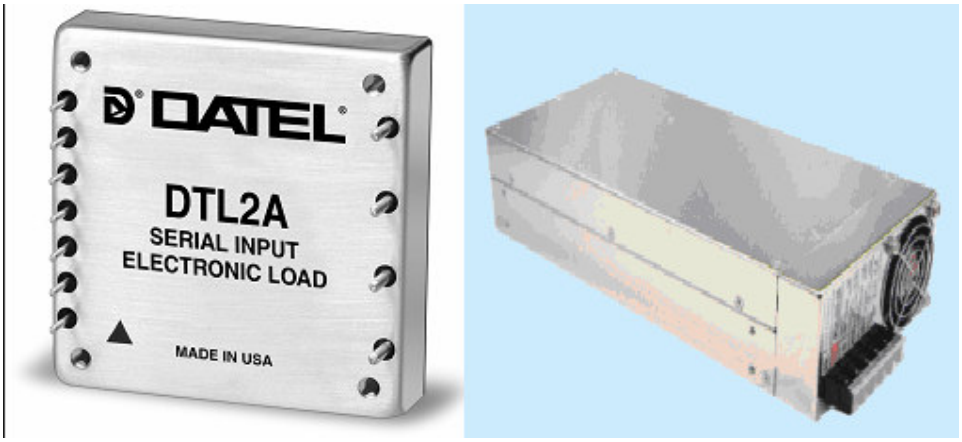

Figure 3.6 Electronic Load and Power supply for heating.

3.1.5 Cooling

Liquid nitrogen is used to cool the specimen from its high temperature austenitic condition to low temperatures. A cryogenic valve controls the flow of nitrogen into the chamber when software sends the cooling order. Upon taking the feedback from the thermocouple, valve opens and allows nitrogen flow until the targeted cooling temperature is reached.

3.1.6 Calibrations

Loadcell calibration is done by using calibrated weights. Offset adjustment is done with an error of 2 - 4 N. This means with the specimen holder, the upper part of the cooling chamber and the load-cell attached, load-cell reads a value between 2-4 N. After the adjustment of offset, calibrated 5, 10 and 20 kgs are hang to the jaw and the readings are controlled.

LVDT is factory calibrated. It represents 0-50 mm between 0-10 V. LVDT can detect 2 μm displacement. Thermocouple amplifier card is also calibrated between -40 and + 260 0C.

3.1.7 Control

Control of the system is done by using a controller designed with Matlab. A schematic diagram of the controller is shown in the Figure 3.7. This controller is processed on a host computer which runs XPC Target. Software does the calculation and sends the order to XPC host computer runs. These two computers are connected to each other by ethernet cards, Figure 3.8.

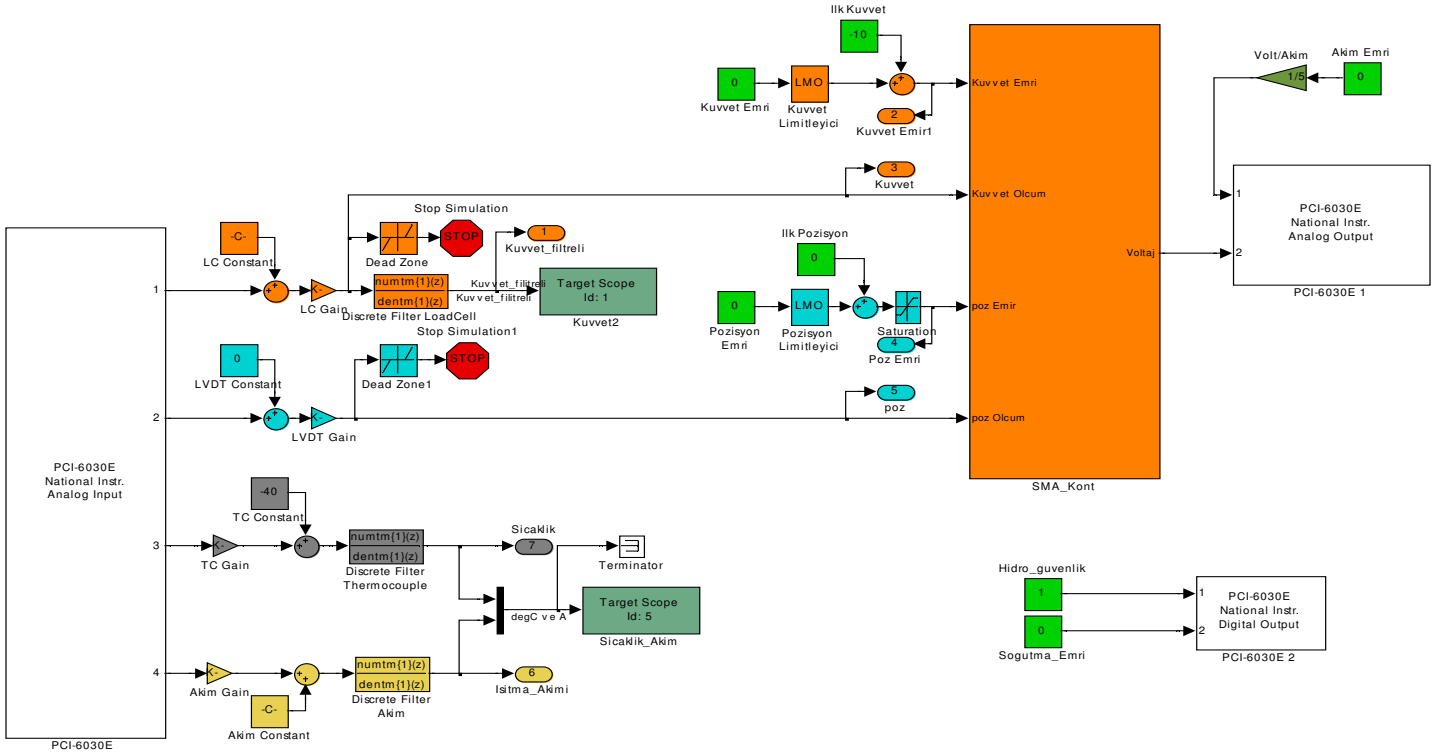

Figure 3.7 Controller of the hydraulic system.

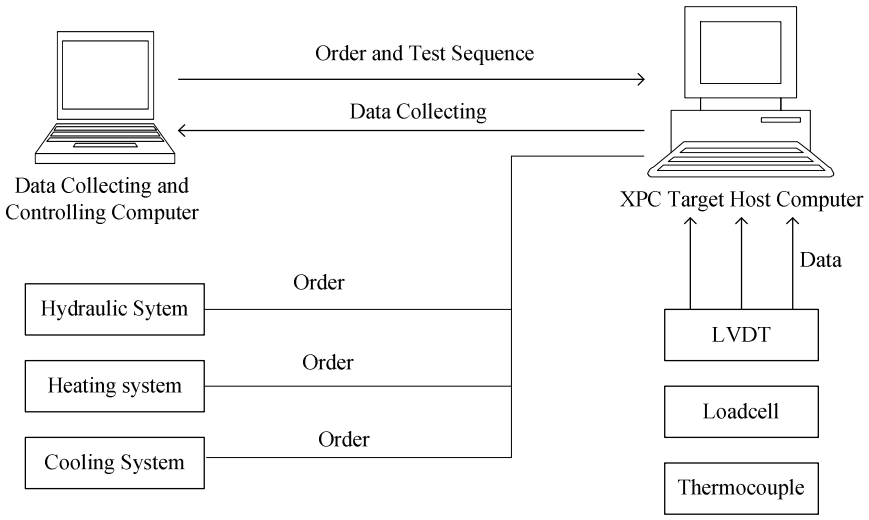

Figure 3.8 Testing machine flow chart.

3.1.8 Software

The software used to create the test sequence, sending order to host computer and collecting data, was written with Delphi. At the start of test user enters the specimen type and dimensions with the number of cycles. Software consisted of process modules to set up any kind of experiment demanded by the user. There are 9 modules for designing the tests. They are as follows:

1. Loading: To set desired load that user wants to apply to the specimen.
2. Unloading: To release the load on the specimen. When this module is used controller try to adjust load on the specimen to zero.
3. % Elongation: To give an elongation order to the system. This module is used when the user wants to apply a specific elongation to the specimen relative to the initial length of it. When this module is used, software calculates the elongation relative to the initial length of the specimen in each cycle.

4. % Elongation (Relative): In this module software calculates elongation relative to the length at the start of each cycle and tries to apply this instruction.
5. Current: With this module user can apply current in the range 0-50 Amps onto the specimen.
6. Heating: This module is used to heat the specimen to the desired temperature assigned by the user.
7. Cooling: Specimen cooling is done by use of this module. User assigns the desired cooling temperature.
8. Waiting: This module is used when the user needs spare time during the test.
9. Position Locked: To measure the force production of shape memory alloy during heating under constant strain.

Once the test is established, software follows the user defined process sequence instructions step by step.

3.2 Alloy Production

A low capacity high frequency vacuum induction melting/casting machine with a vacuum system capable of down to $3x10^{-3}$ mbar evacuation was used for the production of Ti-rich Ti-Ni SMA. Prior to melting, predetermined quantity of 99.2 % purity elemental Titanium and 99.9 % purity Nickel were both cleaned by steel brush and weighed. Crucible material used was alumina-titanate (Al_2O_3-42.8% TiO_2) based and the inner surface was coated with 1-3 mμ thick film of yttria (Y_2O_3). Molds that are made of copper were used in casting operations.

TiNi ingots were swaged and rolled into a bar or a slab at elevated temperatures to break down the cast structure and improve mechanical properties. Hot working

temperature was 900 °C where the alloy is easily workable and the surface oxidation is not too severe. Subsequent to hot working process, TiNi alloys were cold worked and heat-treated to obtain final dimensions with desired physical and mechanical properties.

Cold working was carried out in multiple reduction steps with intermediate annealing at 600°C until the final dimension was obtained. The round wires were produced by rolling through groove profiles. After these production steps, 1.50 mm diameter TiNi shape memory wires were obtained for thermo-mechanical testing.

"Setaram DSC 131" Differential Scanning Calorimeter has been used to determine the effect of heat treatment and deformation on the transformation temperatures of TiNi shape memory alloys. Measurements have been conducted under normal air atmosphere in the temperature range between −50 °C and 150 °C with heating and cooling rates of 10 °C/min, respectively. Transformation temperatures and enthalpies have been determined by use of the software program of the calorimeter.

3.3 Thermomechanical Treatment of the Alloy

Subsequent to the above mentioned standard alloy production process, to investigate the effect of cold working and various heat treatments on the shape memory characteristics of the Ti rich TiNi alloy, various treatments were applied. All the specimens, after acquired in wire form, solution heat treated at 925 ˚C for 30 minutes and then water quenched. While some of the wires are tested in this condition, others are tested after further annealing at 500 C for 30 minutes. Another group of specimens, to see the effect of cold working, subsequent to solutionizing at 925 C and prior to annealing at 500 C are cold deformed by 20%

or 40 %. So, in total there were four differently treated groups of samples to be tested for shape memory behavior.

Differential Scanning Calorimeter has been used at different stages of above mentioned treatment as well as different stages of thermomechanical testing to observe the effect of heat treatment and deformation on the transformation temperatures.

3.4 Thermomechanical Testing Procedure

To determine the thermo-mechanical characteristic of TiNi SMA, a series of experiment is designed and applied to the melt, cast and processed Ti-55wt %Ni wire specimens. The testing equipment used during this investigation is, as mentioned in the previous section, a fully computerized tensile testing machine specially designed and manufactured in the context of the present study. It is capable of accurately measuring a combination of the influence of temperature, stress and strain on the SMA wires.

Four different types of experiment are designed to observe the shape memory characteristics of the specimens in the widest possible spectrum. In all three types of experiments, specimens are deformed to the desired level of stress or strain in martensitic condition and then heated and cooled under various conditions and these were repeated in cycles. During these steps stress-strain-temperature data are collected and stored continuously. Tests designed for inspecting transformations characteristics and behavior under different load and strain condition for untrained SMA wire are as follows:

1. **Constant Stress Free Recovery Test, (Figure 3.9):** A constant amount of load, 700 N, is applied to the specimen at the beginning of each cycle, and after unloading the specimen is heated up to 120ºC to recover the permanent strain,

which is of the order of 10% in the first cycle and decreases with cycling depending on the processing of the alloy.

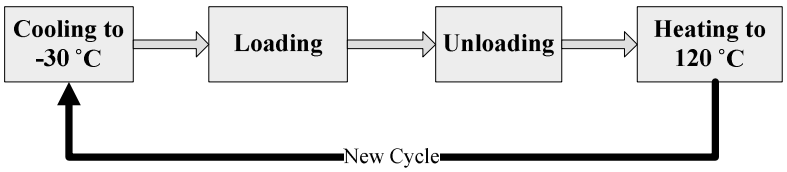

Figure 3.9 Test Sequence of Constant Stress Free Recovery test.

2. Constant Strain Free Recovery Test, (Figure 3.10): The specimen is loaded to yield a constant amount of strain, 2% or 4%, at the beginning of each cycle, and then heated up to 120ºC to recover the permanent strain.

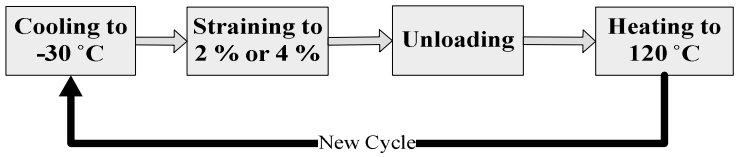

Figure 3.10 Test Sequence of Constant Strain Free Recovery test.

3. Constant Strain Constrained Recovery Test, (Figure 3.11): In this type of test wire was deformed with a predetermined stress and unload. Elastic strain is recovered and a plastic strain remains on the wire. At this point position was fixed and specimen was heated. By heating; since the position fixed stress start to increase. By this test it is observed the maximum load can the wire apply.

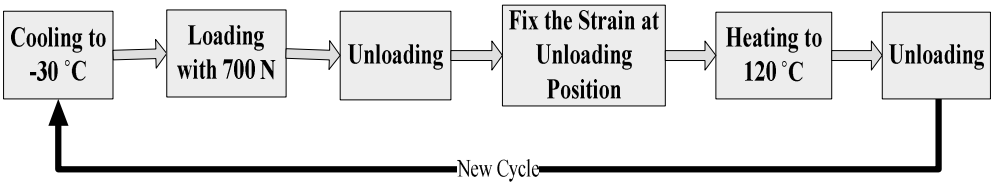

Figure 3.11 Test sequence of Constant Strain Constrained Recovery test.

4. Constant Stress Constrained Recovery Test, (Figure 3.12): In this type of test, SMA wire is deformed with a constant amount of load. After unloading a constant amount of determined stress is applied and the wire is heated with this load, following the shape recovery wire is unloaded and cooled.

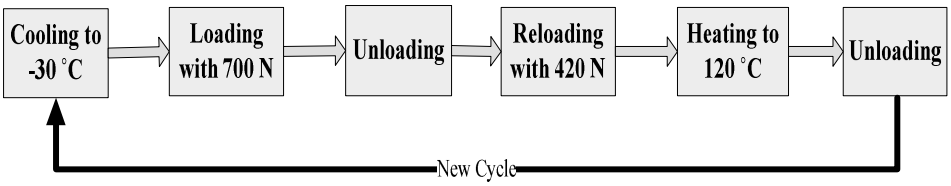

Figure 3.12 Test sequence of Constant Strain Constrained Recovery.

3.5. Overall Testing Scheme:

Overall testing procedure in a summarized form combining the deformation, heat treatment and testing procedures are given in Figure 3.13.

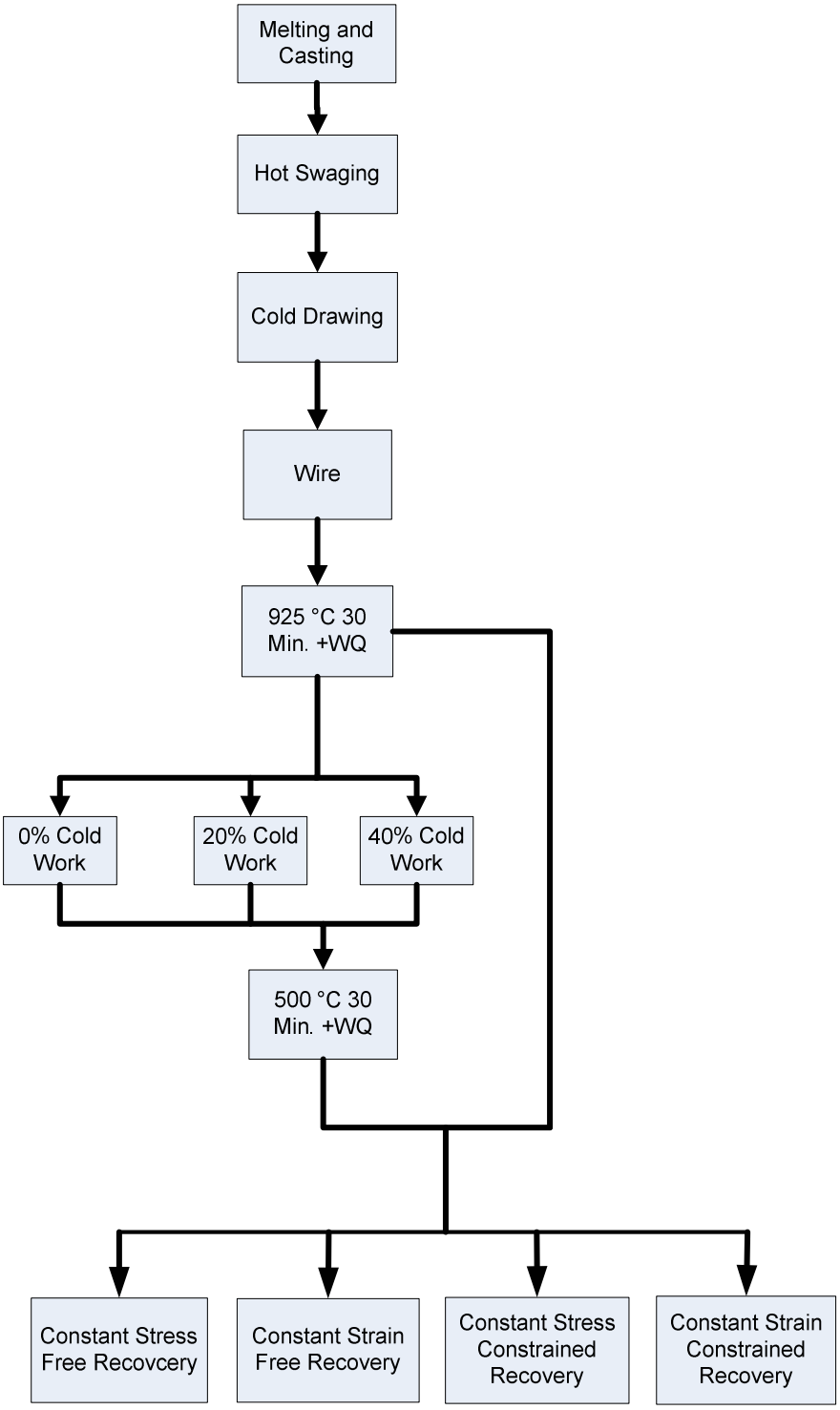

Figure 3.13 Experiment flow chart.

CHAPTER 4

RESULTS AND DISCUSSIONS

Four different types of thermo-mechanical test cycles, namely:

Type I: Constant Stress Free Recovery, i.e., free recovery after loading to the same predetermined stress level before each cycle,
Type II: Constant Strain Free Recovery, i.e., free recovery after straining by the same predetermined amount before each cycle,
Type III: Constant Strain Constrained Recovery, i.e., heating the deformed sample while holding the strained length constant to prevent any shape recovery,
Type IV: Constant Stress Constrained Recovery, i.e., recovery of the deformed sample is allowed to occur under a predetermined bias stress,

were applied to Ti-rich TiNi wire specimens to characterize their shape memory response under four different heat treatment conditions, which were:

Process I: Annealing at 925 °C for 30 minutes and water quenching.
Process II: Annealing at 500 °C for 30 minutes and water quenching subsequent to Process I,
Process III: 20% cold work applied subsequent to Process I,
Process IV: 40% cold work applied subsequent to Process I.

Behavior of shape memory alloys can be visualized in all respects by use of three dimensional σ-ε-T diagrams. However, since it is difficult to interpret a three dimensional plot, the results of the tests in the following sections are presented by

use of appropriate two dimensional graphical sections of the three dimensional σ-ε-T plots given in Appendix A. Below, for each type of test, the results for samples subjected to different heat treatments will be presented as (1) Stress-Strain (σ-ε) diagram during loading and the subsequent heating, (2) Strain-Temperature (ε-T) diagram during heating and (3) Critical Strains diagram showing the effect of cycling on some critical strain values. For each type of test, finally, one way and two way shape recovery, OWSR and TWSR, respectively, of differently heat treated samples will be compared on a OWSR and TWSR versus number of cycles graphs.

4.1 Type I (Constant Stress Free Recovery) Test

Results of Constant Stress Free Recovery tests for samples subjected to Process I, II, III and IV are shown in Figures 4.1.1 to 4.1.4, respectively, as (a) σ-ε, (b) ε-T and (c) Critical Strains - # of cycles diagrams. Considering the difference in the strength and therefore martensite inducing stress of samples subjected to different treatments, samples subjected to processes I and II were stressed to 310 Mpa, 20 % cold worked samples to 350 Mpa and 40% cold worked samples to 400 Mpa.
The diagrams displaying the results are similar in shape but differ somewhat in magnitudes for the four different heat treatments. The initial cycles of the (σ-ε) curves in all cases, subsequent to the elastic deformation, show a plateau where strain increases without an increase in the stress level. The plateau stress, which is around 175 MPa for all heat treatments in the present study, is the critical stress for martensite deformation by the reversible motion of the variant boundaries, which is also known as detwinning of martensite. Such a deformation is quite expected since it is the basis of shape memory behavior. The subsequent strain hardening region where stress increases with strain corresponds to plastic deformation of detwinned martensite by dislocation mechanisms. The plateau strain and therefore the total permanent deformation which is around 10% for the first two heat treatments is reduced to around 6% for the later two treatments

which involve cold working. The plateau region almost completely disappears and the σ-ε curves are stabilized after the second cycle, and the total permanent strain is reduced by an amount approximately corresponding to the plateau strain. ε-T curves obtained during heating show the A_s and A_f temperatures at the point of deviation from linearity on the two ends of the curves. ε-T diagrams indicate that applying cyclic thermomechanical tests decrease the A_s temperature and widens the range of hysterisis. A_s decreases approximately by 10°C in five cycles. But quantitative analysis of transformation temperatures and the hysterisis ranges based on these curves is not adequate due to the accuracy and response time limitations of the thermocouples used. Results of a concise study consisting of DSC cycles on samples before and after free recovery tests to determine the transformation temperatures are shown in Figure 4.1.6. A_s temperatures are observed to be considerably increased, as much as 28° C, in some of the samples during the free recovery tests without any systematic dependence on the heat treatment, Figure 4.1.6.a. But in few DSC cycles, the difference is reduced to few degrees, indicating that the origin of the A_s difference is the substructure formed during testing and it is recovered during DSC cycles. M_s Temperatures, on the other hand, are found to vary by free recovery testing at most by 2°C as shown in Figure 4.1.6.b. The reason why M_s temperatures are not affected from free recovery testing as much as the A_s temperatures is that, since the M_s temperatures are measured during cooling after a heating in the DSC, they actually represent the values for recovered structure. That is also why they show very limited variation during DSC cycling. Figure 4.1.6 c and d show the austenite and martensite transformation hysterisis (T_s-T_f), respectively. While austenite hysterisis is in the range 15° to 25° C and exhibits no systematic variation with testing or heat treatment (probably due to insufficient data), martensite transformation hysterisis is found to be around 15° C before mechanical testing and around 35° C after free recovery tests. Martensite hysterisis of free recovery tested samples have a tendency to decrease with DSC cycling.

Recovered strain upon heating is shown in Figure 4.1.5 as a function of cycling. One way shape recovery, OWSR, improves with cycling and approaches to a value around 4 %.after couple of cycles for the first two heat treatments. For the last two heat treatments involving cold working, OWSR is not affected from cycling but has a relatively low level around 2.5%. Two way shape recovery, TWSR, which is the elongation during cooling as if trying to achieve the initial deformed dimensions, also exhibit an increase with cycling but magnitude is much smaller than OWSR, varies in the range from about 1.5% (non-cold worked specimens) to about 0.6% (cold worked specimens).

From these results one can see the strong effect of deformation on shape memory behavior and reach to the conclusion that the observed dependence on cycling is closely related to dislocation generation in the early cycles. The considerably large unrecovered strain of the first cycle is probably due to strain imposed by irreversible dislocation mechanisms and cannot be recovered. Those dislocated regions can not contribute to the strain during detwinning in the next cycles. As a result, in the later cycles only the regions which are not dislocated and therefore active do take part in deformation and in recovery as well, so that fractional recovery approaches from about 40% in the first cycle to about 100% in 5 cycles. Actually, this phenomenon is the basis of the commercial training of shape memory alloys.

It is interesting to note that the plateau region exists also in the first cycle of the heavily cold worked samples indicating that the dislocation structures generated during detwinning is different than that of cold working. Most probably the random dislocation structure of cold working is not as effective as the dislocations generated on the variant boundaries during detwinning. Further interpretation on the subject requires a detailed transmission electron microscopy study. Increase of OWSR of the non-cold worked samples with cycling while the total recovery after cooling remains constant with cycling due to the contribution

of the two way shape recovery is difficult to explain and should be considered in the same context.

If OWSR is used as the performance criteria of shape memory alloys, Process I seems to be the best heat treatment that can be applied. Additional intermediate annealing heat treatment decreases OWSR property nearly by 0.5 %. Specimens cold worked during Process III and Process IV show similar characteristics, and OWSR is considerably lower than that for Process I and Process II. But, on the other hand, Process III and Process IV specimens show more stable behavior than Process I and Process II specimens starting from the first cycle and they can be used without any training.

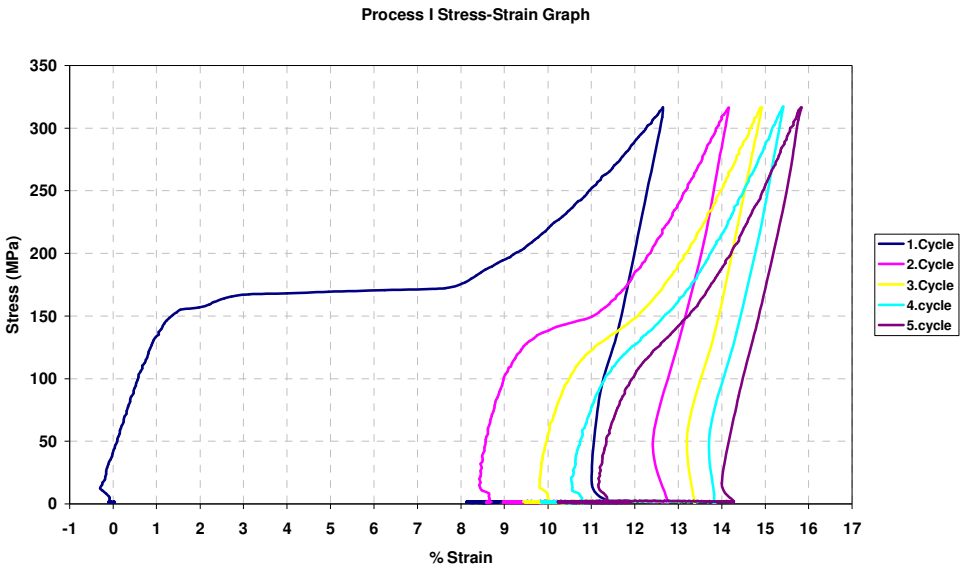
Process I Stress-Strain Graph
Stress (MPa)
% Strain
1.Cycle
2.Cycle
3.Cycle
4.cycle
5.cycle

(a)

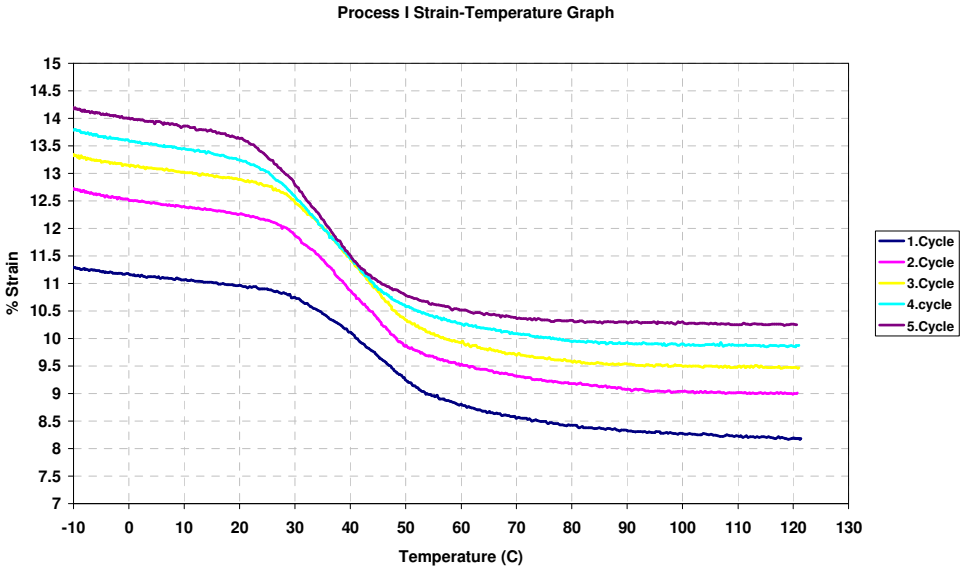
Process I Strain-Temperature Graph
% Strain
Temperature (C)
1.Cycle
2.Cycle
3.Cycle
4.cycle
5.Cycle

(b)

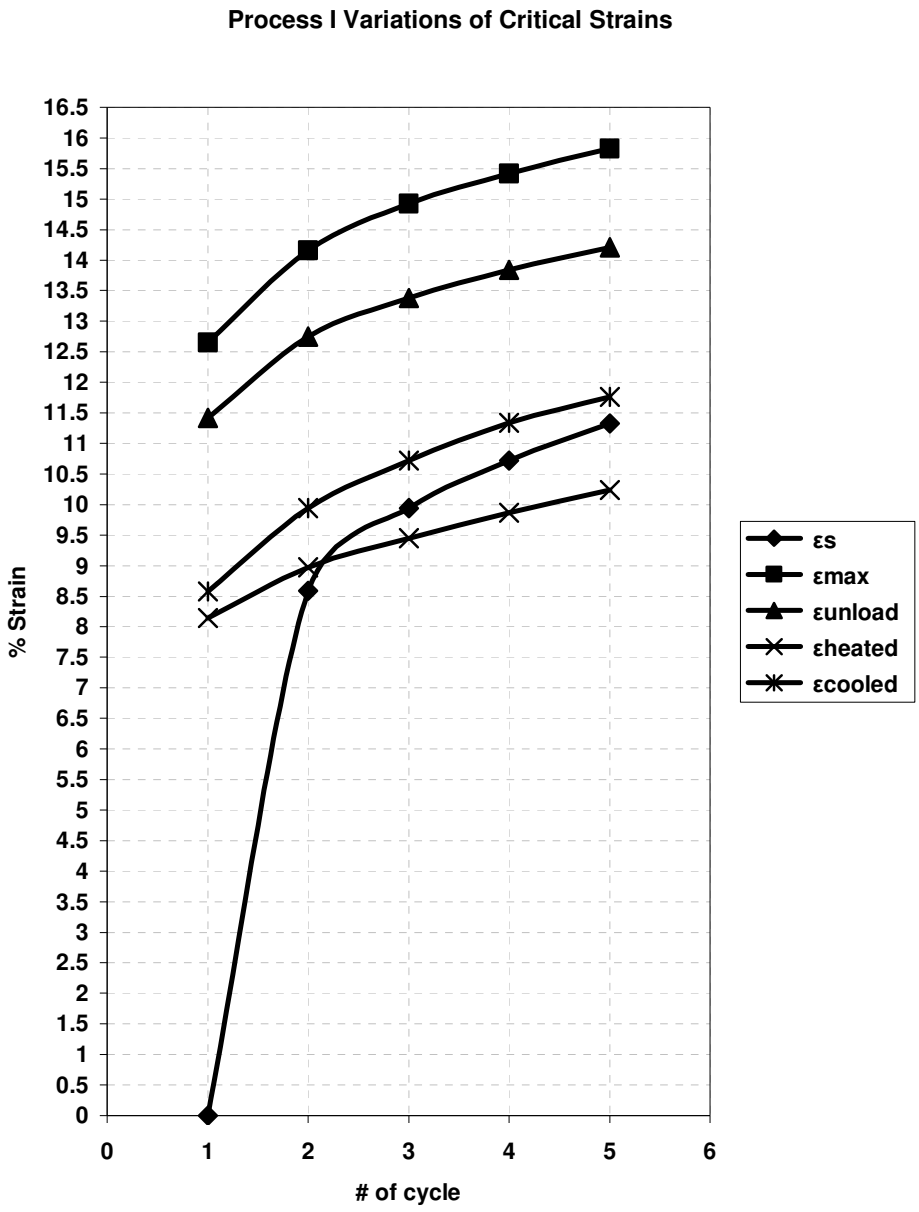

(c)

Figure 4.1.1 Type I (Constant Stress Free Recovery), test results for samples subjected to Process I. (a) σ-ε, (b) ε-T and (c) Critical Strains - # of cycles diagrams.

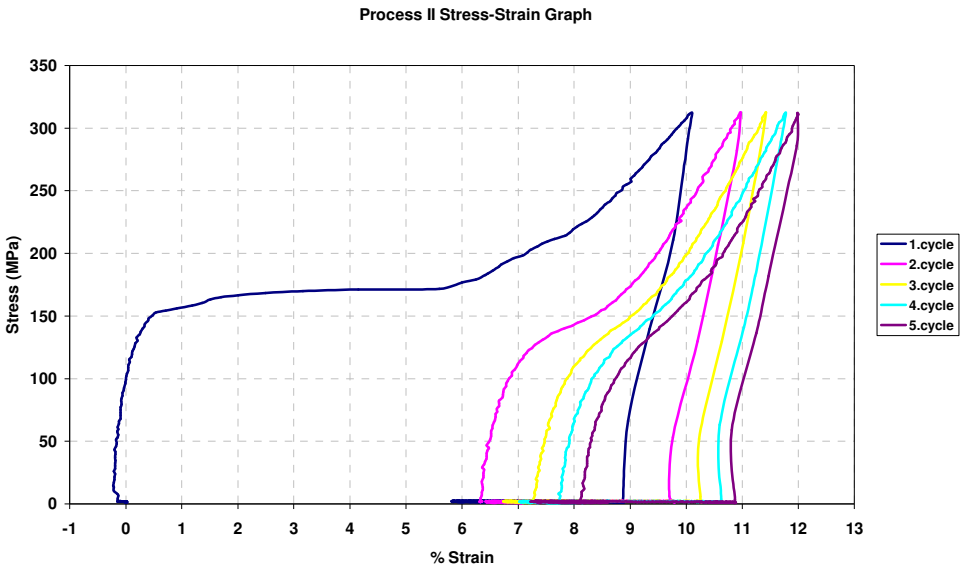
Process II Stress-Strain Graph
Stress (MPa)
% Strain
1.cycle
2.cycle
3.cycle
4.cycle
5.cycle

(a)

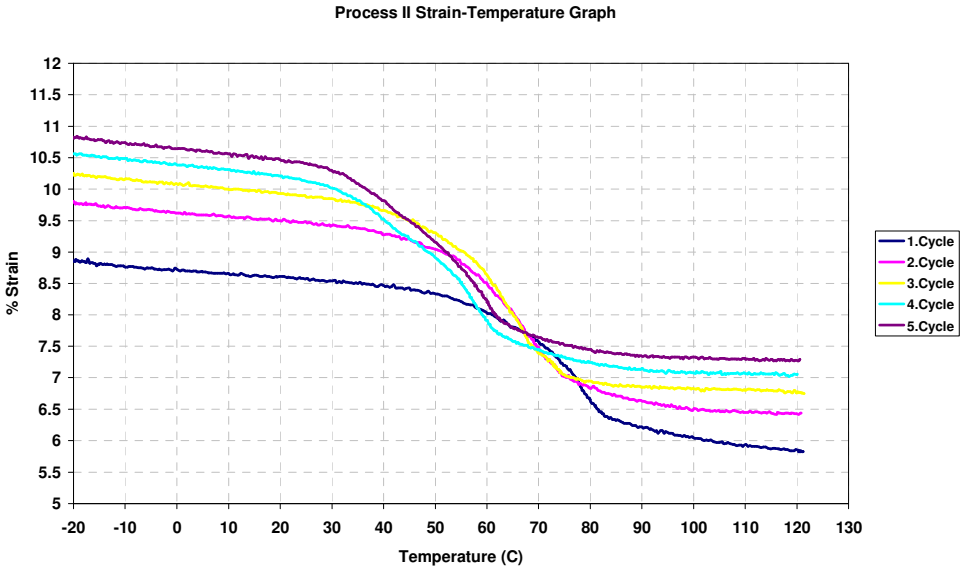
Process II Strain-Temperature Graph
% Strain
Temperature (C)
1.Cycle
2.Cycle
3.Cycle
4.Cycle
5.Cycle

(b)

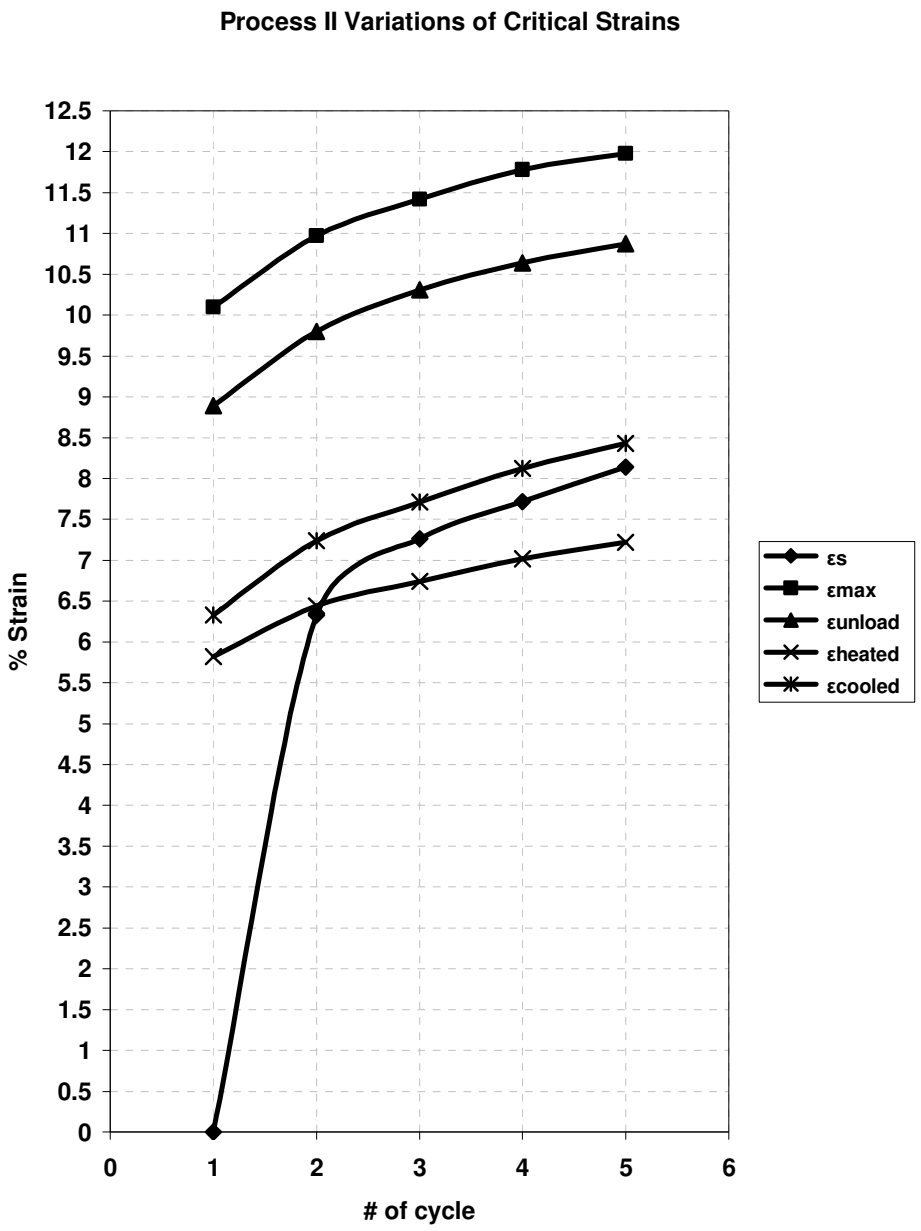

(c)

Figure 4.1.2 Type I (Constant Stress Free Recovery), test results for samples subjected to Process II. (a) σ-ε, (b) ε-T and (c) Critical Strains - # of cycles diagrams.

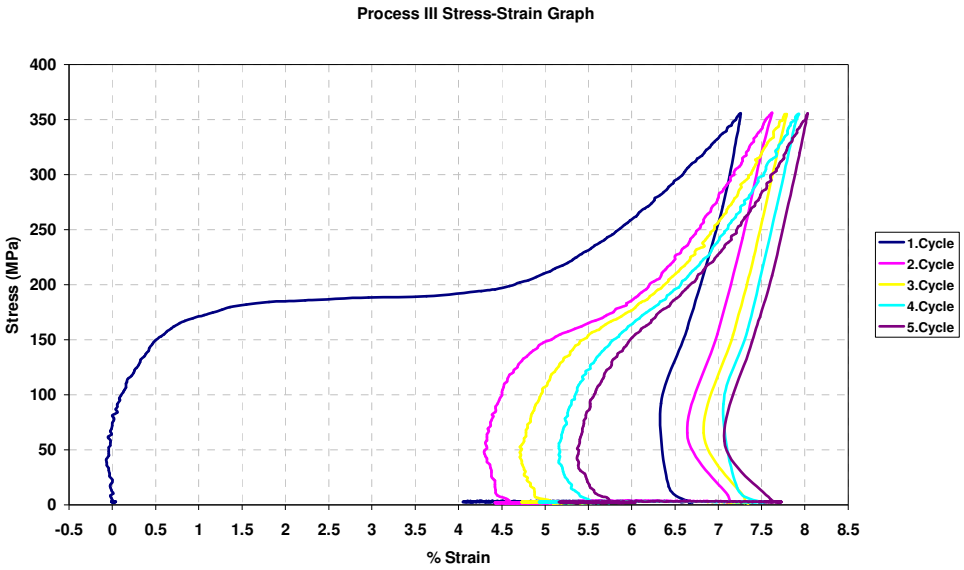
Process III Stress-Strain Graph
Stress (MPa)
% Strain
1.Cycle
2.Cycle
3.Cycle
4.Cycle
5.Cycle

(a)

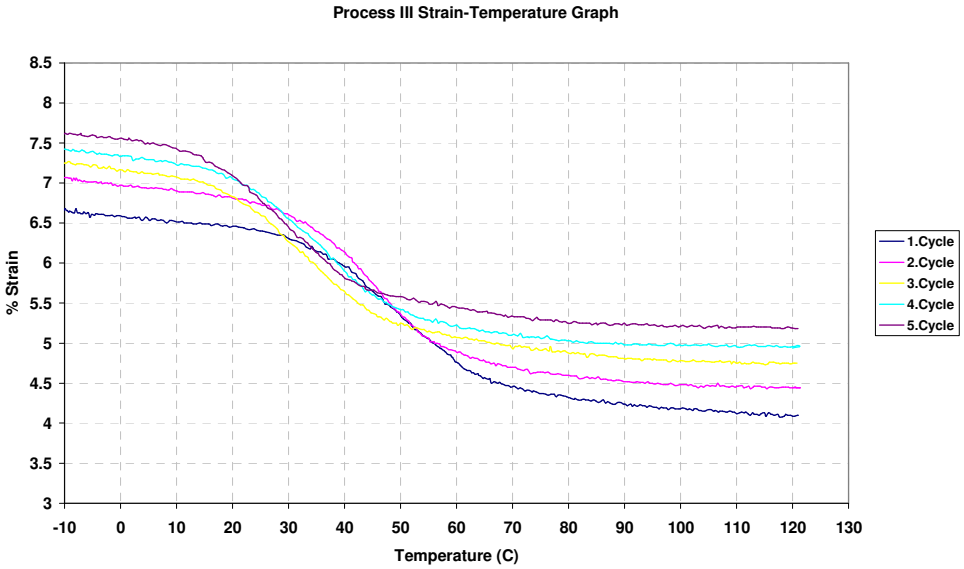
Process III Strain-Temperature Graph
% Strain
Temperature (C)
1.Cycle
2.Cycle
3.Cycle
4.Cycle
5.Cycle

(b)

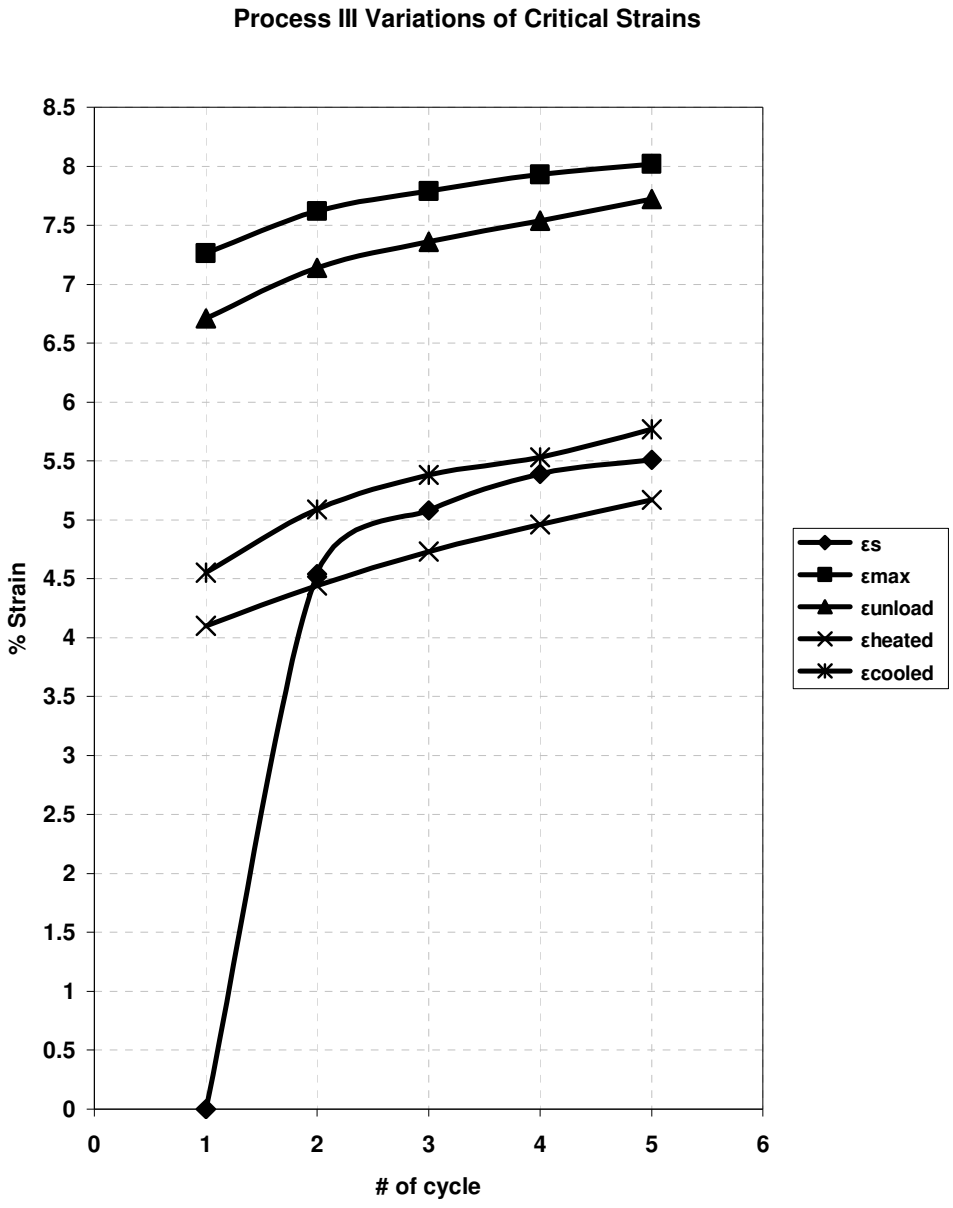

(c)

Figure 4.1.3 Type I (Constant Stress Free Recovery), test results for samples subjected to Process III. (a) σ-ε, (b) ε-T and (c) Critical Strains - # of cycles diagrams.

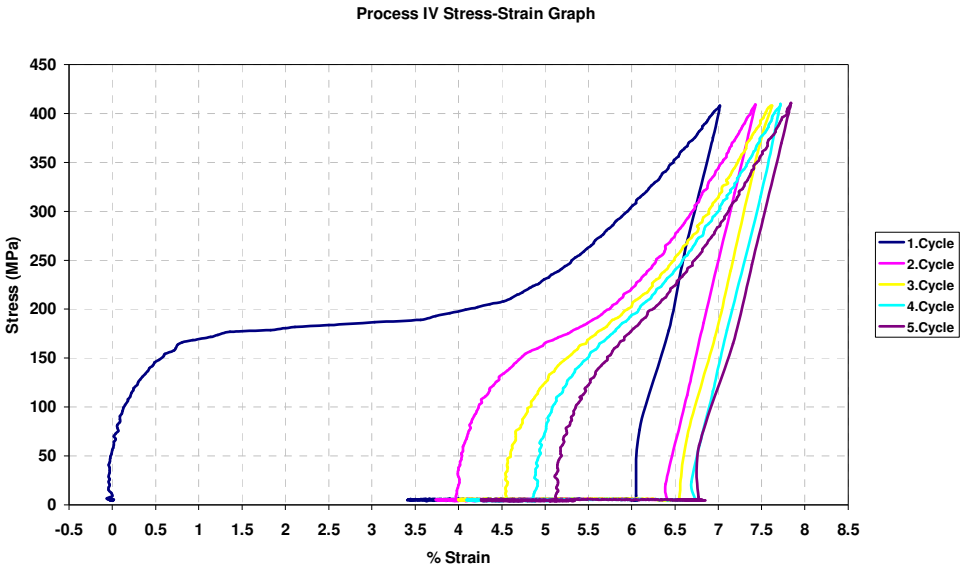
Process IV Stress-Strain Graph
Stress (MPa)
% Strain
1.Cycle
2.Cycle
3.Cycle
4.Cycle
5.Cycle

(a)

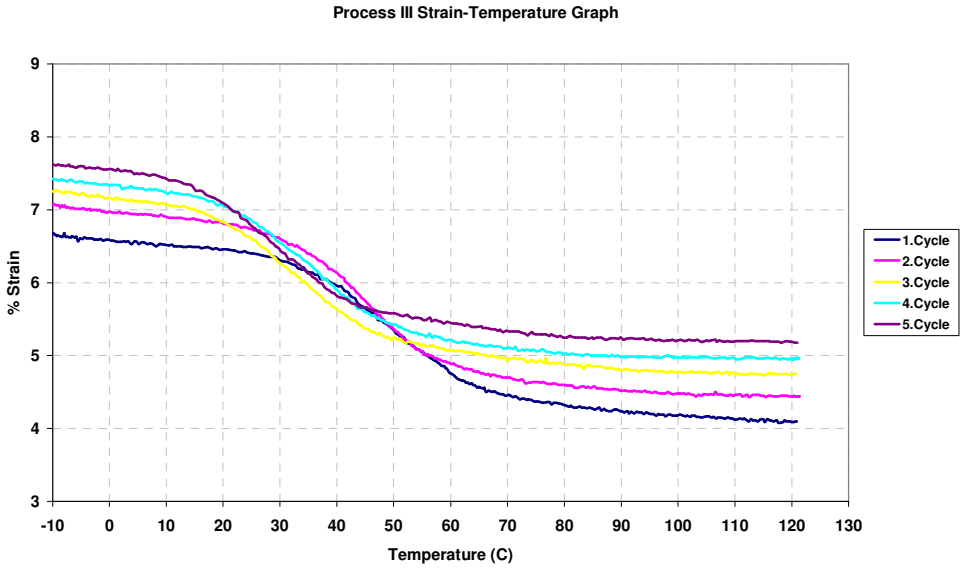
Process III Strain-Temperature Graph
% Strain
Temperature (C)
1.Cycle
2.Cycle
3.Cycle
4.Cycle
5.Cycle

(b)

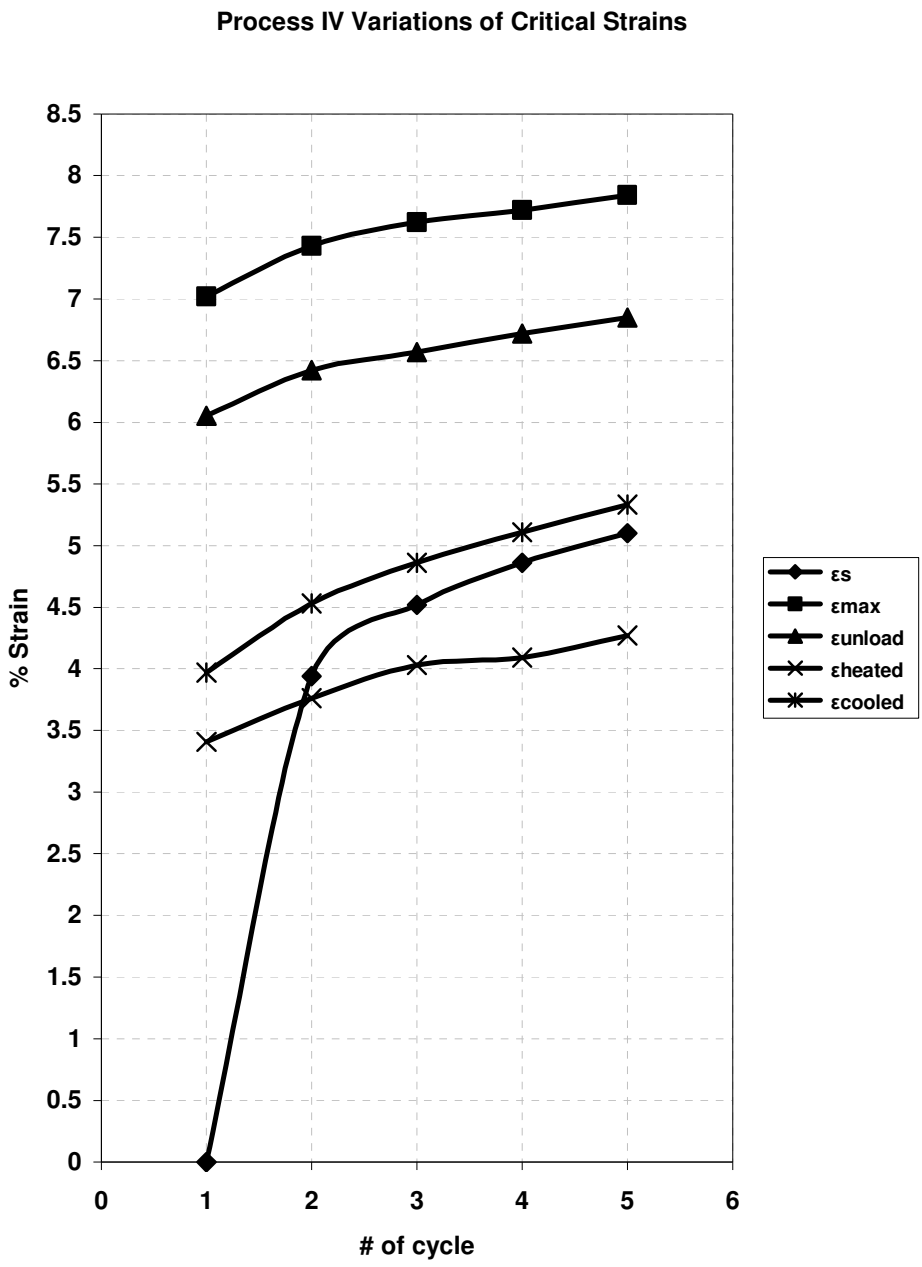

(c)

Figure 4.1.4 Type I (Constant Stress Free Recovery), test results for samples subjected to Process IV. (a) σ-ε, (b) ε-T and (c) Critical Strains - # of cycles diagrams.

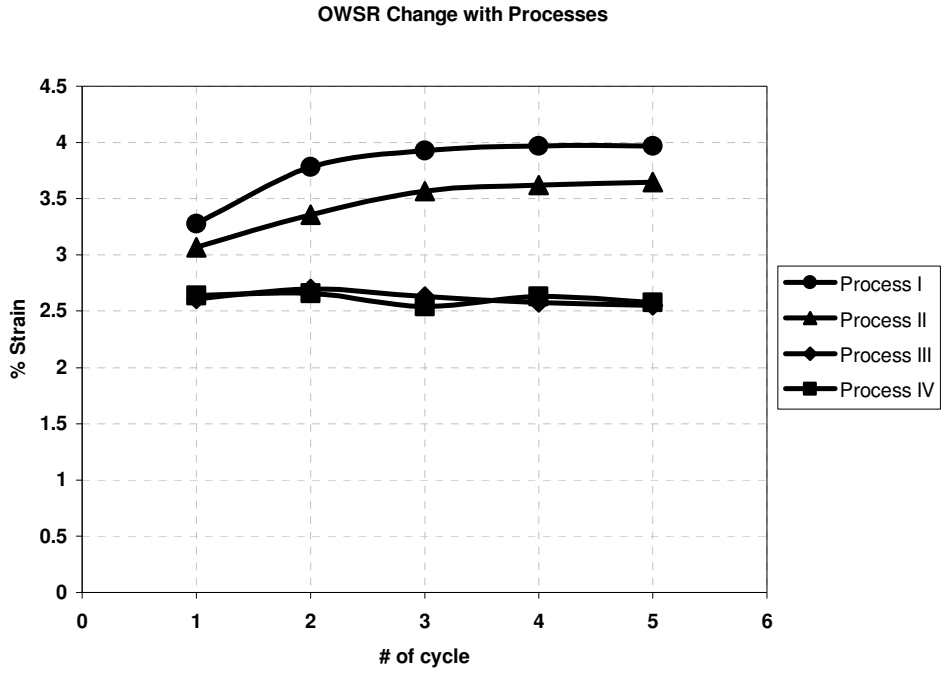

(a)

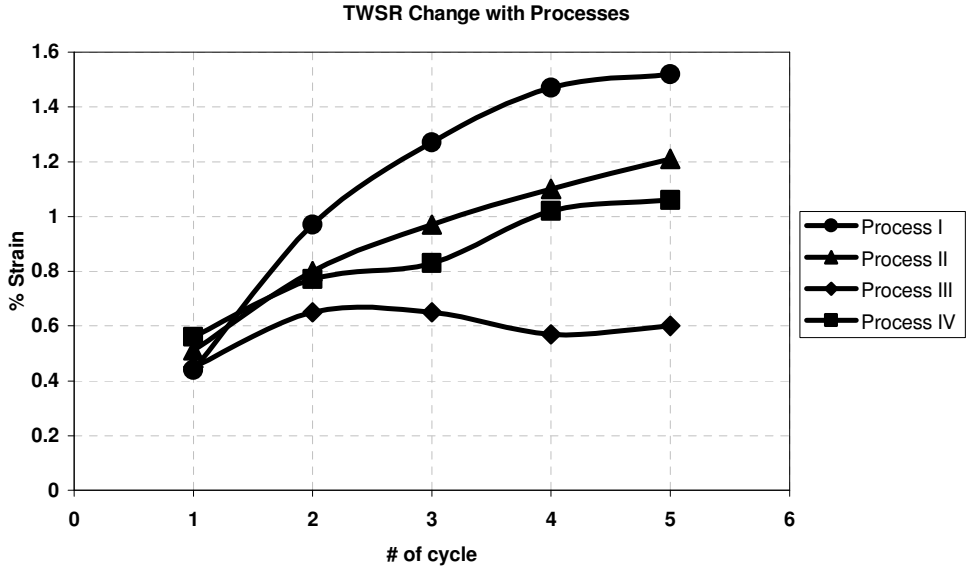

(b)

Figure 4.1.5 OWSR (a) and TWSR (b) change with processes at Constant Stress Free Recovery test.

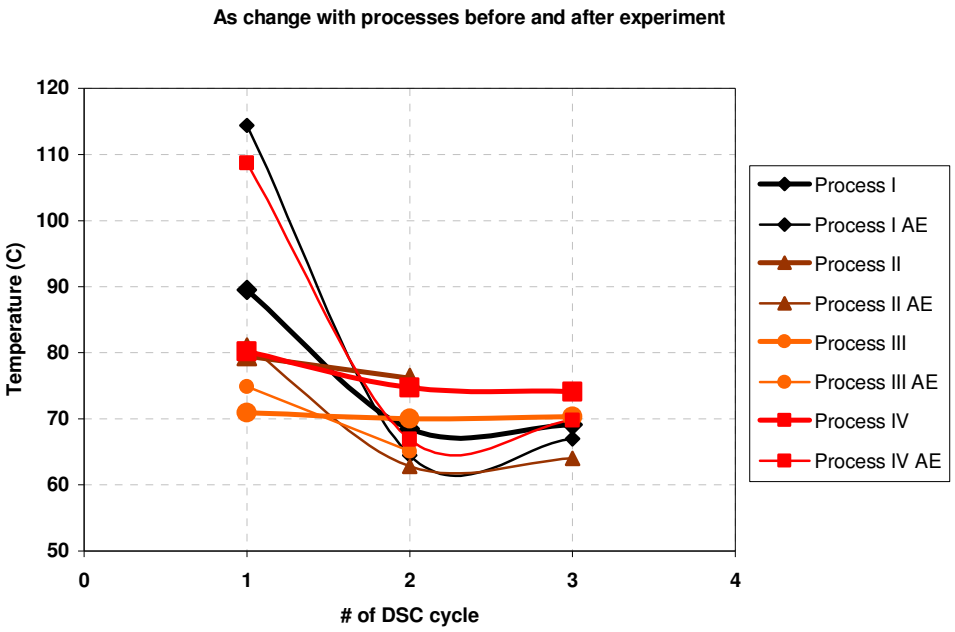
As change with processes before and after experiment
Temperature (C)
120
110
100
90
80
70
60
50
0
1
2
3
4
# of DSC cycle
Process I
Process I AE
Process II
Process II AE
Process III
Process III AE
Process IV
Process IV AE

(a)

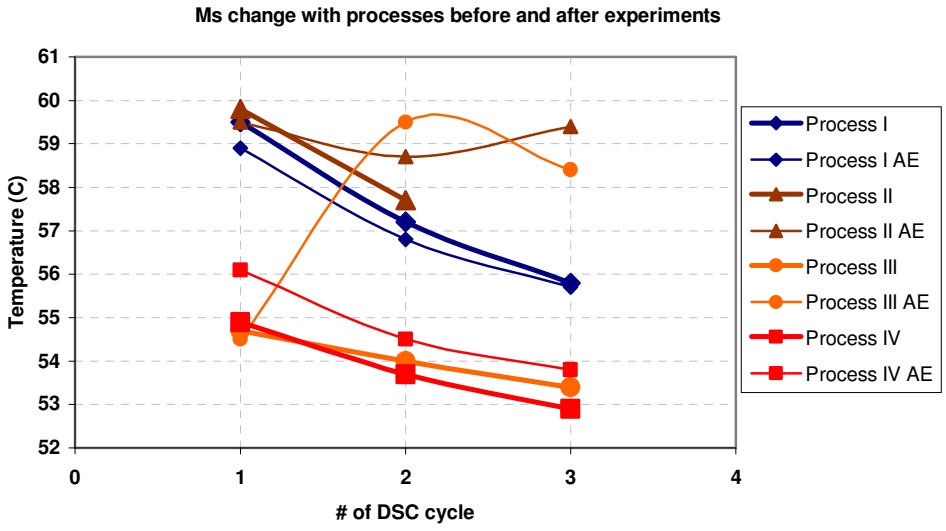
Ms change with processes before and after experiments
Temperature (C)
61
60
59
58
57
56
55
54
53
52
0
1
2
3
4
# of DSC cycle
Process I
Process I AE
Process II
Process II AE
Process III
Process III AE
Process IV
Process IV AE

(b)

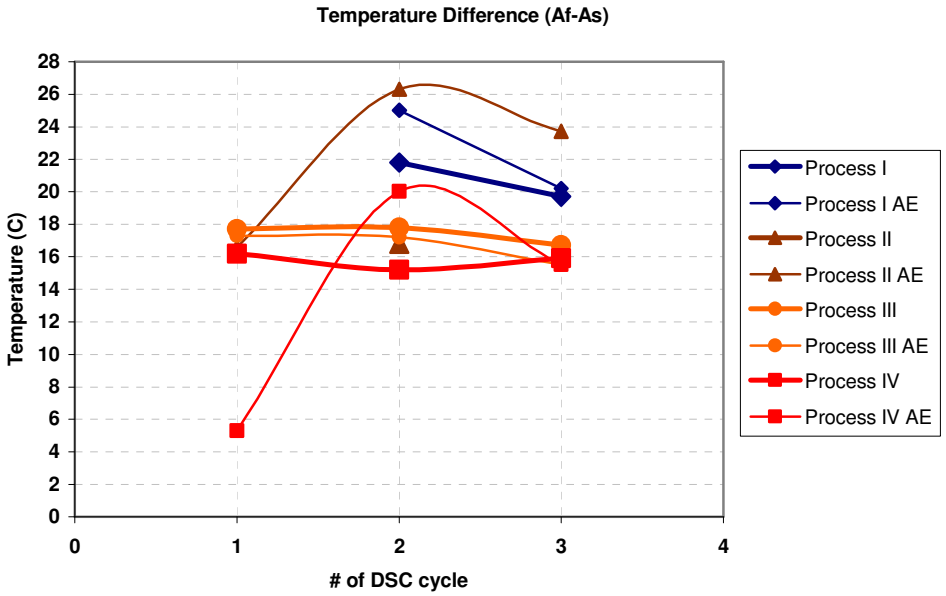

(c)

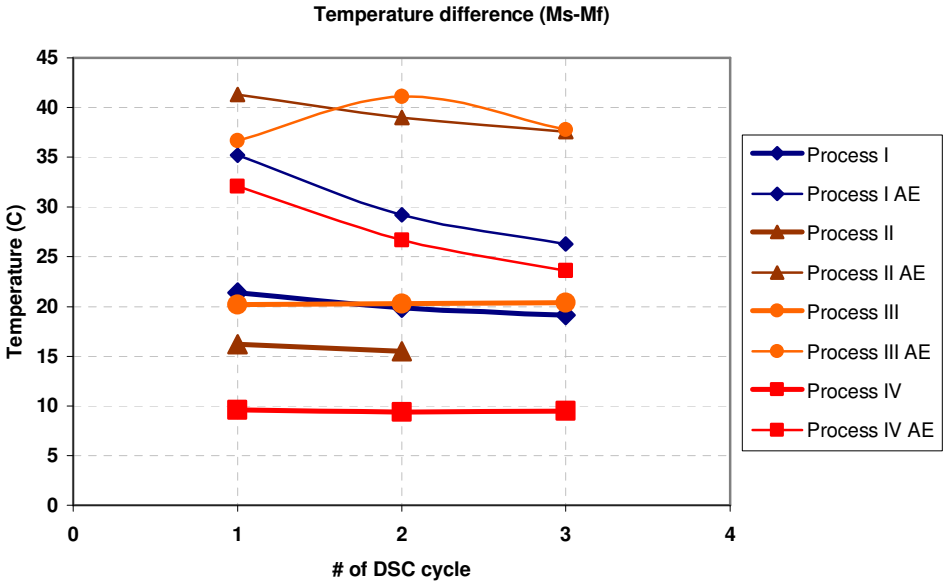

(d)

Figure 4.1.6. (a) Austenite and (b) martensite transformation temperatures (A_s and M_s), and(c) austenite and (d) martensite transformation hysterisis (T_s-T_f), measured by DSC before and after free recovery testing.

4.2 Type II (Constant Strain Free Recovery) Test

As mentioned in the previous chapter, Type II tests, namely the Constant Strain Free Recovery tests, involve loading to yield a constant amount of strain in the plateau region, 2% or 4%, at the beginning of each cycle, and then heating up to 120ºC to recover the permanent strain. The applied strain values were chosen specifically in the plateau region to prevent the irreversible dislocation deformation in the first cycle. However, since testing machine was load controlled, it has not been possible to stop the tests at the desired strain levels in the first few cycles but still remained in the plateau region. As before, results of Constant Strain Free Recovery tests for samples subjected to Process I, II, III and IV are shown in Figures 4.2.1 to 4.2.4, respectively, for constant strain of 2% and in Figures 4.2.6 to 4.2.9, respectively, for constant strain of 4%, as (a) σ-ε, (b) ε-T and (c) Critical Strain Change - # of cycles diagrams. Figures 4.2.5 and 4.2.10 show the OWSR and TWSR change with process during all cycles. The plateau stress for first two heat treatment were found to be around 150 MPa and around 175 MPa for the last two due to cold work. For both 2 % and 4 % strain level experiments, plateau region in the σ-ε curves disappeared in few cycles and it has been possible to control and stop the tests at the desired strain levels. In both 2 % and 4 % constant strain experiments σ-ε curves and the stress to obtain the desired strain stabilized with cycling. While the rise in the stress for stabilization in 2 % constant strain experiments was only around 10 % in non-cold worked specimens, it was almost 80 % for the cold worked specimens. On the other hand, in 4 % constant strain experiments, the stress increased by three to four folds in 15 cycles for all heat treatments. Obviously, the stress rise was more apparent in the cold work samples. The permanent strain after unloading and before heating for shape recovery was about 1.5% in the 2 % total constant strain experiments and was about 3% during the initial cycles but dropped down to as low as 1.5% with increasing stress with the cycles in the 4 % total constant strain experiments

ε-T curves indicate that applying constant strain cyclic thermomechanical tests decrease the A_s temperature by nearly 20 °C in the 2 % constant strain experiments and by 30 °C in the 4 % constant strain experiments.

As can be seen from the Critical Strain Variations graphs as well, OWSR, shown in Figure 4.2.5 as a function of cycling for the 2% constant strain experiments improves with cycling and after the 3rd cycle becomes nearly constant around 2%. for the first two heat treatments and around 1.5% for the last two heat treatments involving cold working. Recalling that the permanent strain is only 1.5%, 2% strain recovery in the non-cold worked samples corresponds to about 130% fractional recovery upon heating. But upon cooling, because of two way recovery effect, total fractional recovery reduces to reasonable values close to 100%. This anomalous behavior, which has been also observed in Constant Stress Free Recovery tests and cannot be attributed to thermal expansion, is apparent in the critical strain-# of cycles curves denoted as (c) in the corresponding figures since the starting strain is normalized to begin from zero in the plots. This seems to be related to the unrecovered strain of the first two cycles because in the cold worked samples such a anomalous higher than 100% fractional recovery is not observed because of the relatively limited unrecovered strain in the first cycles and fractional recovery was about 100% starting from the second cycle. TWSR of the non-cold worked samples initially strained to 2 % are also much better than the free recovery, i.e., 1% TWSR observed corresponds to about 50% of the OWSR compared to 30% in the free recovery.

Figure 4.2.10 shows the OWSR change of 4 % constant strain experiments. It is seen that OWSR increase with each cycles and almost stabilize after 7-8 cycles. As can also be seen from critical strain-# of cycles curves, after stabilization, the anomalous higher than 100% recovery upon heating is observed in 4 % constant strain experiments similar to the previous experiment. But this time, probably because of the high level of applied strain and the resulting stresses, cold worked samples also behaved in the same manner and displayed high unrecovered strain

during the first cycles and the same anomalous high recovery behavior. TWSR of the samples initially strained to 4 % is in the range 1.5% to 1% for all the samples and improve with cycling comparable to that in free recovery.

As a general conclusion, it can be stated that the specimens deformed to a smaller strain show a more stable shape memory behavior and more over, in all free recovery tests conducted, OWSR characteristics was observed to deteriorate with heat treatment in the order from Process I to Process IV.

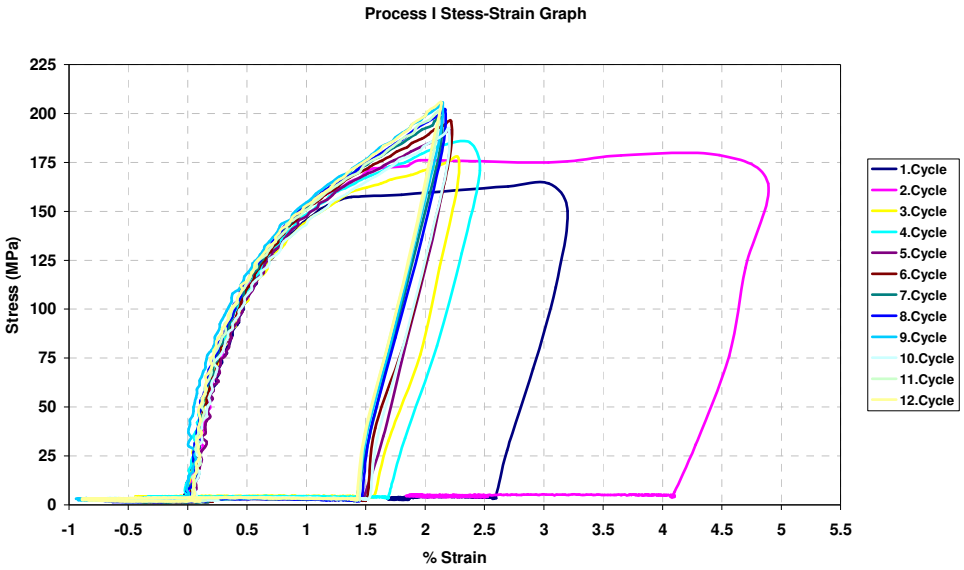
Process I Stess-Strain Graph
Stress (MPa)
% Strain
1.Cycle
2.Cycle
3.Cycle
4.Cycle
5.Cycle
6.Cycle
7.Cycle
8.Cycle
9.Cycle
10.Cycle
11.Cycle
12.Cycle

(a)

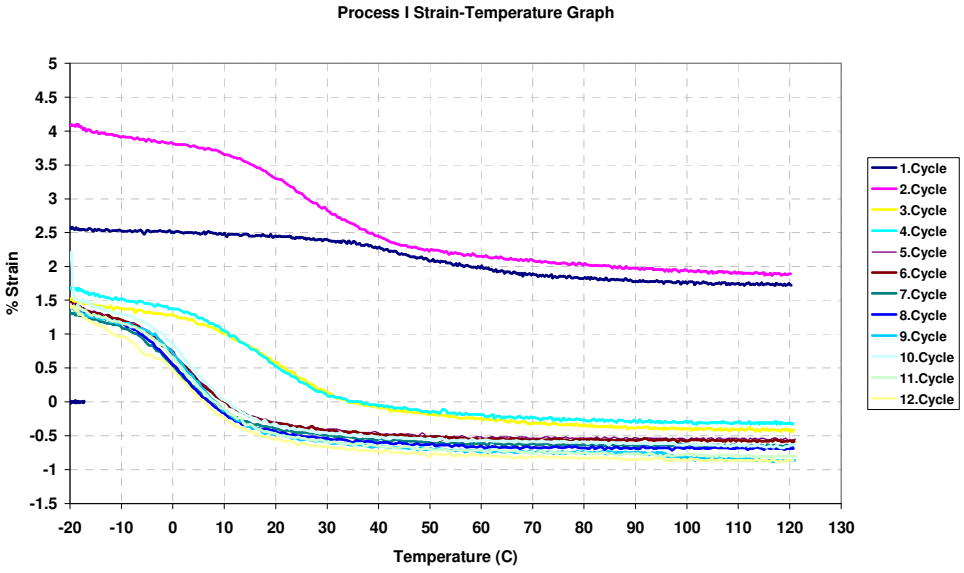
Process I Strain-Temperature Graph
% Strain
Temperature (C)
1.Cycle
2.Cycle
3.Cycle
4.Cycle
5.Cycle
6.Cycle
7.Cycle
8.Cycle
9.Cycle
10.Cycle
11.Cycle
12.Cycle

(b)

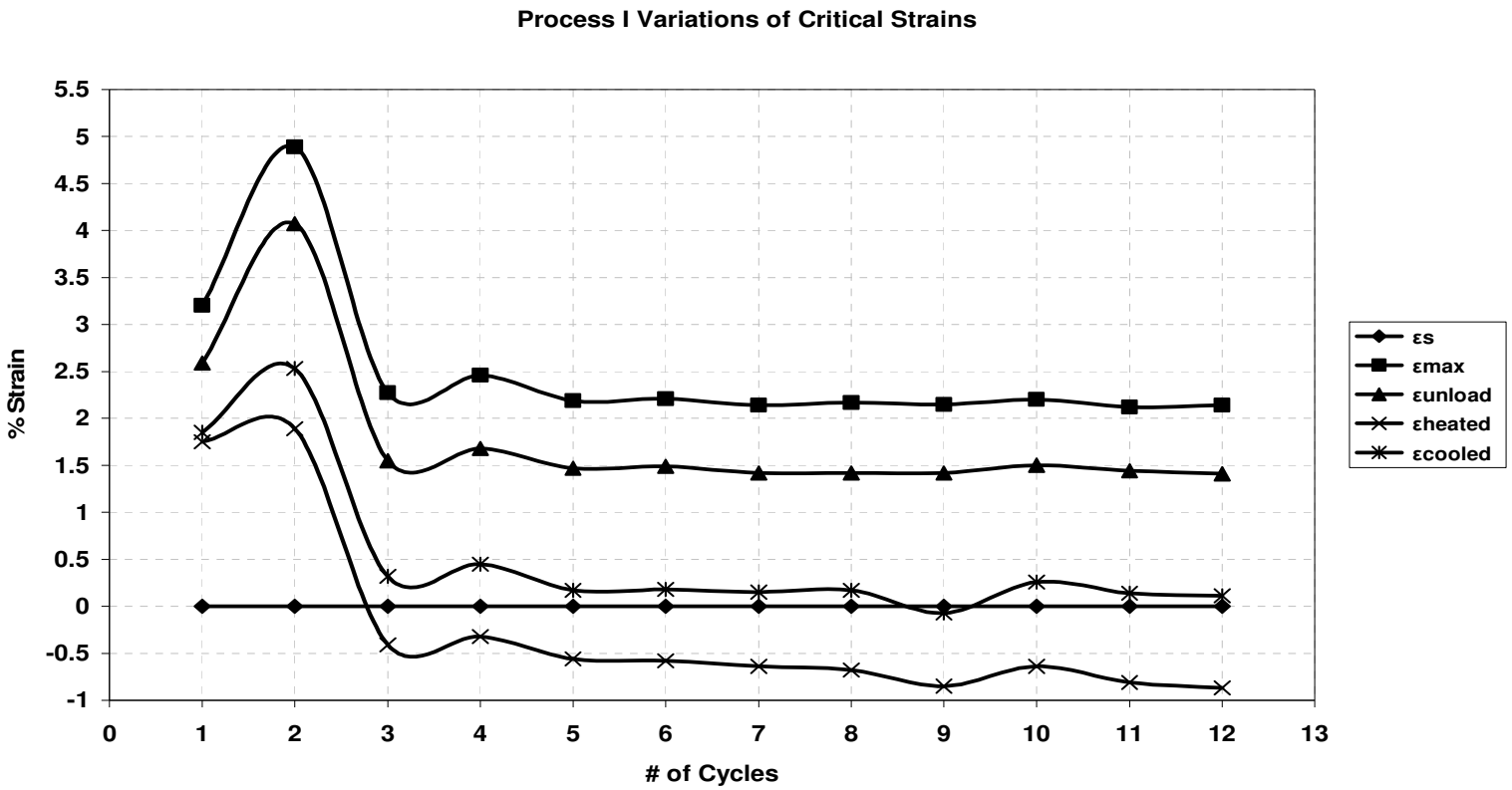

(c)

Figure 4.2.1 Type II (Constant Strain Free Recovery), test results for samples subjected to Process I and 2% strained. (a) σ-ε, (b) ε-T and (c) Critical Strains - # of cycles diagrams.


Process II Stress-Strain Graph
Stress (MPa)
% Strain
Cycle 1
Cycle 2
Cycle 3
Cycle 4
Cycle 5
Cycle 6
Cycle 7
Cycle 8
Cycle 9
Cycle 10
Cycle 11
Cycle 12

(a)

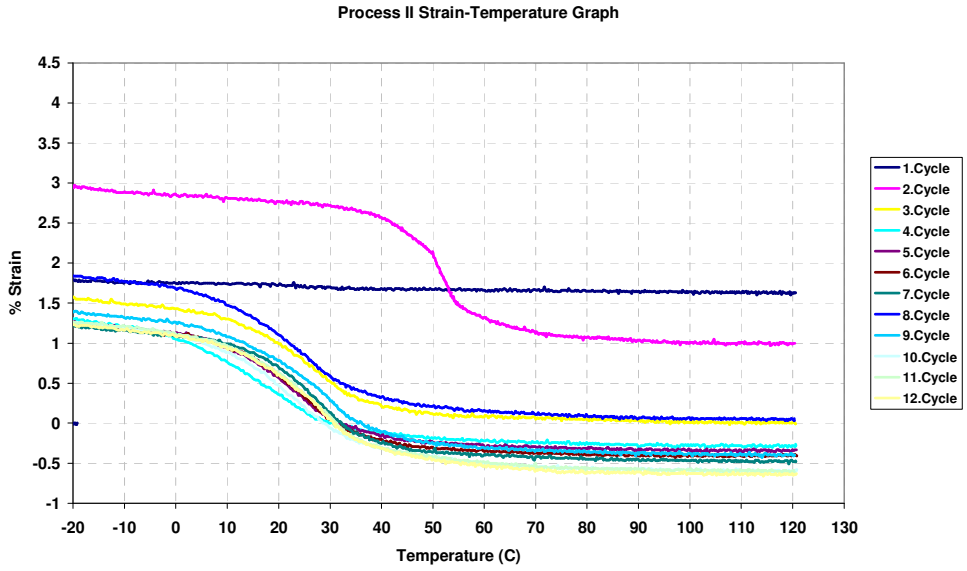
Process II Strain-Temperature Graph
% Strain
Temperature (C)
1.Cycle
2.Cycle
3.Cycle
4.Cycle
5.Cycle
6.Cycle
7.Cycle
8.Cycle
9.Cycle
10.Cycle
11.Cycle
12.Cycle

(b)

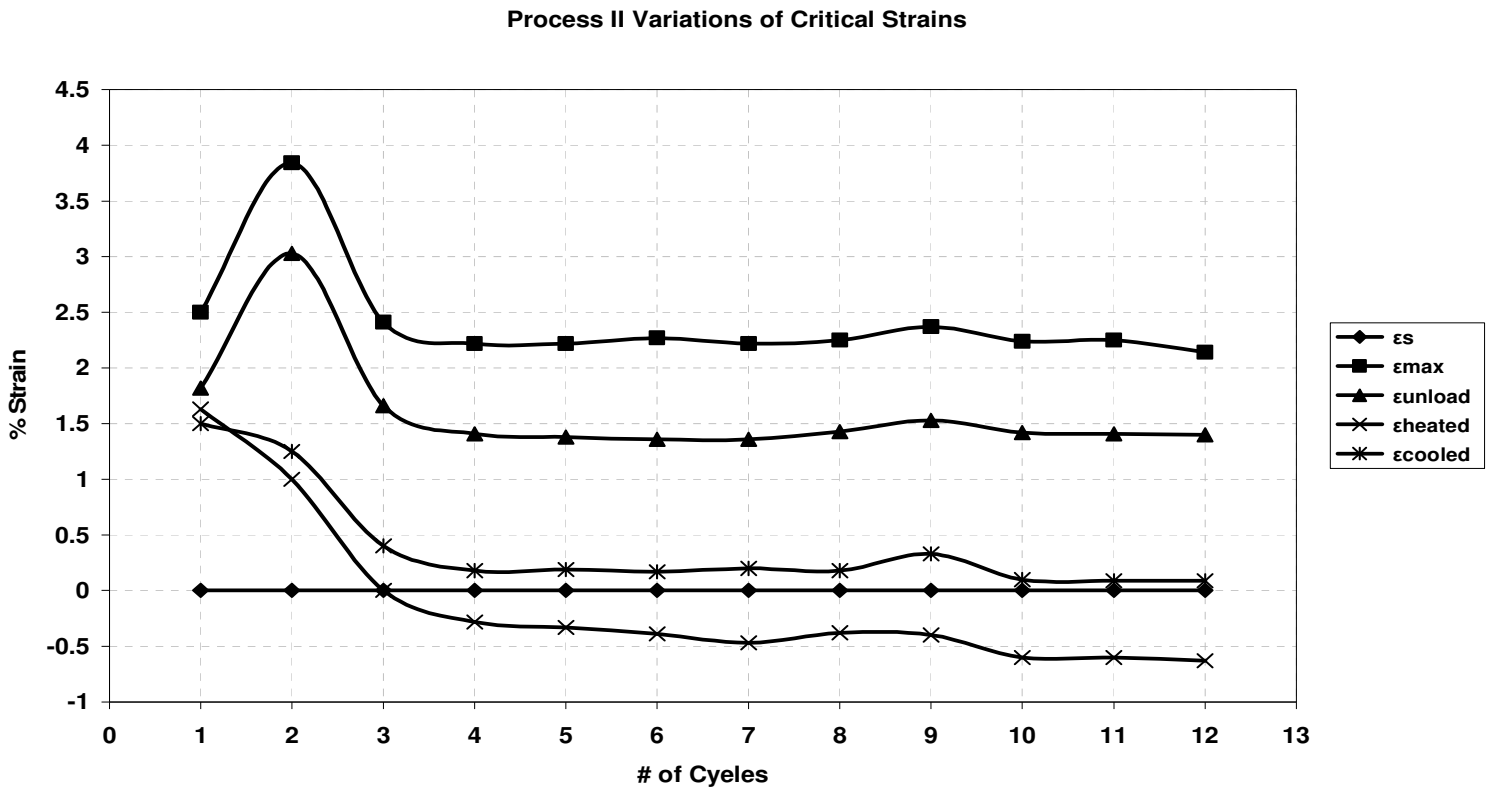

(c)

Figure 4.2.3. Type II (Constant Strain Free Recovery), test results for samples subjected to Process II and 2% strained. (a) σ-ε, (b) ε-T and (c) Critical Strains - # of cycles diagrams.

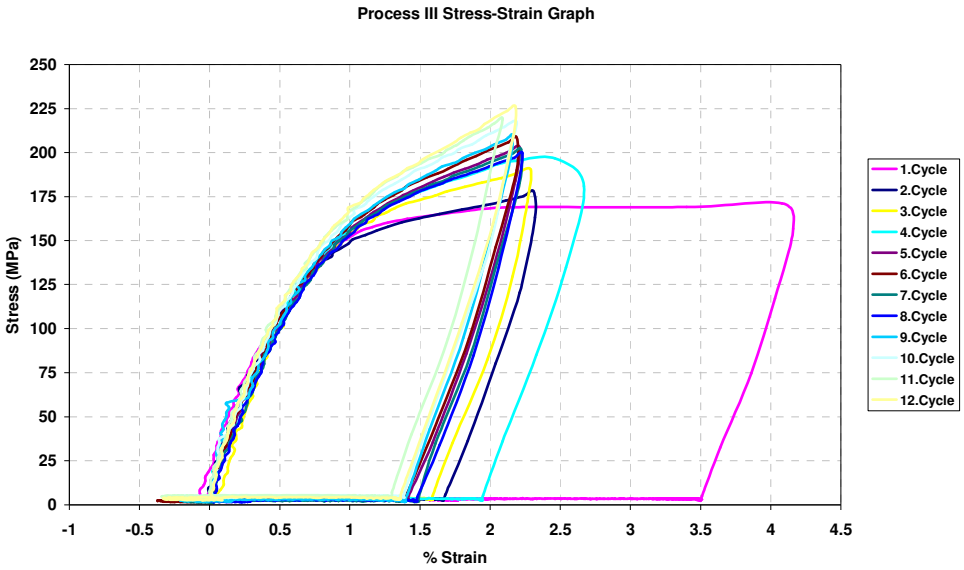
Process III Stress-Strain Graph
Stress (MPa)
% Strain
250
225
200
175
150
125
100
75
50
25
0
-1
-0.5
0
0.5
1
1.5
2
2.5
3
3.5
4
4.5
1.Cycle
2.Cycle
3.Cycle
4.Cycle
5.Cycle
6.Cycle
7.Cycle
8.Cycle
9.Cycle
10.Cycle
11.Cycle
12.Cycle

(a)

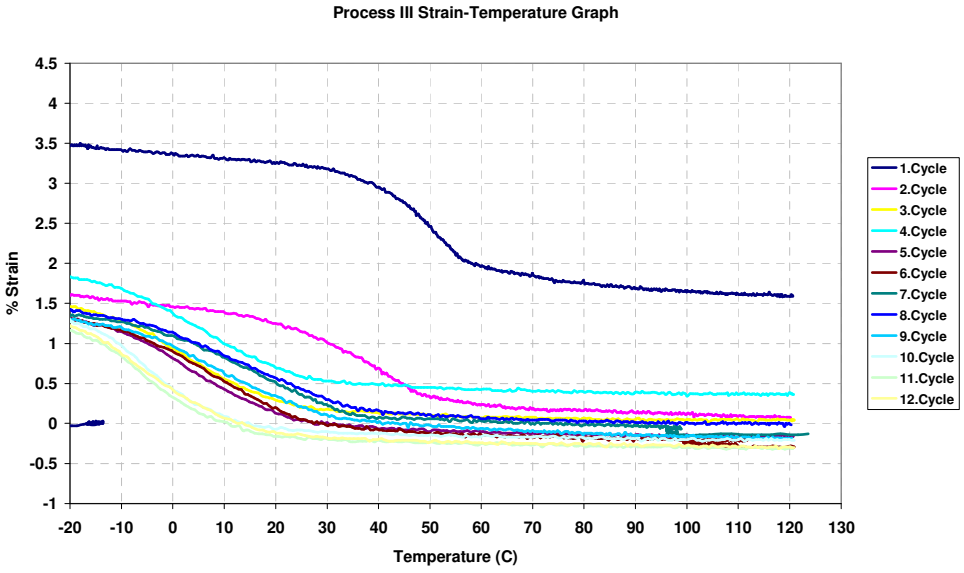
Process III Strain-Temperature Graph
% Strain
Temperature (C)
4.5
4
3.5
3
2.5
2
1.5
1
0.5
0
-0.5
-1
-20
-10
0
10
20
30
40
50
60
70
80
90
100
110
120
130
1.Cycle
2.Cycle
3.Cycle
4.Cycle
5.Cycle
6.Cycle
7.Cycle
8.Cycle
9.Cycle
10.Cycle
11.Cycle
12.Cycle

(b)

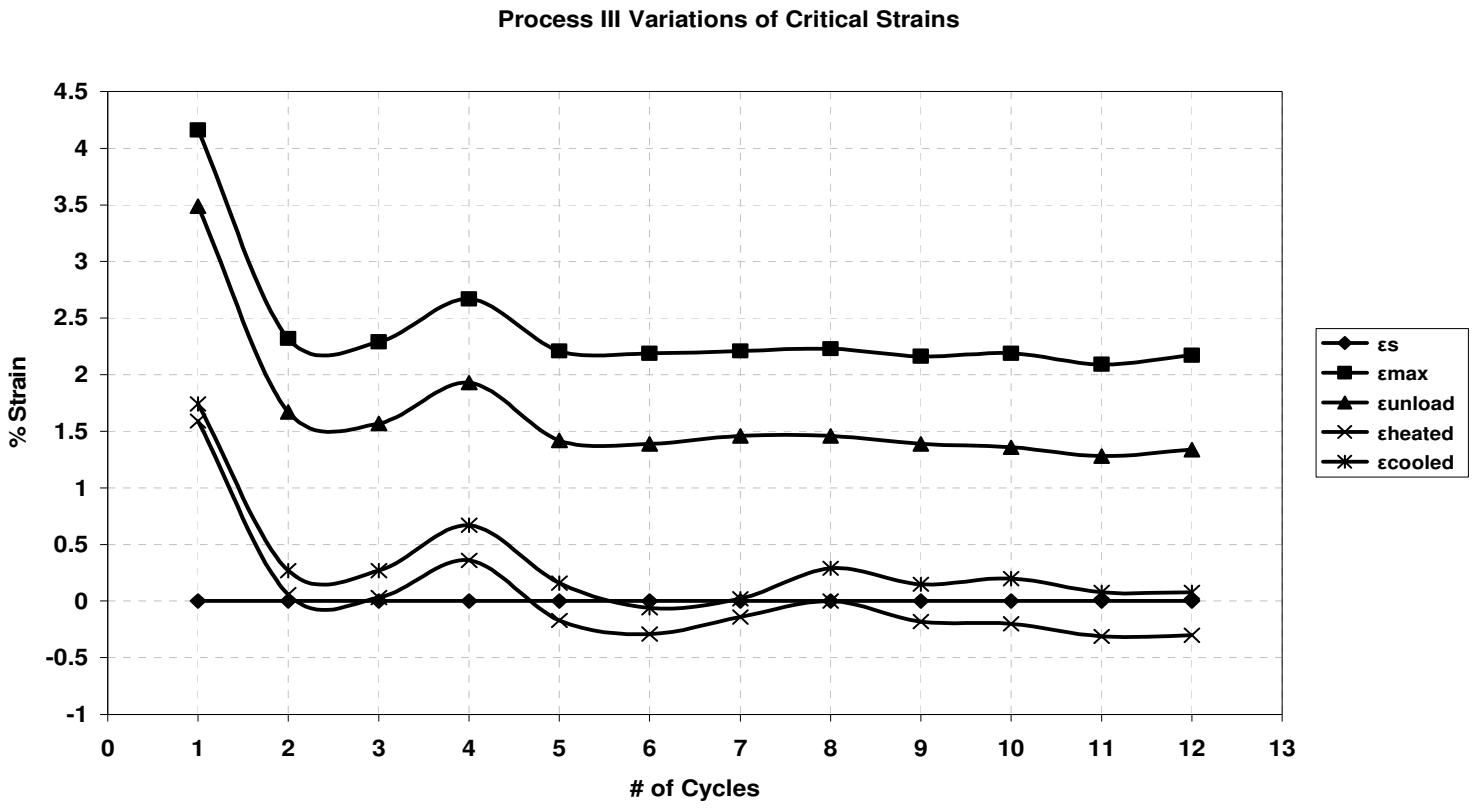

(c)

Figure 4.2.3. Type II (Constant Strain Free Recovery), test results for samples subjected to Process III and 2% strained. (a) σ-ε, (b) ε-T and (c) Critical Strains - # of cycles diagrams.

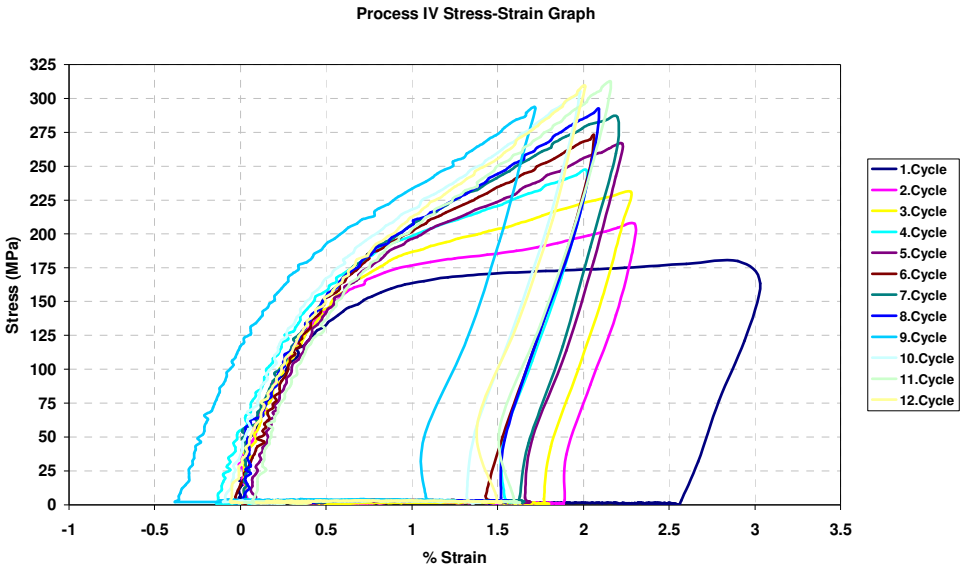
Process IV Stress-Strain Graph
Stress (MPa)
% Strain
1.Cycle
2.Cycle
3.Cycle
4.Cycle
5.Cycle
6.Cycle
7.Cycle
8.Cycle
9.Cycle
10.Cycle
11.Cycle
12.Cycle

(a)

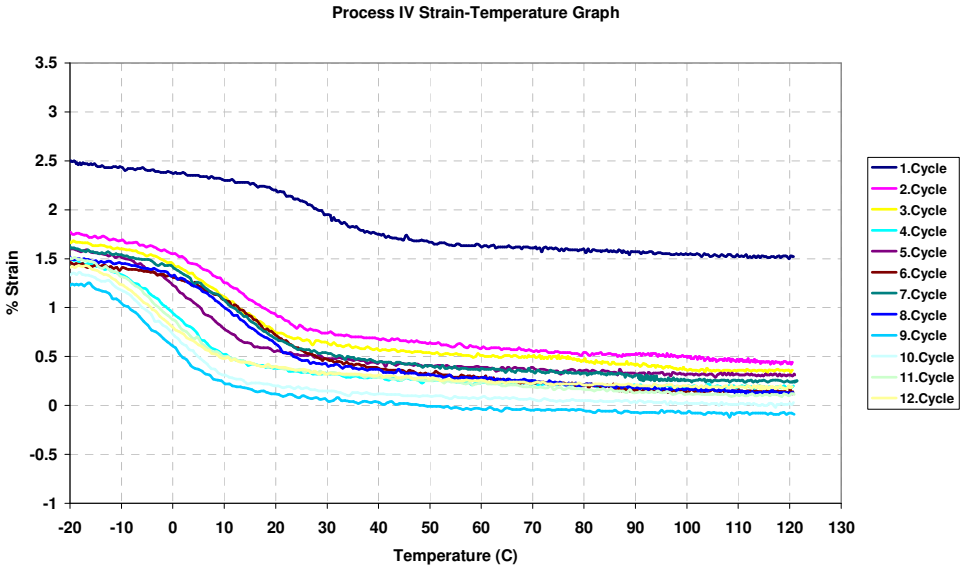
Process IV Strain-Temperature Graph
% Strain
Temperature (C)
1.Cycle
2.Cycle
3.Cycle
4.Cycle
5.Cycle
6.Cycle
7.Cycle
8.Cycle
9.Cycle
10.Cycle
11.Cycle
12.Cycle

(b)

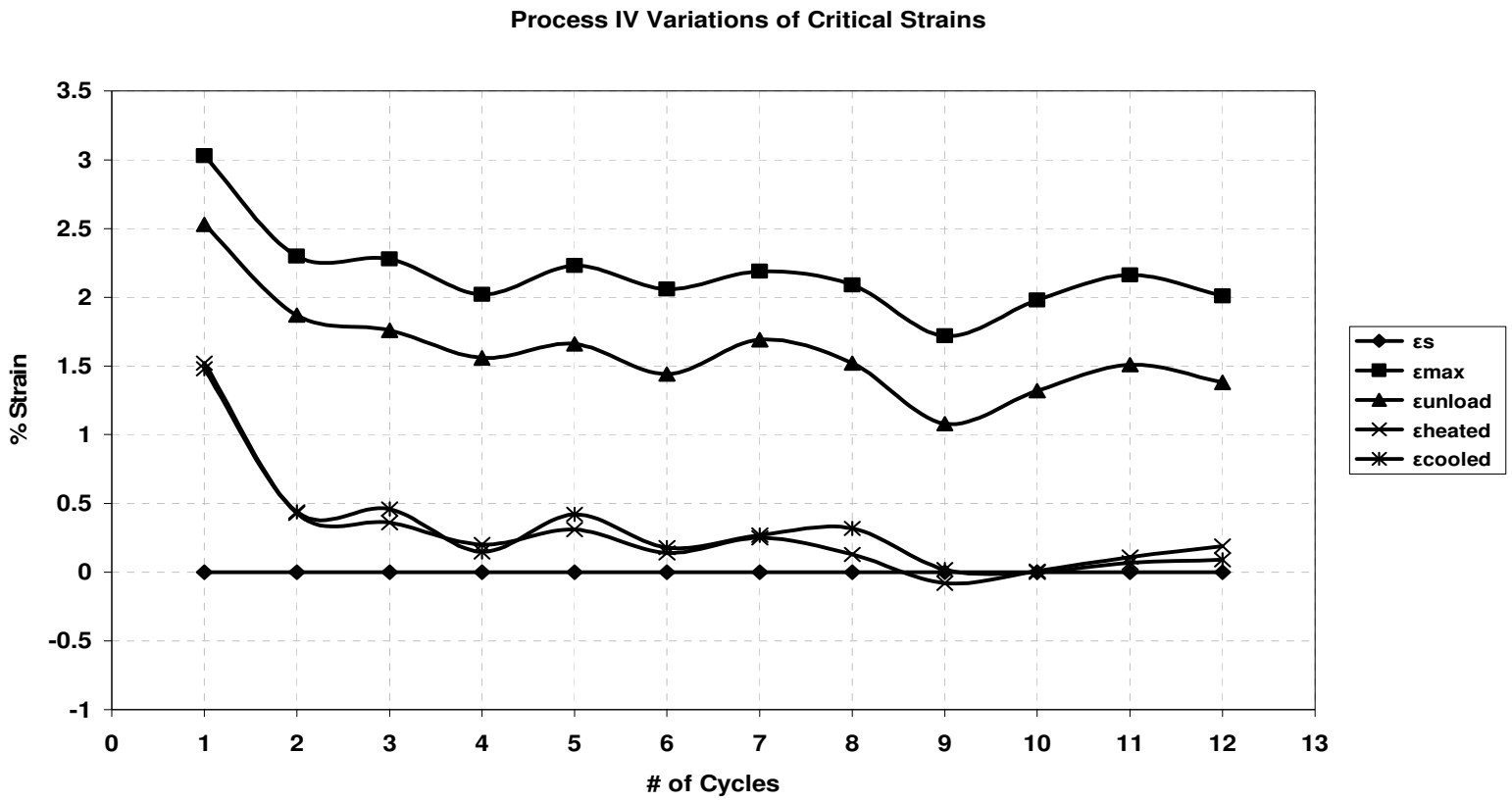

(c)

Figure 4.2.4. Type II (Constant Strain Free Recovery), test results for samples subjected to Process IV and 2% strained. (a) σ-ε, (b) ε-T and (c) Critical Strains - # of cycles diagrams

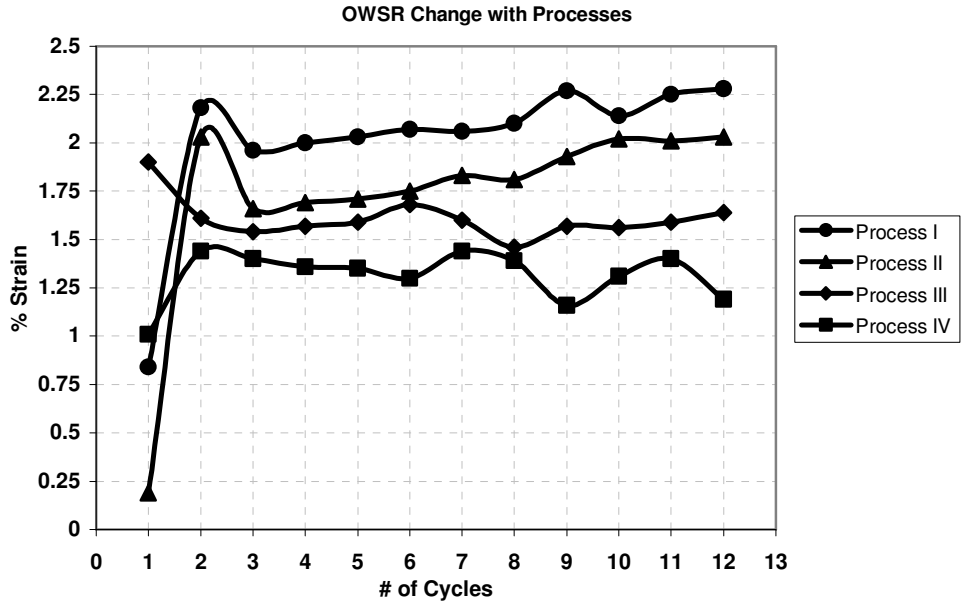

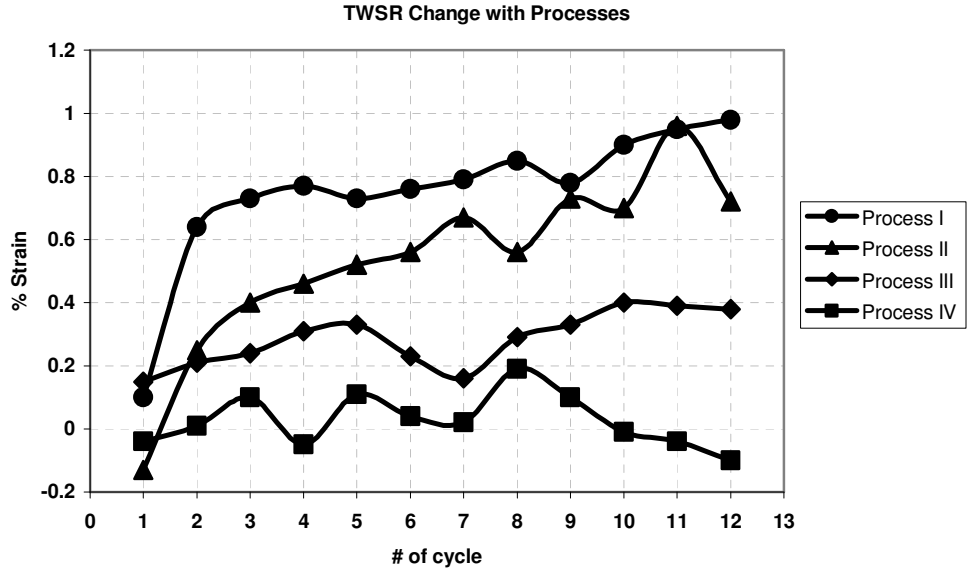

Figure 4.2.5 OWSR (a) and TWSR (b) change with processes at Constant Strain (2%) Free Recovery Test.

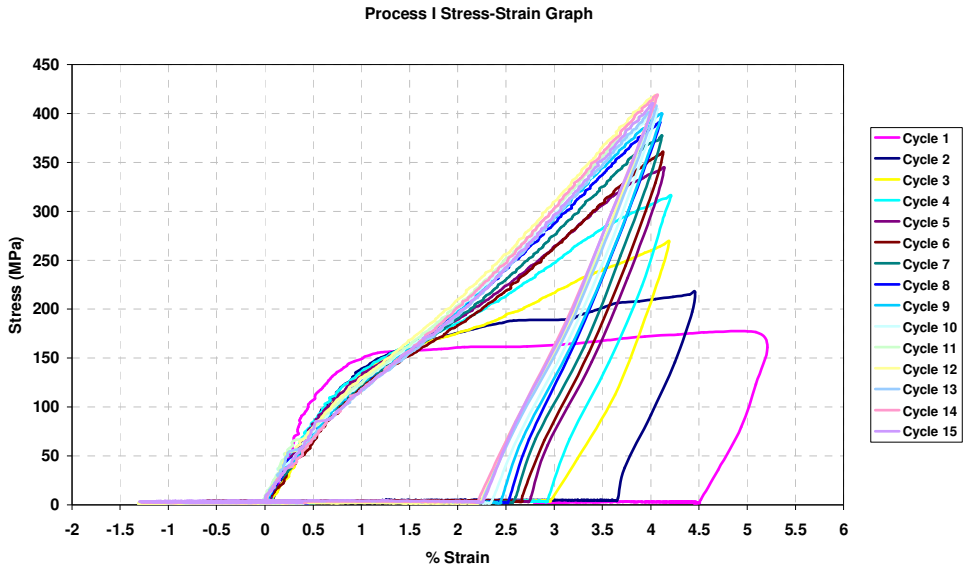
Process I Stress-Strain Graph
Stress (MPa)
% Strain
Cycle 1
Cycle 2
Cycle 3
Cycle 4
Cycle 5
Cycle 6
Cycle 7
Cycle 8
Cycle 9
Cycle 10
Cycle 11
Cycle 12
Cycle 13
Cycle 14
Cycle 15

(a)

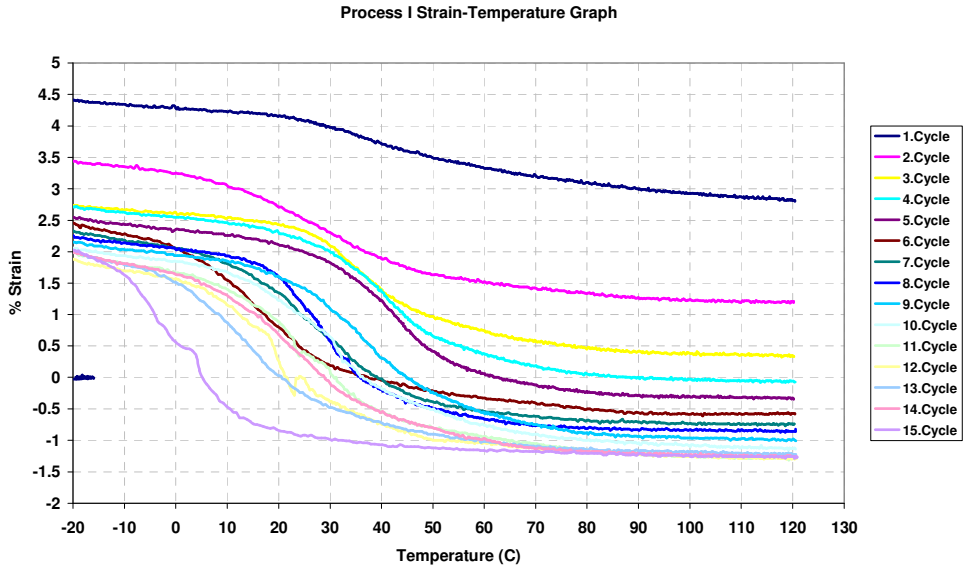
Process I Strain-Temperature Graph
% Strain
Temperature (C)
1.Cycle
2.Cycle
3.Cycle
4.Cycle
5.Cycle
6.Cycle
7.Cycle
8.Cycle
9.Cycle
10.Cycle
11.Cycle
12.Cycle
13.Cycle
14.Cycle
15.Cycle

(b)

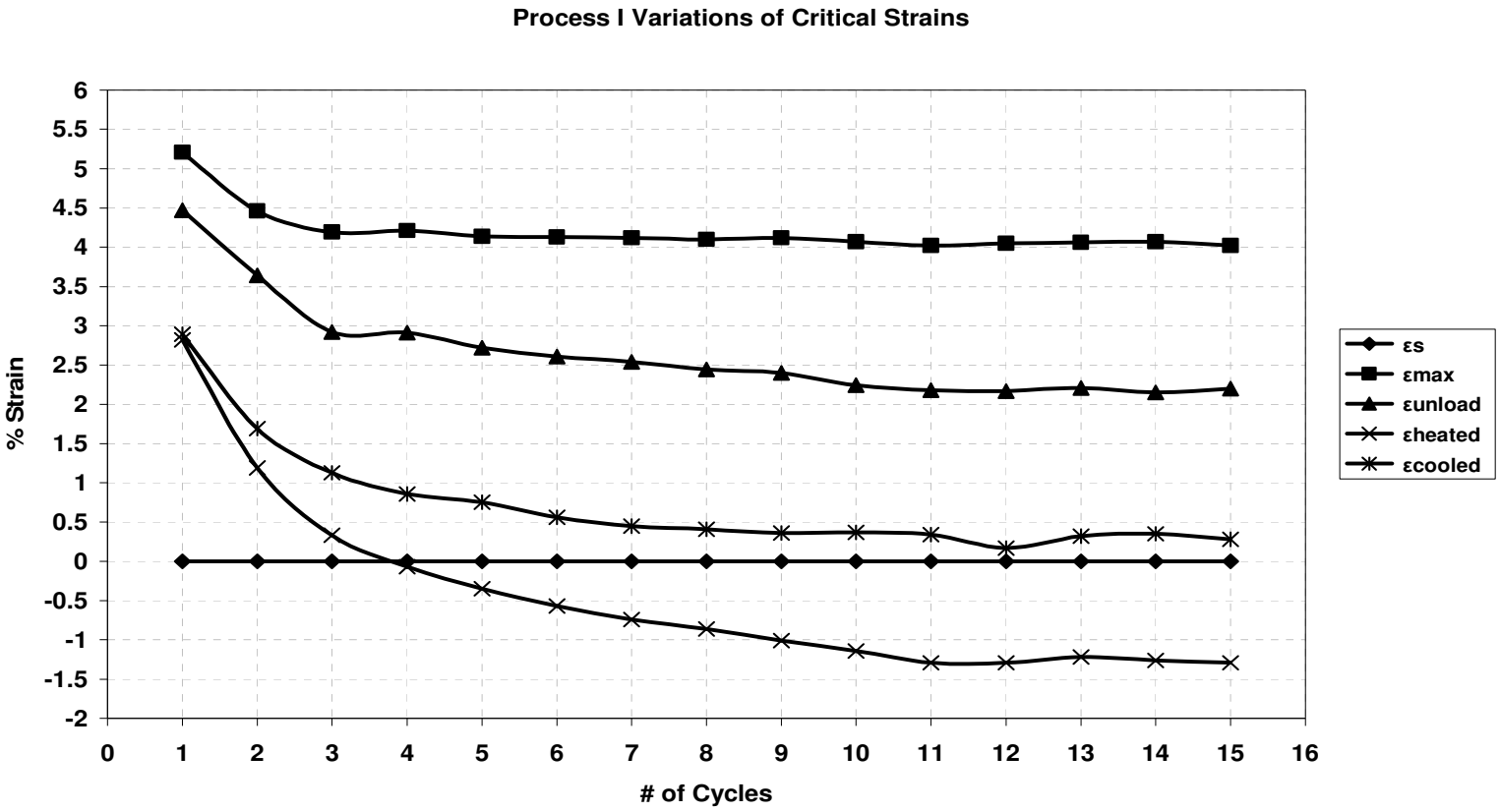

(c)

Figure 4.2.6 Type II (Constant Strain Free Recovery), test results for samples subjected to Process I and 4% strained. (a) σ-ε, (b) ε-T and (c) Critical Strains - # of cycles diagrams

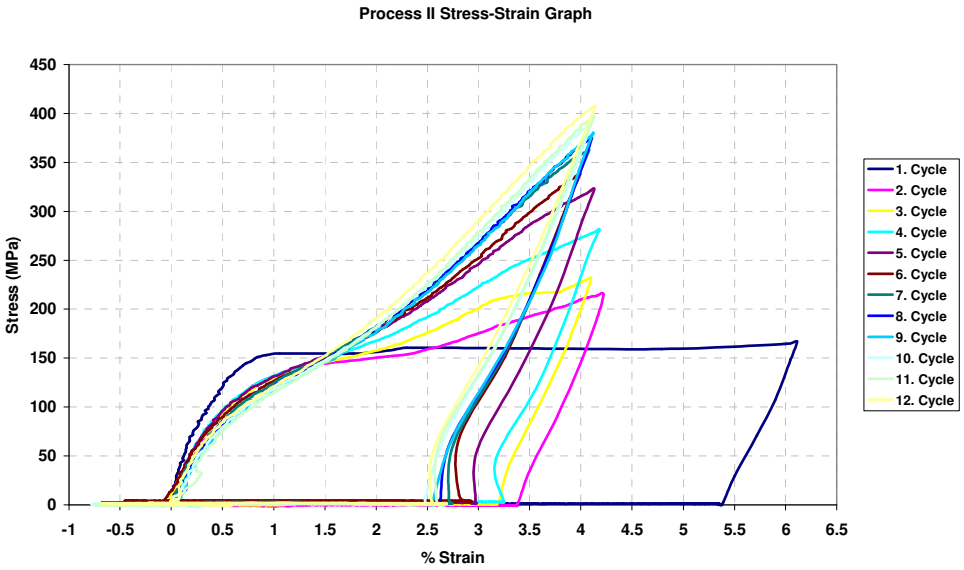
Process II Stress-Strain Graph
Stress (MPa)
% Strain
1. Cycle
2. Cycle
3. Cycle
4. Cycle
5. Cycle
6. Cycle
7. Cycle
8. Cycle
9. Cycle
10. Cycle
11. Cycle
12. Cycle

(a)

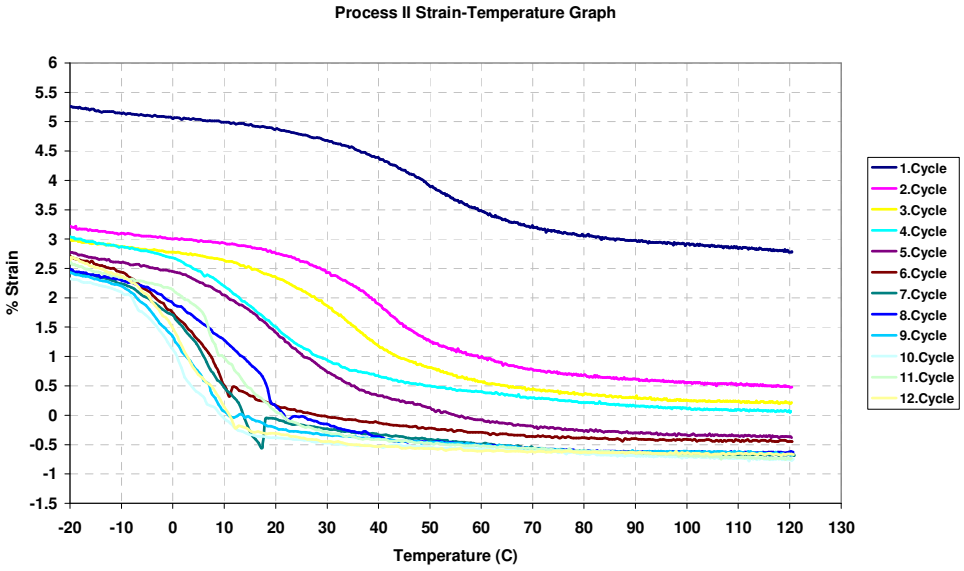
Process II Strain-Temperature Graph
% Strain
Temperature (C)
1.Cycle
2.Cycle
3.Cycle
4.Cycle
5.Cycle
6.Cycle
7.Cycle
8.Cycle
9.Cycle
10.Cycle
11.Cycle
12.Cycle

(b)

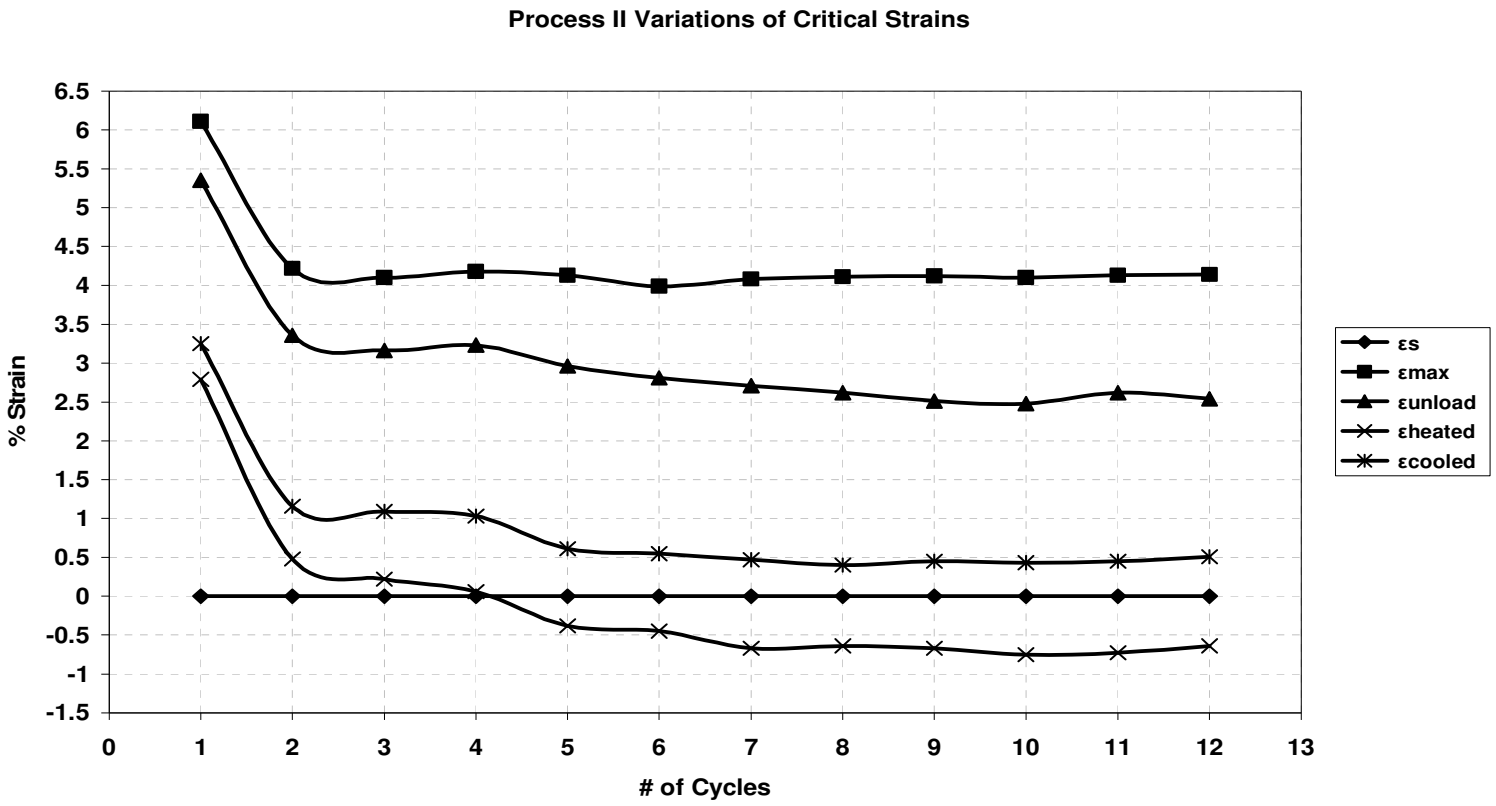

(c)

Figure 4.2.7 Type II (Constant Strain Free Recovery), test results for samples subjected to Process II and 4% strained. (a) σ-ε, (b) ε-T and (c) Critical Strains - # of cycles diagrams

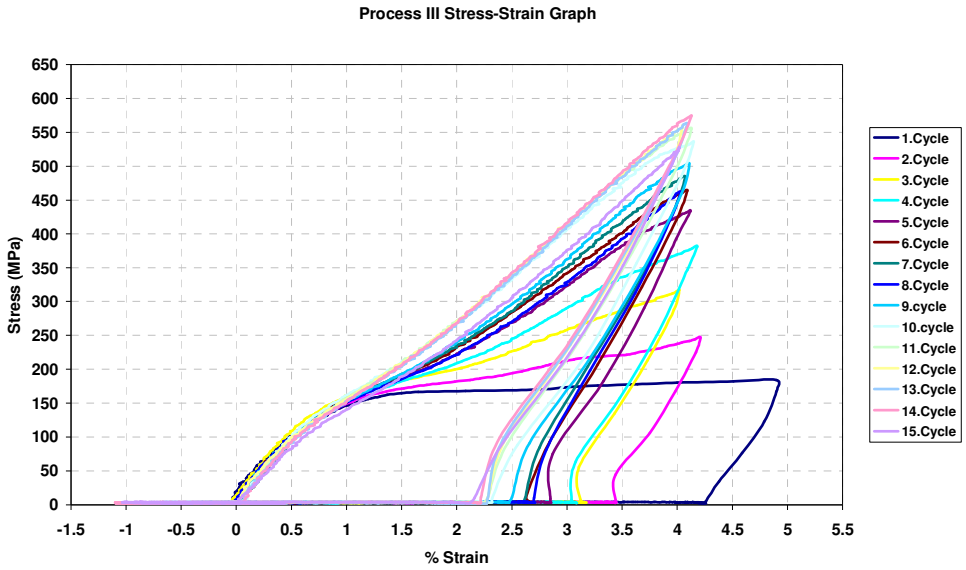
Process III Stress-Strain Graph
Stress (MPa)
650
600
550
500
450
400
350
300
250
200
150
100
50
0
-1.5
-1
-0.5
0
0.5
1
1.5
2
2.5
3
3.5
4
4.5
5
5.5
% Strain
1.Cycle
2.Cycle
3.Cycle
4.Cycle
5.Cycle
6.Cycle
7.Cycle
8.Cycle
9.cycle
10.cycle
11.Cycle
12.Cycle
13.Cycle
14.Cycle
15.Cycle

(a)

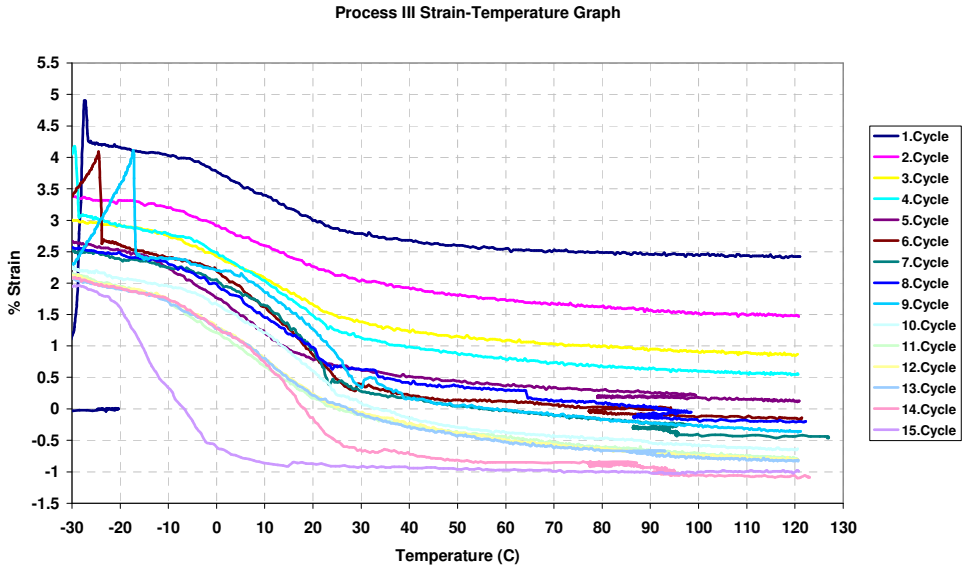
Process III Strain-Temperature Graph
% Strain
5.5
5
4.5
4
3.5
3
2.5
2
1.5
1
0.5
0
-0.5
-1
-1.5
-30
-20
-10
0
10
20
30
40
50
60
70
80
90
100
110
120
130
Temperature (C)
1.Cycle
2.Cycle
3.Cycle
4.Cycle
5.Cycle
6.Cycle
7.Cycle
8.Cycle
9.Cycle
10.Cycle
11.Cycle
12.Cycle
13.Cycle
14.Cycle
15.Cycle

(b)

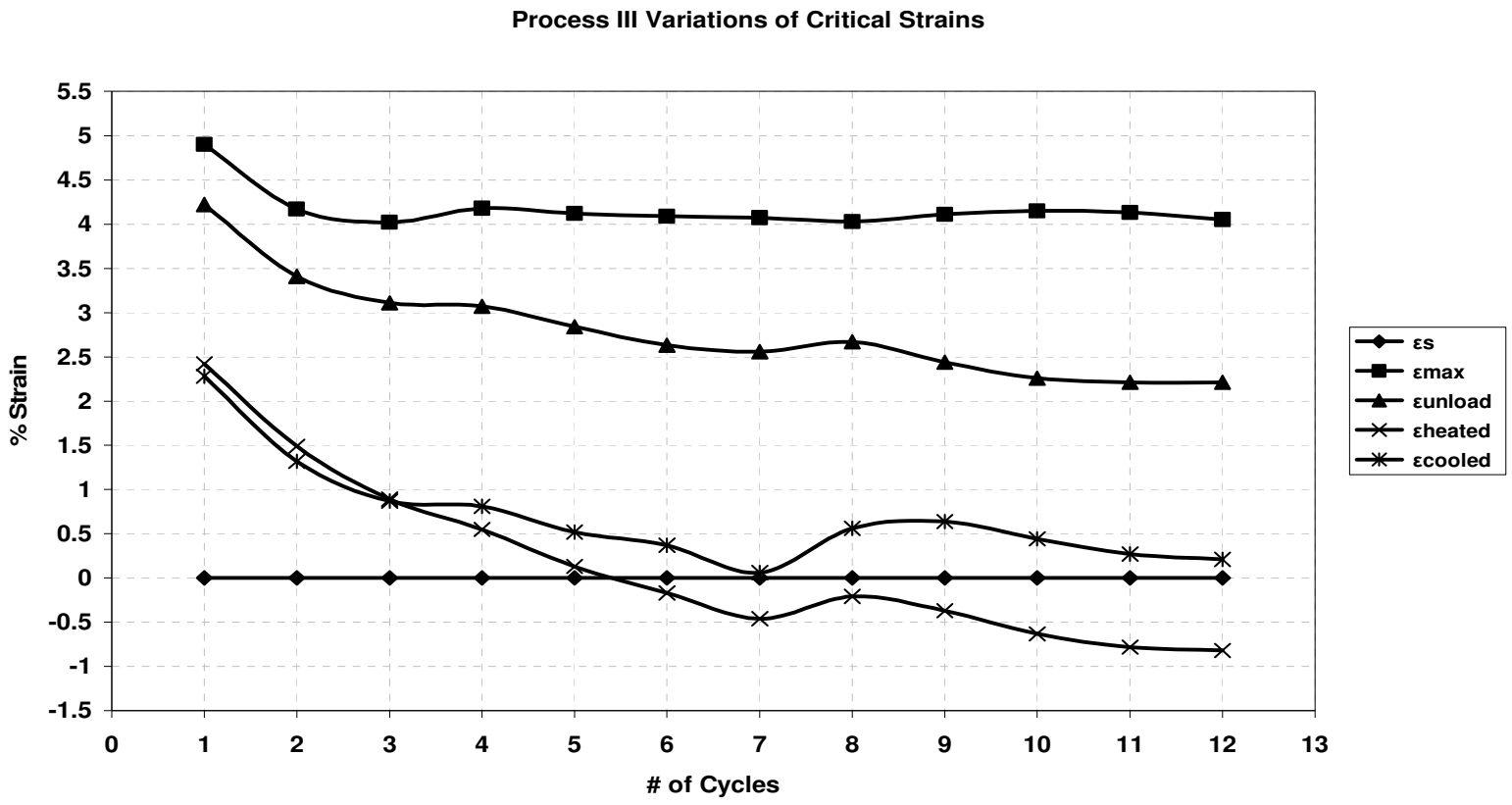

(c)

Figure 4.2.8 Type II (Constant Strain Free Recovery), test results for samples subjected to Process III and 4% strained. (a) σ-ε, (b) ε-T and (c) Critical Strains - # of cycles diagrams

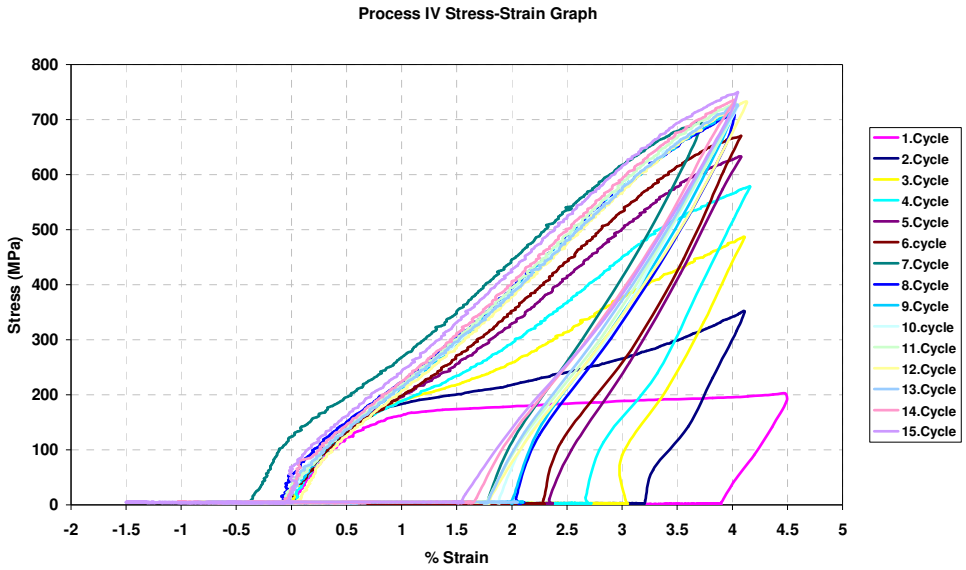
Process IV Stress-Strain Graph
Stress (MPa)
% Strain
800
700
600
500
400
300
200
100
0
-2
-1.5
-1
-0.5
0
0.5
1
1.5
2
2.5
3
3.5
4
4.5
5
1.Cycle
2.Cycle
3.Cycle
4.Cycle
5.Cycle
6.cycle
7.Cycle
8.Cycle
9.Cycle
10.cycle
11.Cycle
12.Cycle
13.Cycle
14.Cycle
15.Cycle

(a)

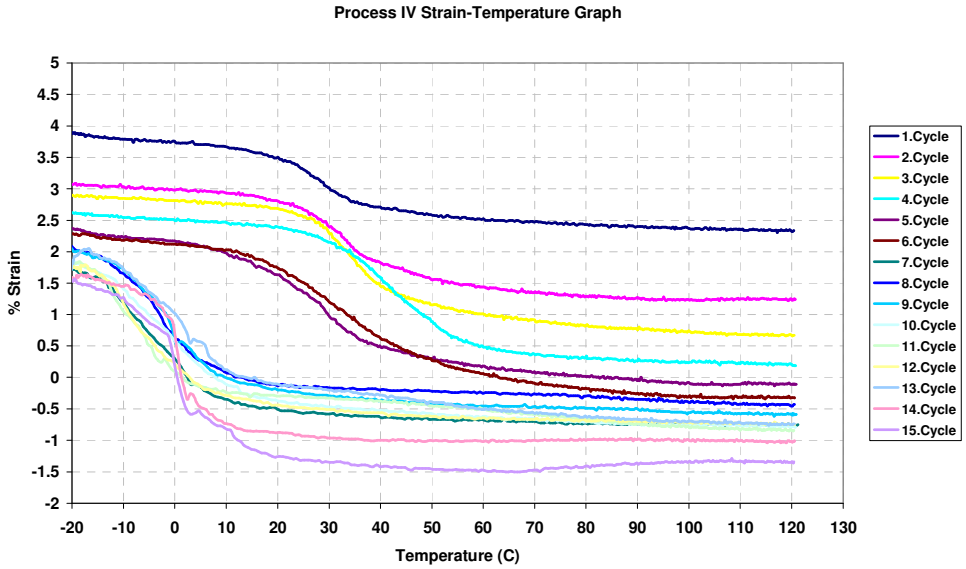
Process IV Strain-Temperature Graph
% Strain
Temperature (C)
5
4.5
4
3.5
3
2.5
2
1.5
1
0.5
0
-0.5
-1
-1.5
-2
-20
-10
0
10
20
30
40
50
60
70
80
90
100
110
120
130
1.Cycle
2.Cycle
3.Cycle
4.Cycle
5.Cycle
6.Cycle
7.Cycle
8.Cycle
9.Cycle
10.Cycle
11.Cycle
12.Cycle
13.Cycle
14.Cycle
15.Cycle

(b)

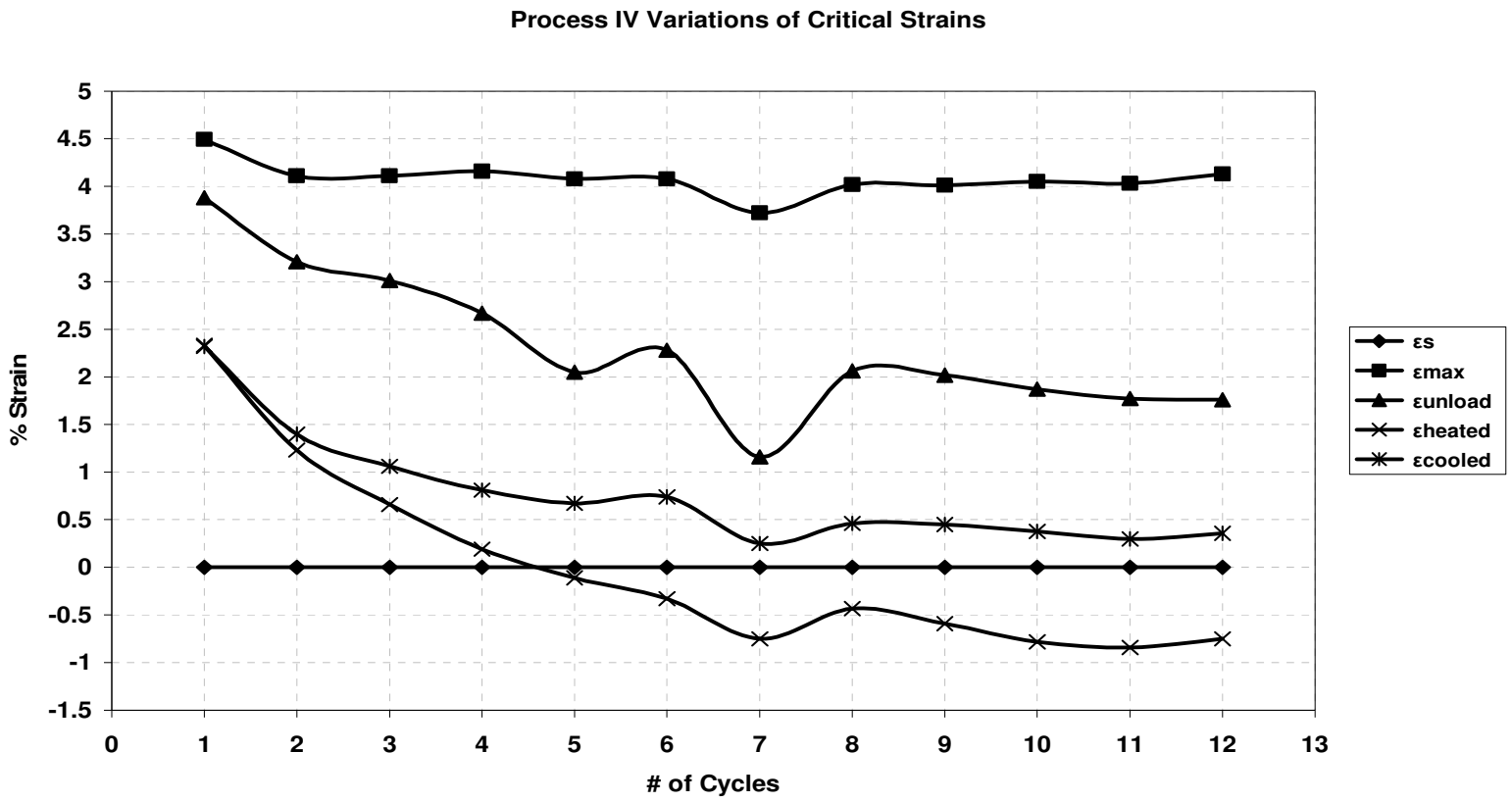

(c)

Figure 4.2.9 Type II (Constant Strain Free Recovery), test results for samples subjected to Process IV and 4% strained. (a) σ-ε, (b) ε-T and (c) Critical Strains - # of cycles diagrams.

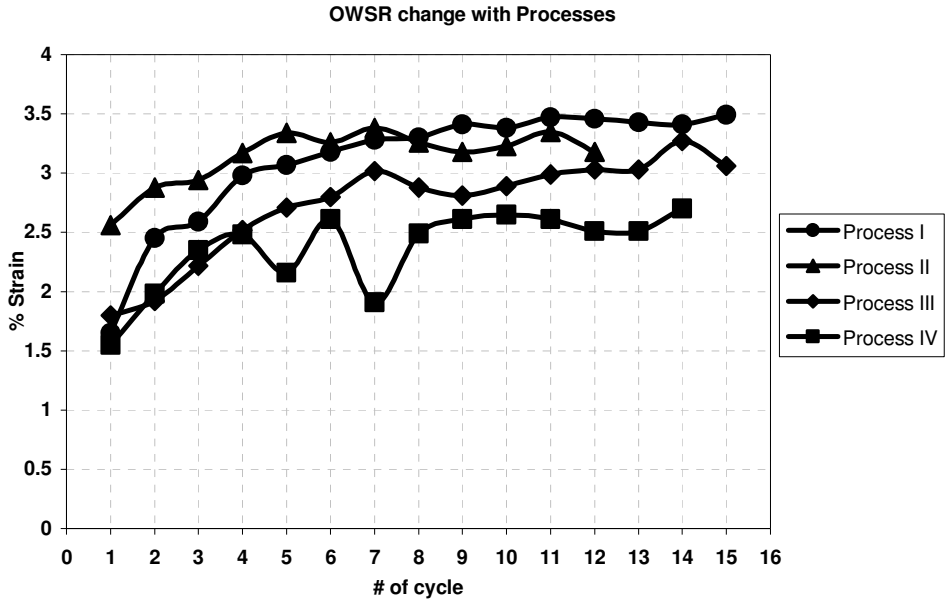

(a)

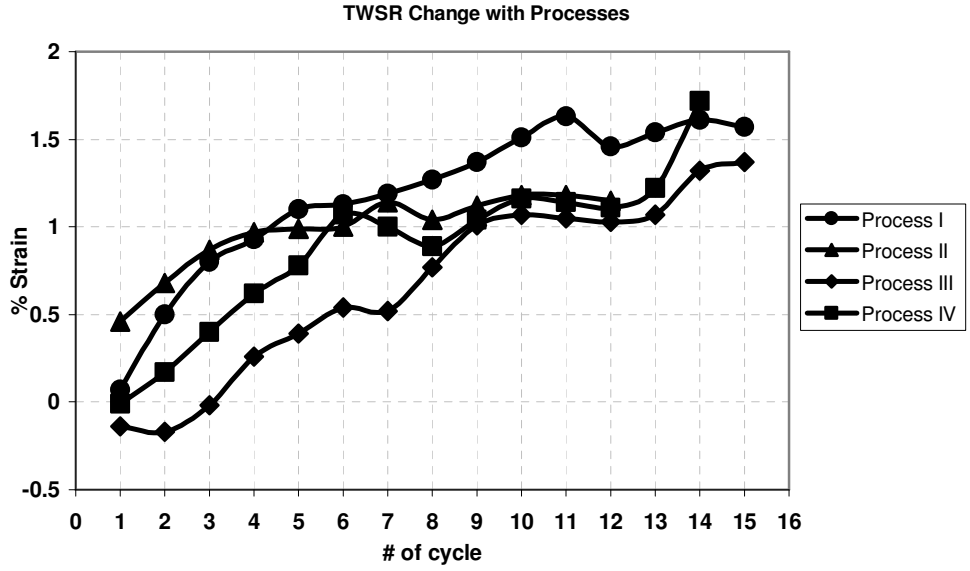

(b)

Figure 4.2.10 OWSR (a) and TWSR (b) change with processes at Constant Strain (4%) Free Recovery test.

4.3 Type III (Constant Strain Constrained Recovery) Test

Constant strain constrained recovery test were done by deforming by a constant predetermined stress, unloading and then fixing the position at the obtained permanent strain prior to heating. Due to the difference in the strength, as mentioned previously, samples subjected to processes I and II were stressed to 310 Mpa, 20 % cold worked samples to 350 Mpa and 40% cold worked samples to 400 Mpa. Main concern of this type of experiment was to observe the recovery force generation during heating by fixing the specimen dimensions after deformation. With different treated specimens effect of heat treatment and cold working on recovery force generation are observed. From Figure 4.3.1 to Figure 4.3.4 σ-ε and σ-T graphs of selected cycles are given.

As in the previous experiments, constant stress plateau that appears after elastic deformation in the first cycle disappears with cycling. Increase of the maximum recovery force developed upon heating the samples with cycles for all four types of heat treatments is the common feature as can bee seen from Figure 4.3.5. The characteristic feature for the first two heat treatments is that the recovery force instantaneously rises from zero to almost a steady value at a transformation start temperature and exhibit only a very gradual increase with temperature during the first cycle. This unexpected behavior resembles burst martensitic transformations in some alloy steels, which is attributed to inducing of martensite plates by the previously formed ones and known as autocatalytic effect in martensite terminology. It is interesting because burst martensites are quite rare and always partial (few tens percent of the total transformation contrary to almost 100 % observed in the present case) as precursor of the athermal martensitic transformation. With further cycling while the initial recovery force at the starting temperature decreases, the maximum recovery force approaches to a stabilized value. The transformation start temperature varies unpredictably from cycle to cycle in a 20 ˚C range, which also seems to support the burst martensite mechanism. In the cold worked specimens, on the other hand, for all cycles

starting from the first, after a quite limited burst recovery force gradually increases to the maximum value with temperature. The much smaller initial instantaneous recovery stress (burst) in the cold worked samples and its decrease with cycling indicates that presence of dislocations with their own random stress field impede stress induced martensite formation.

Effect of cycling on the maximum recovery stress and on its fraction with respect to the maximum stress applied in each cycle is given in Figure 4.3.5. Apart from the increase of the recovery stress with cycling one can also conclude that recovery stress increases in the reverse order, i.e., from process IV to Process I. But since the experiment has not been repeated at different initial deformation stresses, it is difficult to judge whether the higher recovery stress of the cold worked samples is due to their microstructure or the higher level of the initially applied stress. To clarify this point the fractional recovery stress, i.e., the ratio of the recovery stress to the initial applied stress, is plotted as a function of the cycles in Figure 4.3.5, but any reasonable conclusion could not be reached.

Process I

1. Cycle

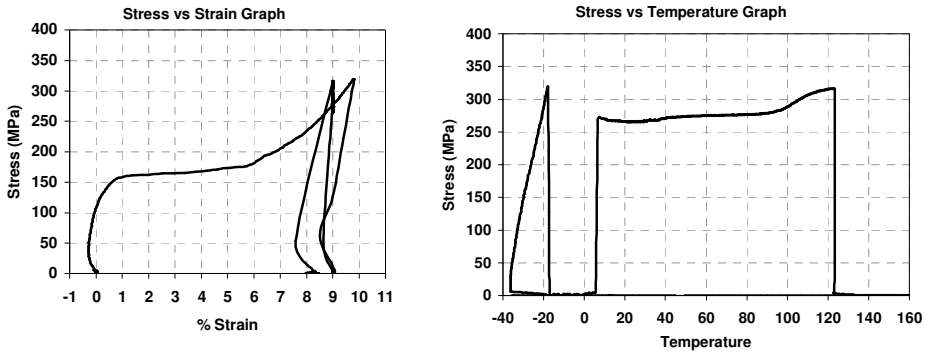

3. Cycle

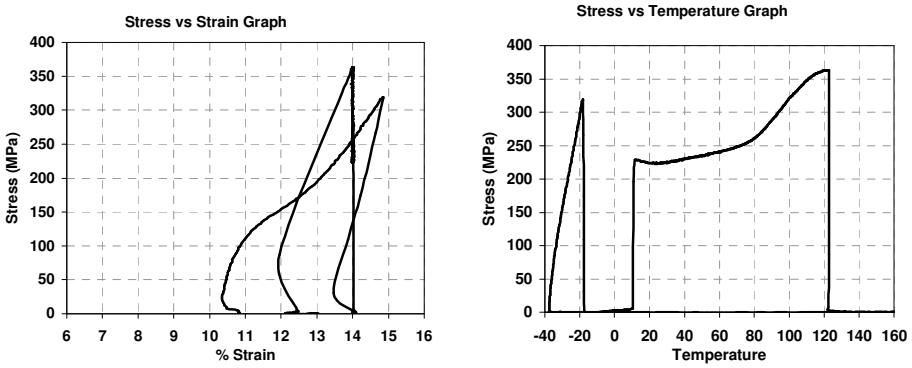

5. Cycle

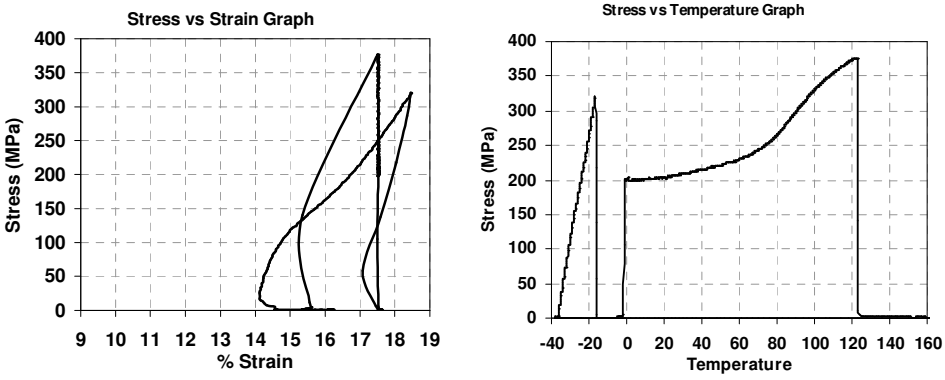

Figure 4.3.1 Stress-strain and Strain Temperature graphs of selected cycles for Constant Strain Constrained Recovery test for specimens subjected to Process I.

Process II

1. Cycle

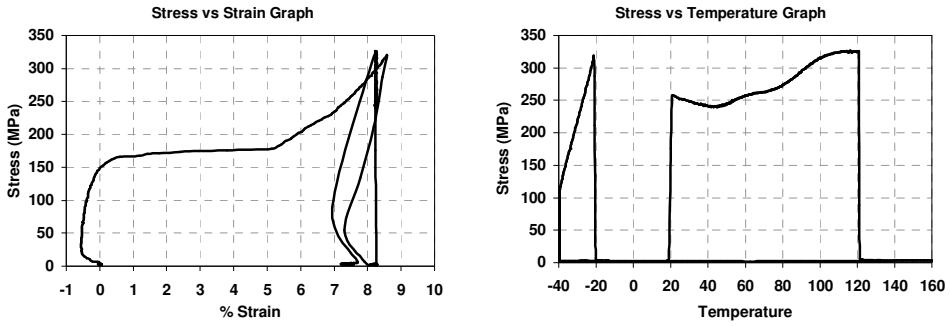

3. Cycle

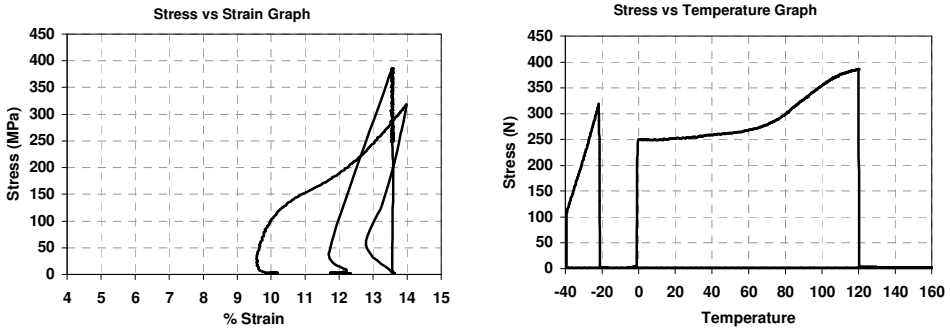

5. Cycle

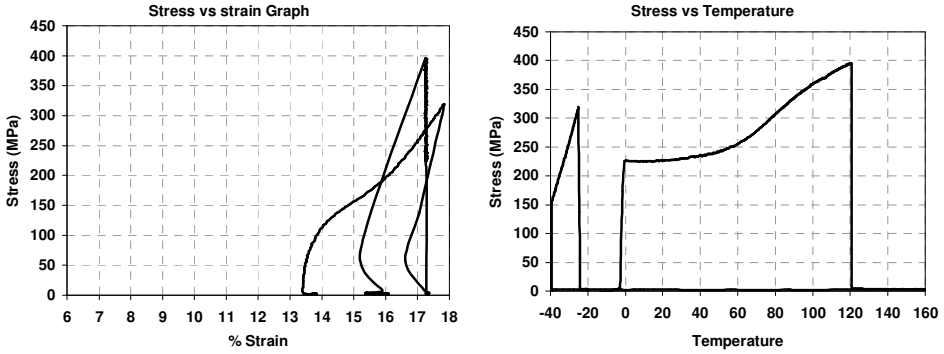

Figure 4.3.2 Stress-strain and Strain Temperature graphs of selected cycles for Constant Strain Constrained Recovery test for specimens subjected to Process II.

Process III

1. Cycle

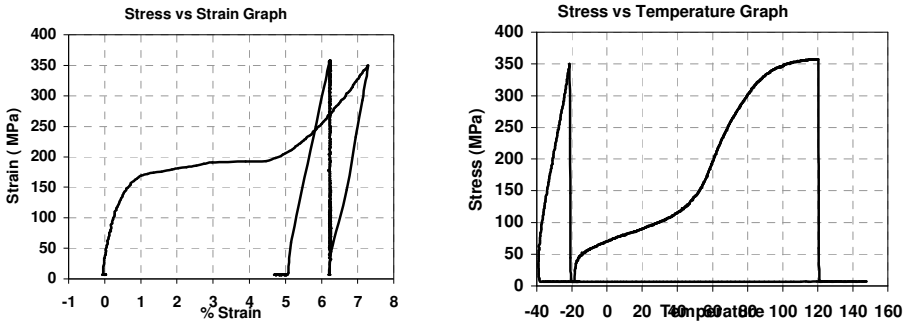

3. Cycle

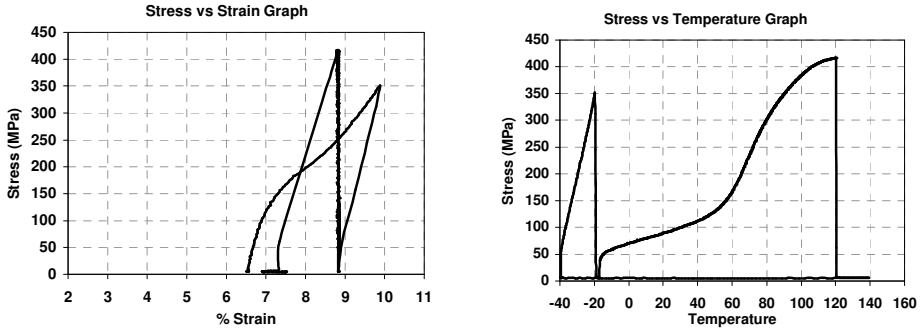

5. Cycle

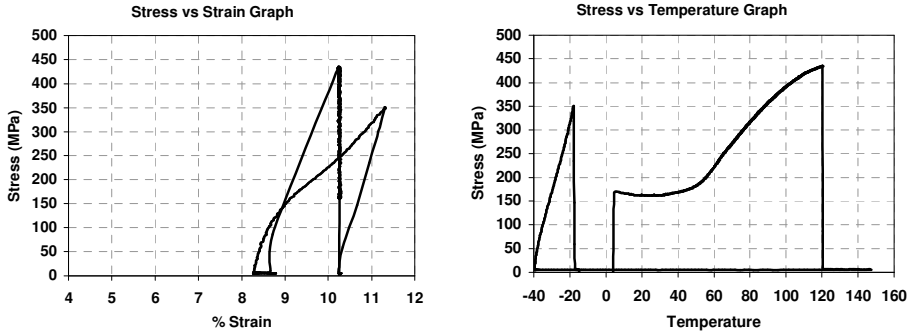

Figure 4.3.3 Stress-strain and Strain Temperature graphs of selected cycles for Constant Strain Constrained Recovery test for specimens subjected to Process III.

Process IV

1. Cycle

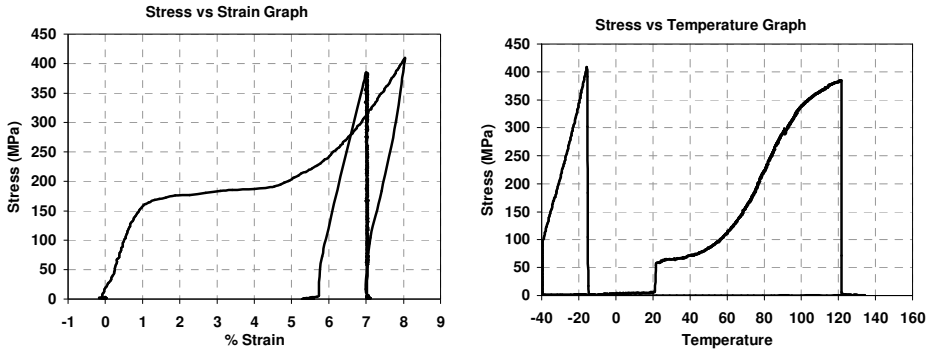

3. Cycle

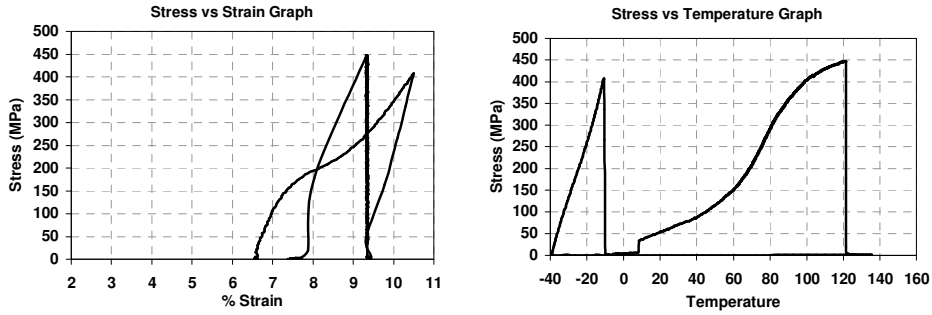

5. Cycle

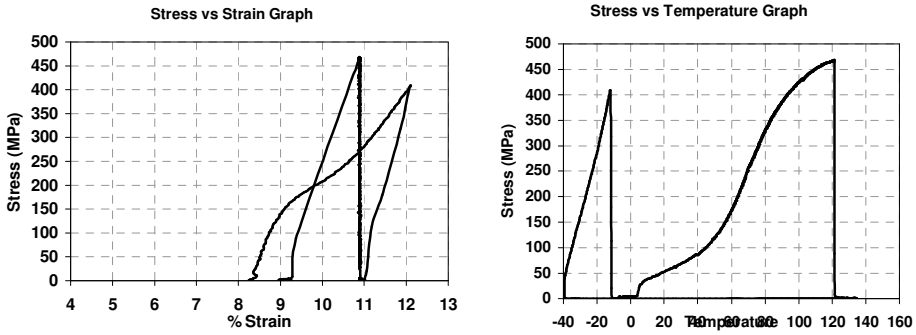

Figure 4.3.4 Stress-strain and Strain Temperature graphs of selected cycles for Constant Strain Constrained Recovery test for specimens subjected to Process IV.

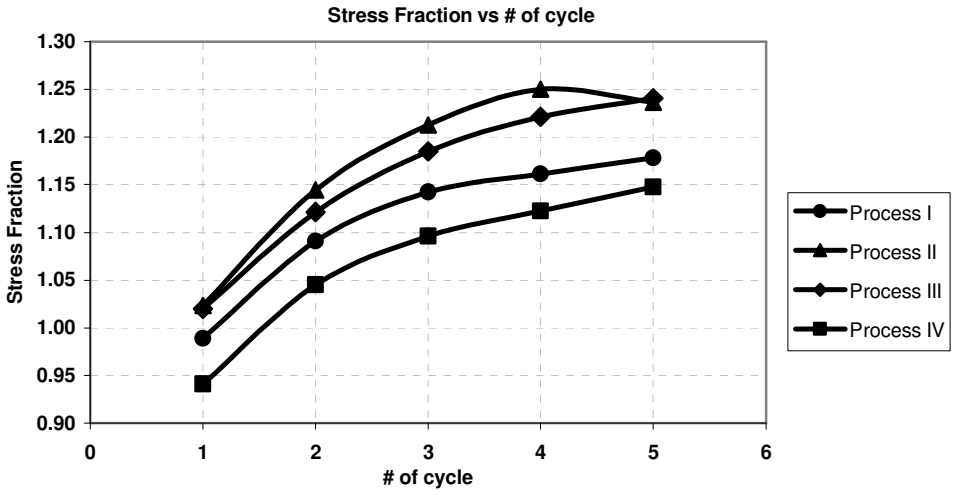

(a)

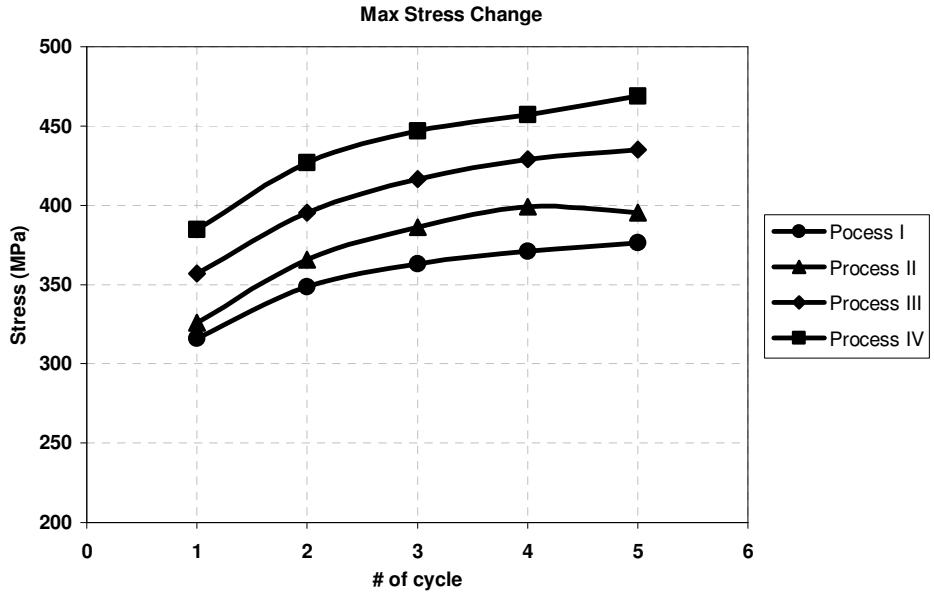

(b)

Figure 4.3.5 (a) Stress Fraction and (b) Max Stress change with cycling for all four processes.

4.4 Type IV (Constant Stress Constrained Recovery) Test

Results of Constant Stress Constrained Recovery tests for samples subjected to Process I, II, III and IV are shown in Figures 4.4.1 to 4.4.4, respectively, as (a) σ-ε, (b) ε-T and (c) Critical Strains Change - # of cycles diagrams. Test was done by heating the deformed shape memory wire under a bias stress equal to 0.6 of the deformation stress. One way shape recovery characteristics under bias load and the effect of cycling and different thermal treatments was the main concern of these tests.

From σ-ε graphs of all four different treatments it can be seen that recovery under bias load improves with cycling. The recovery under bias load, as expected, is found to be about 40% lower than in free recovery. Different than in free recovery, under bias load specimens subjected to Process II exhibit better recovery than Process I and also recovery of specimens subjected to Process III is unusually high. While an account for the former observation requires further microstructrural study, the later may be resulting from an experimental error.

Decrease of A_s temperatures with cycle, but not as much as constant stress free recovery test, can be observed from ε-T graphs. In addition, A_s temperatures are higher than that in free recovery tests. This indicates that applied stress during transformation increases the transformation temperatures.

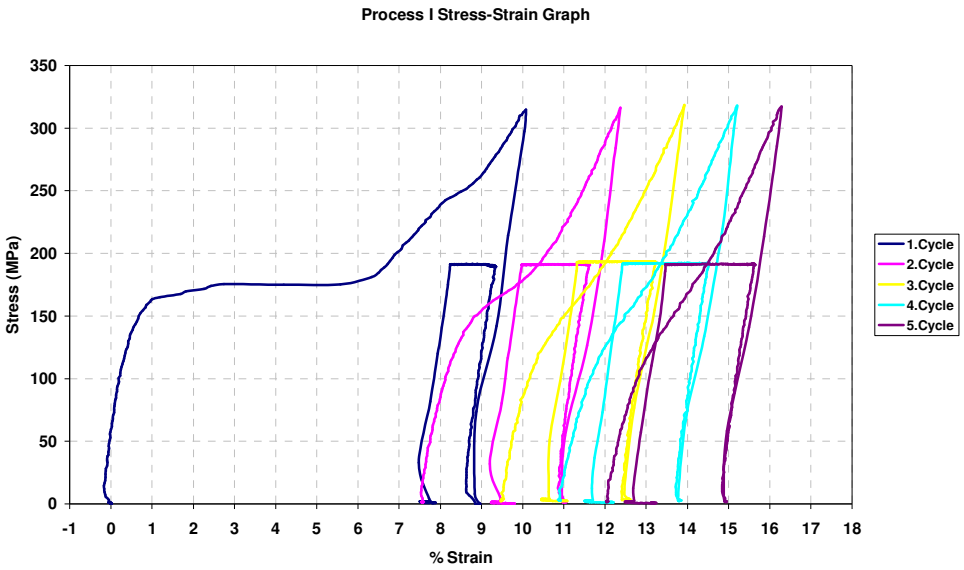
Process I Stress-Strain Graph
Stress (MPa)
% Strain
1.Cycle
2.Cycle
3.Cycle
4.Cycle
5.Cycle

(a)

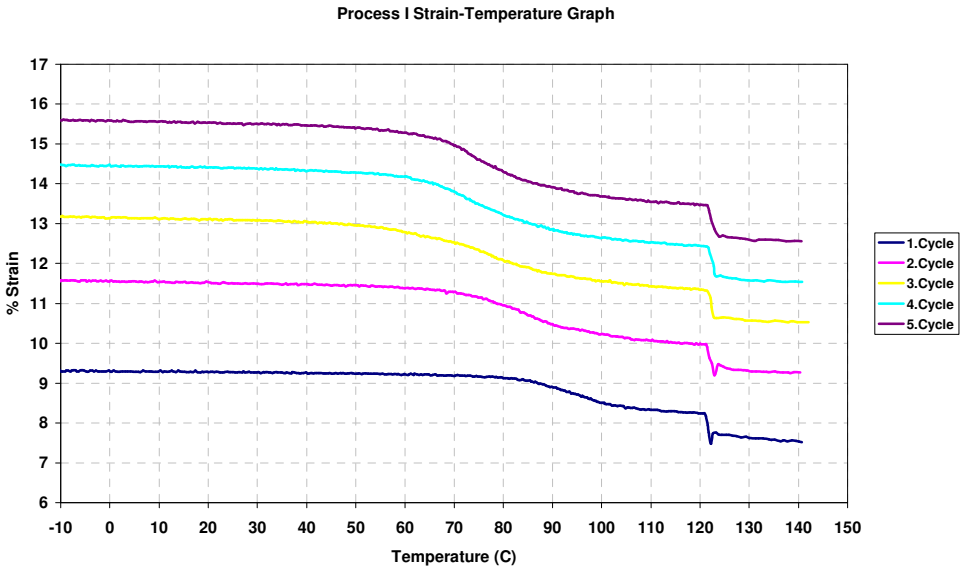
Process I Strain-Temperature Graph
% Strain
Temperature (C)
1.Cycle
2.Cycle
3.Cycle
4.Cycle
5.Cycle

(b)

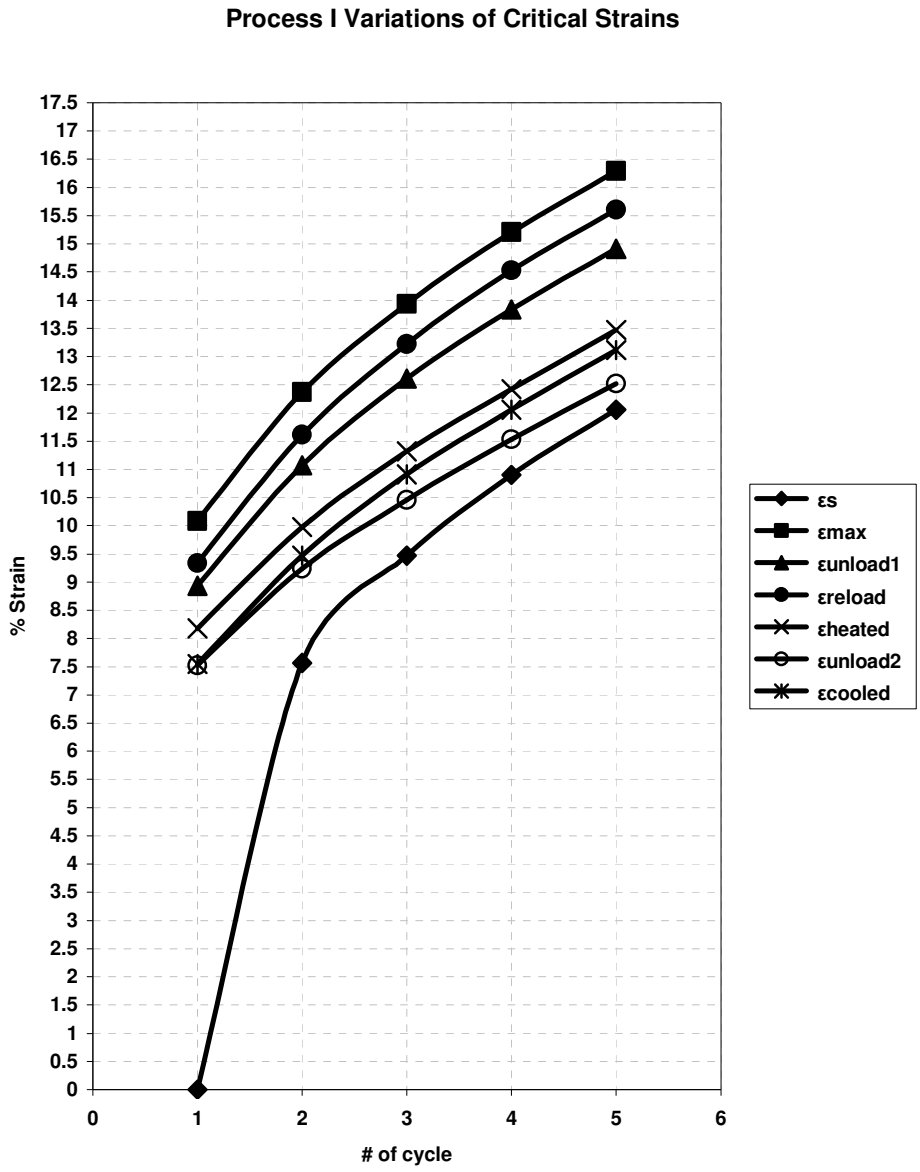

(c)

Figure 4.4.1 Type IV (Constant Stress Constrained Recovery), test results for samples subjected to Process I. (a) σ-ε, (b) ε-T and (c) Critical Strains - # of cycles diagrams.

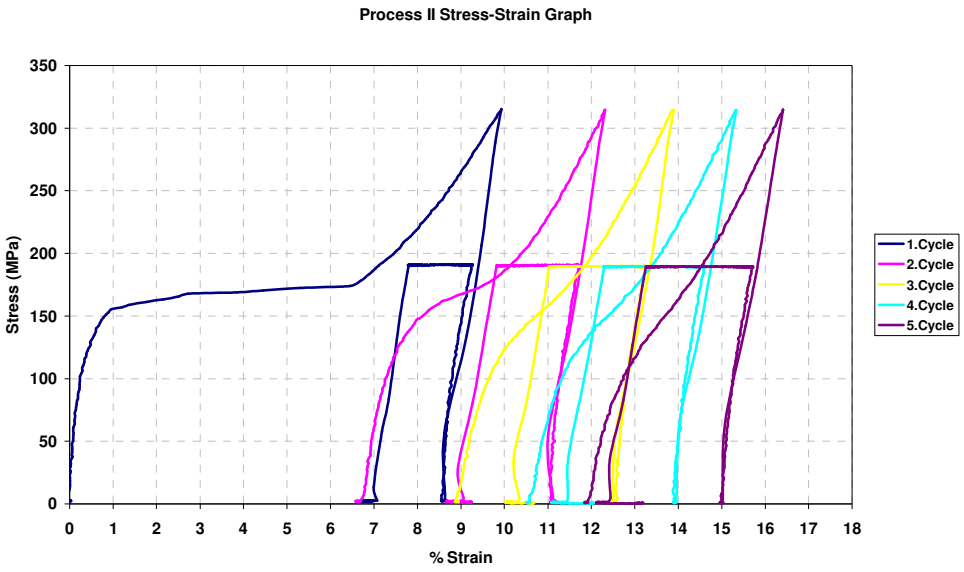
Process II Stress-Strain Graph
Stress (MPa)
% Strain
1.Cycle
2.Cycle
3.Cycle
4.Cycle
5.Cycle

(a)

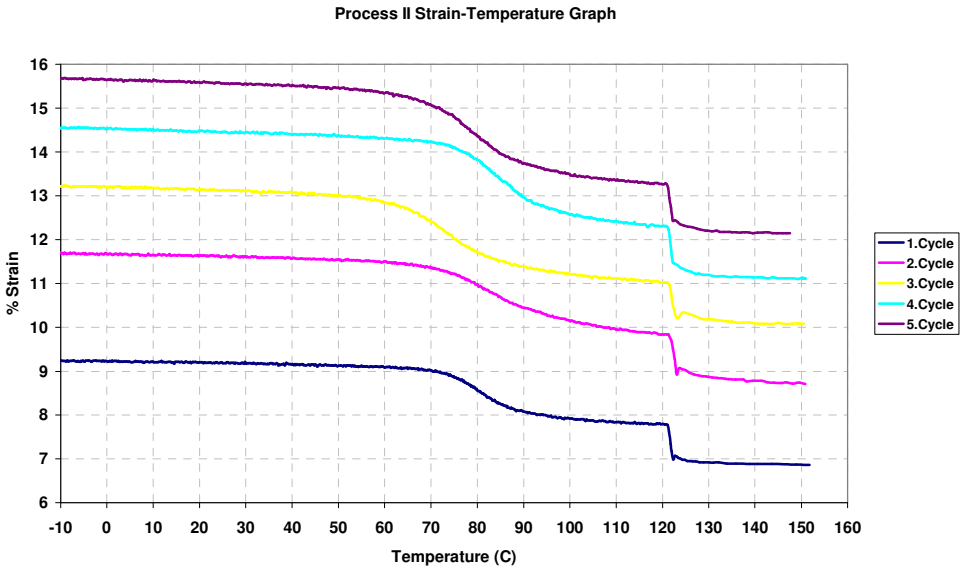
Process II Strain-Temperature Graph
% Strain
Temperature (C)
1.Cycle
2.Cycle
3.Cycle
4.Cycle
5.Cycle

(b)

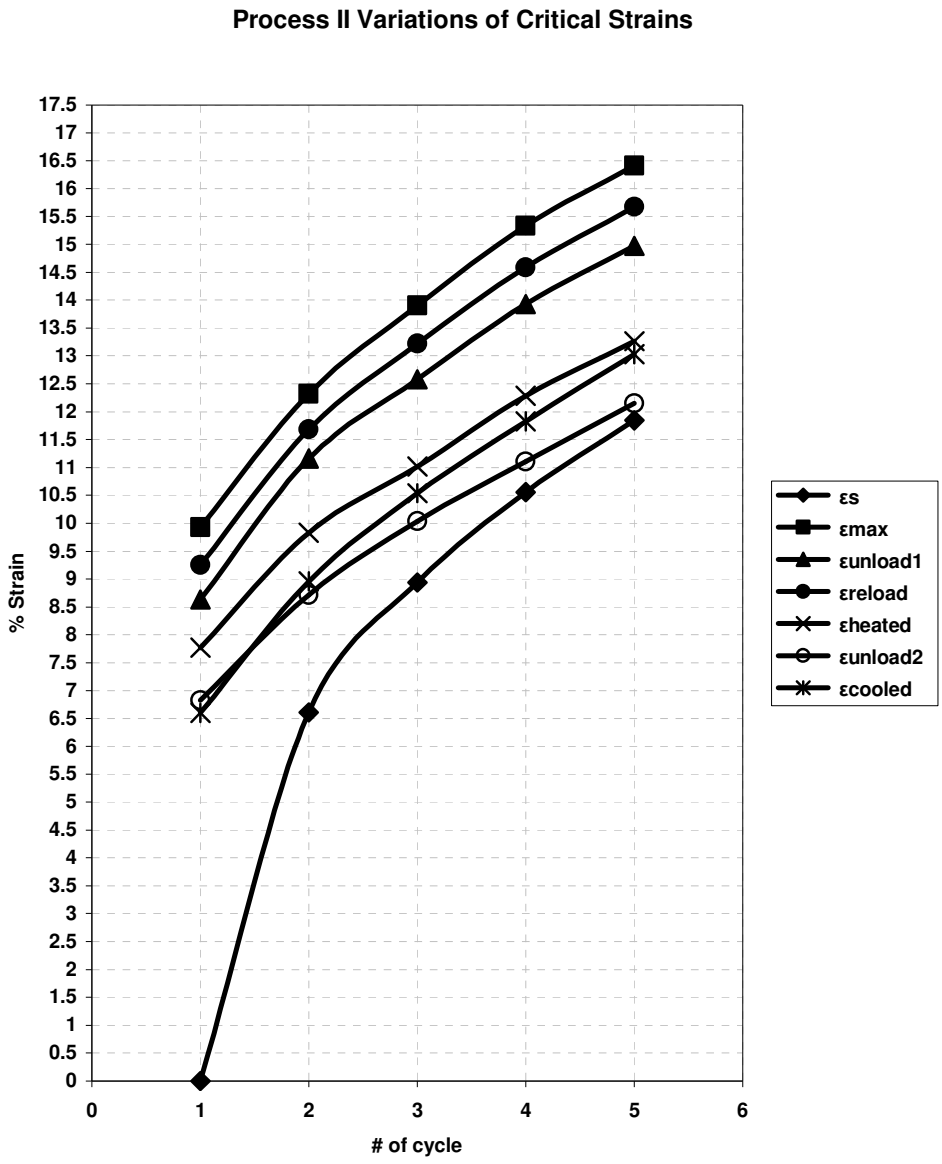

(c)

Figure 4.4.2 Type IV (Constant Stress Constrained Recovery), test results for samples subjected to Process II. (a) σ-ε, (b) ε-T and (c) Critical Strains - # of cycles diagrams.

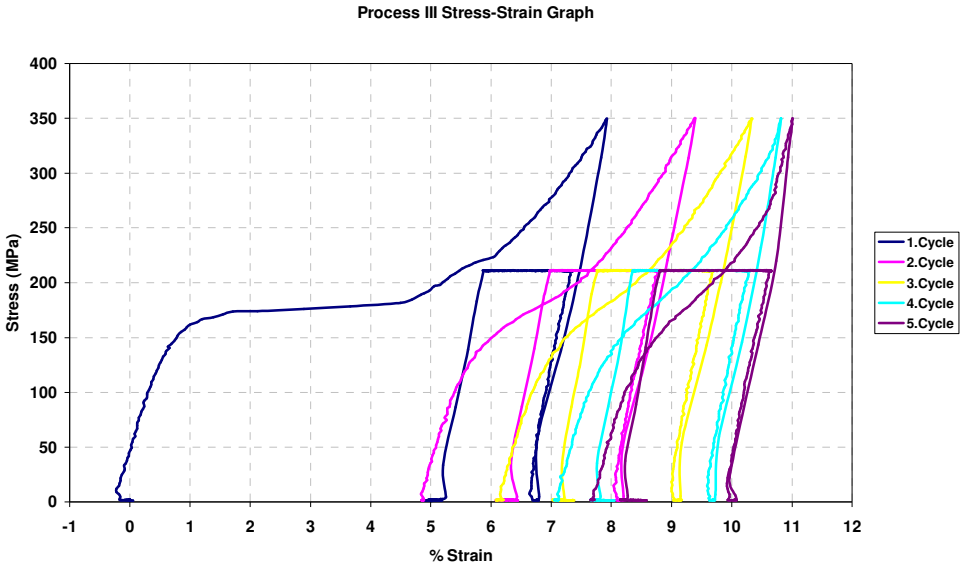
Process III Stress-Strain Graph
Stress (MPa)
% Strain
1.Cycle
2.Cycle
3.Cycle
4.Cycle
5.Cycle

(a)

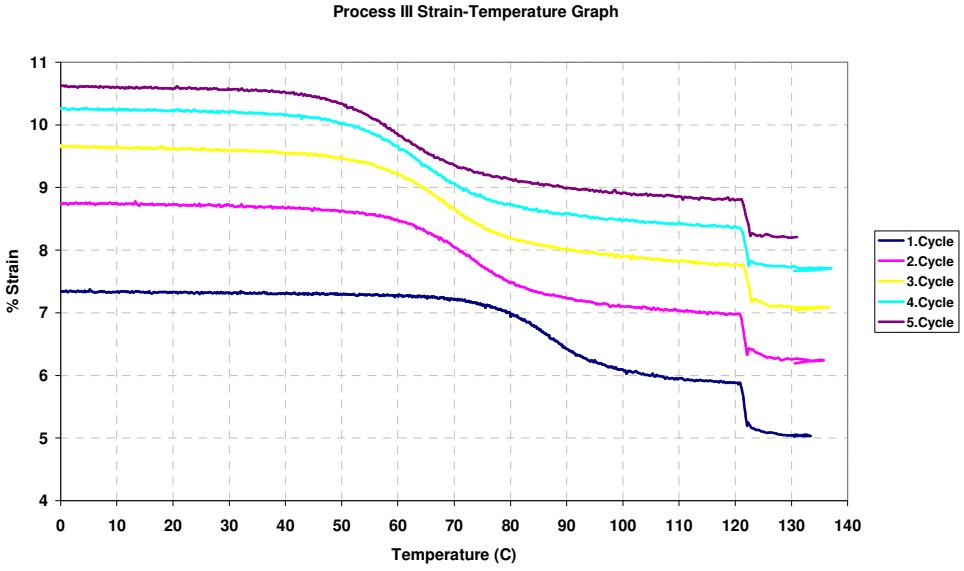
Process III Strain-Temperature Graph
% Strain
Temperature (C)
1.Cycle
2.Cycle
3.Cycle
4.Cycle
5.Cycle

(b)

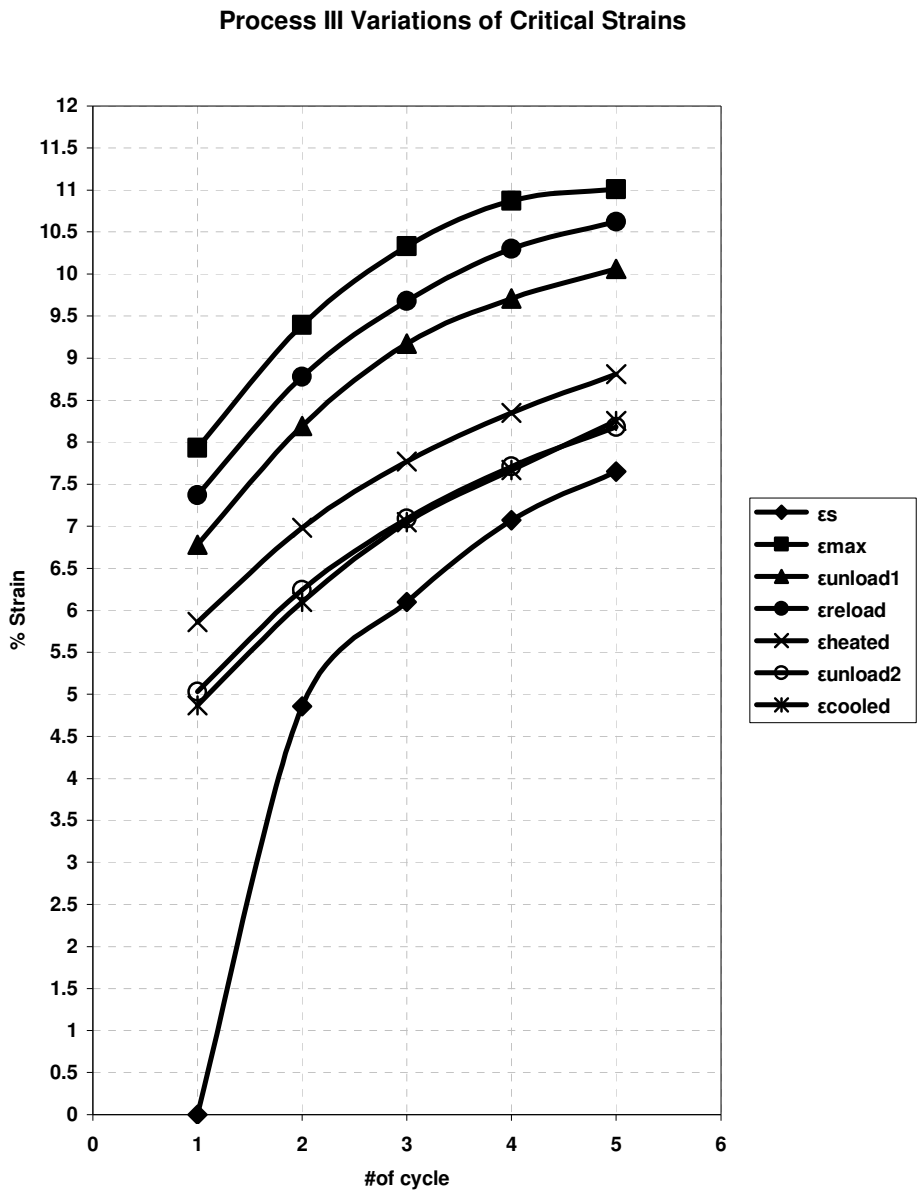

(c)

Figure 4.4.3 Type IV (Constant Stress Constrained Recovery), test results for samples subjected to Process III. (a) σ-ε, (b) ε-T and (c) Critical Strains - # of cycles diagrams**.**

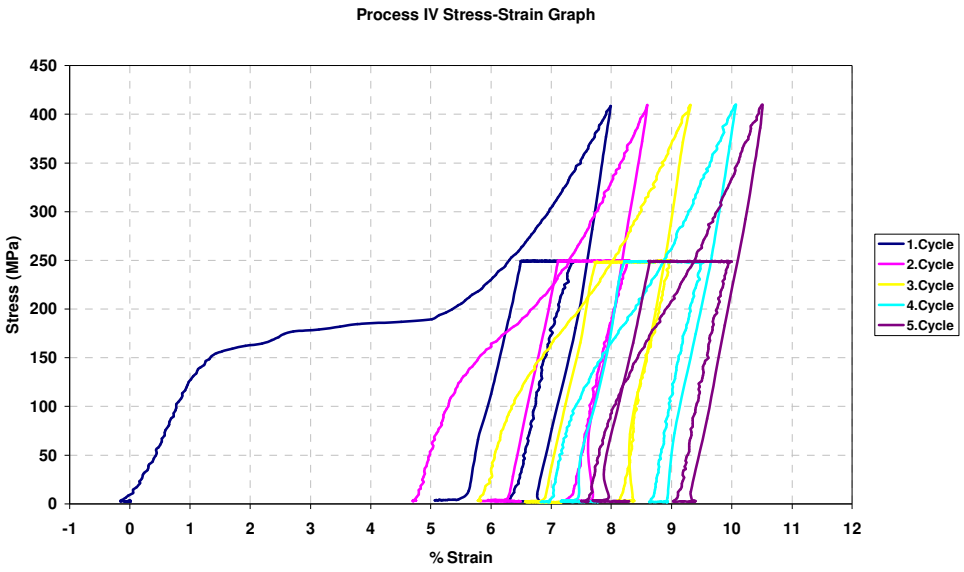
Process IV Stress-Strain Graph
Stress (MPa)
% Strain
1.Cycle
2.Cycle
3.Cycle
4.Cycle
5.Cycle

(a)

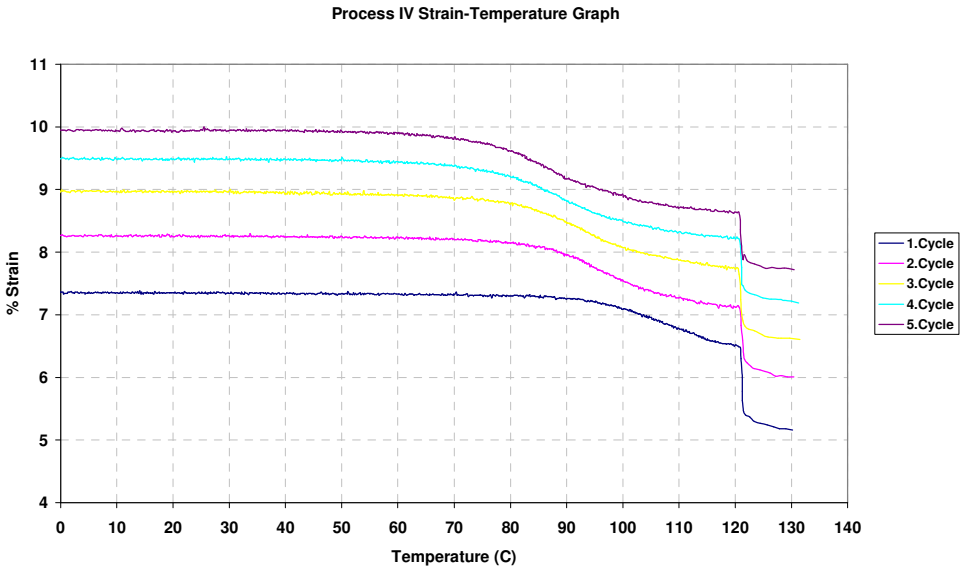
Process IV Strain-Temperature Graph
% Strain
Temperature (C)
1.Cycle
2.Cycle
3.Cycle
4.Cycle
5.Cycle

(b)

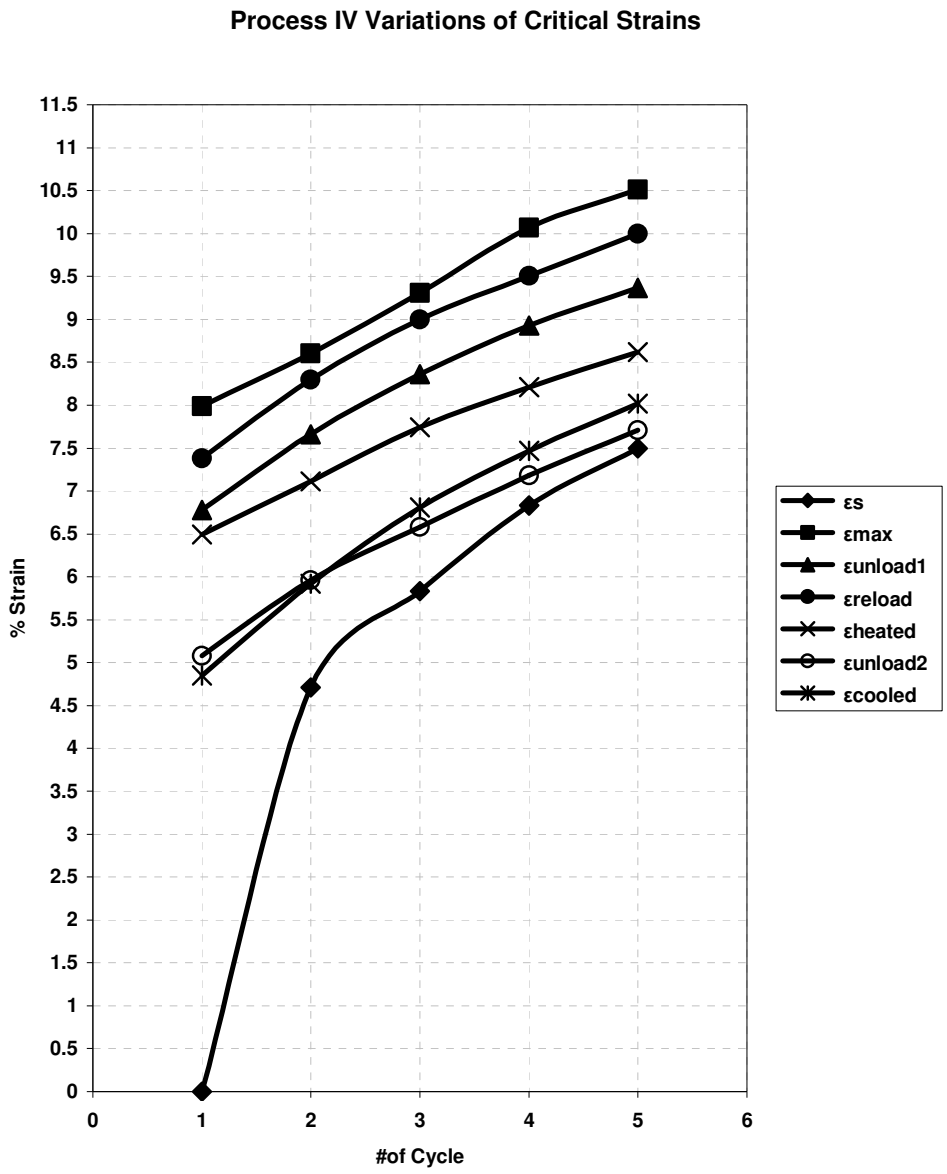

(c)

Figure 4.4.4 Type IV (Constant Stress Constrained Recovery), test results for samples subjected to Process IV. (a) σ-ε, (b) ε-T and (c) Critical Strains - # of cycles diagrams.

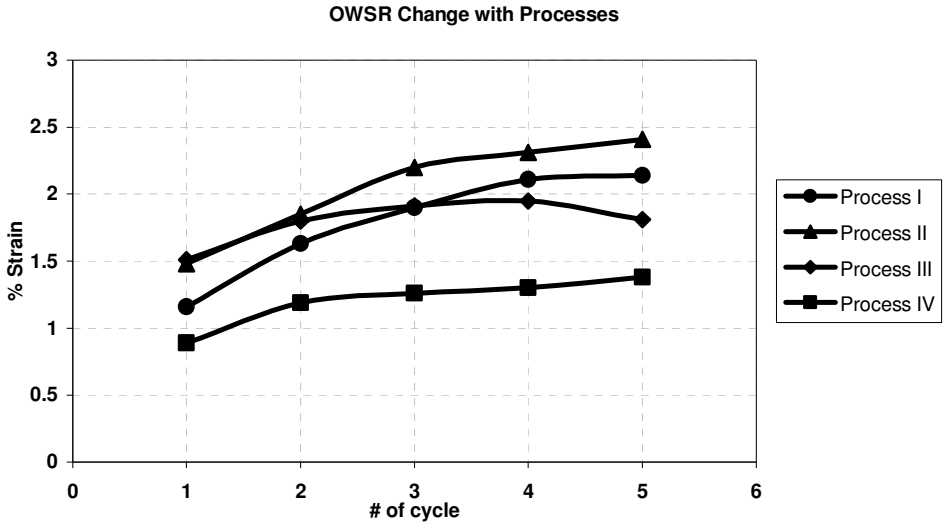

(a)

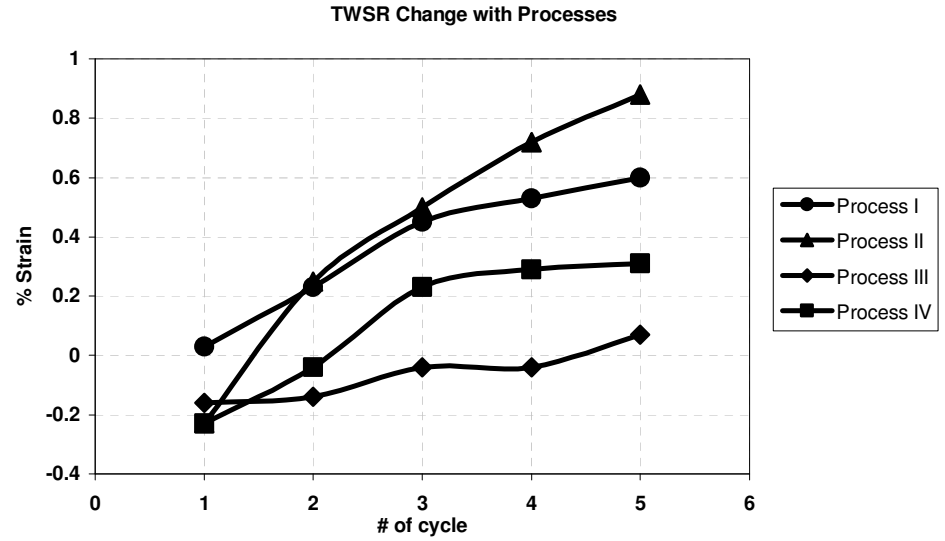

(b)

Figure 4.4.5 (a) OWSR and (b) TWSR change with cycling for all four processes in Constant Stress Constrained Recovery tests.

CHAPTER 5

CONCLUSION

Thermomechanical testing machine designed, constructed and testing has shown that self resistance heating and gas cooling of the samples are very effective but hydraulic load application causes problems in strain controlled tests due to the stress plateau observed in SMAs and a servo motor controlled system would be better for such an application.

The considerably large stress plateau observed in the first cycle of all tests and samples is due to detwinning of martensite and unrecoverable nature of this strain is attributed to the irreversible dislocation mechanisms that operate specially after the plateau region.

In all tests and samples cycling is found to improve the shape memory characteristics and stabilize the behavior probably through an optimization of dislocation microstructure.

Constant Stress Free Recovery tests have shown that after training for about 5 cycles 100% fractional recovery can be achieved for all processes. Due to higher strength, the imposed and recovered strains at a constant stress level are smaller in cold worked samples but they are already stabilized (trained) starting with the first cycle. Process I seems to be the best heat treatment but requires some training.

Constant Strain Free Recovery test have shown that the specimens deformed to a smaller strain show a more stable shape memory behavior and more over, in all free recovery tests conducted, OWSR characteristics was observed to deteriorate with heat treatment in the order from Process I to Process IV.

Constant Strain and Constant Stress Constrained Recovery tests have shown that in samples subjected to all four processes, stresses about 20 % greater than the applied can be generated by preventing shape recovery and partial recovery is possible even under a bias stress.

REFERENCES

1. E. Cydzik, T.W. Deurig, K.N. Melton, D. Stöckel, C.M.Wayman (Eds.), Engineering Aspects of Shape Memory Alloys, Butterworth-Heinemann Ltd., pp. 9-39, 1990.

2. D.A. Porter and K.E. Easterling, Chapter 6, Diffusionless Transformations, Phase Transformations in Metals and Alloys, 2nd ed., Chapman & Hall, 1992.

3. Martensitic Structures, ASM Handbooks. Online
http://products.asminternational.org.

4. Crystallographic Theory, ASM Handbooks Online.
http://products.asminternational.org

5. S. Pai Mizar, Worcester Polytechnic Institute, Phd. Thesis, pp.36-39, 2005.

6. K.Shimizu and T.Tadaki, Shape Memory Alloys Edited By H.Funakubo, Gordon and Breach Science Publishers, pp.1-17, 1984.

7. M. Cohen and C. M. Wayman, Metallurgical Treaties, AIME, N.Y., pp 445, 1981.

8. J.Perkins, Materials Science and Engineering, 51, pp.181-192, 1981.

9. H. C. Tong and C. M. Wayman, Scripta. Met.,8 , pp.93-100, 1974.

10. G. B. Olson and M. Cohen, Scripta Metallurgica, 9, pp.1247-1254, 1974.

11. K.Shimizu and T.Tadaki, Shape Memory Alloys Edited By H.Funakubo, Gordon and Breach Science Publishers, pp.4, 1984.

12. H. Kessler and W. Pitsch, Acta Metall. 13, pp.871-874, 1965.

13. P. Verhoven, Fundementals of Physical Metallurgy, John Willey and Sons, N.Y., pp.49, 1975.

14. C. M. Wayman, Progress in Materials Science Vol. 36, pp. 203-224, 1992.

15. R.J. Salzbrenner and M. Cohen, Acta Metall, 27, pp.739, 1979.

16. L.C. Brinson, Journal of Intelligent Material Systems and Structures, Vol. 4, pp. 229-242, 1993.

17. X. D. Zhang, C.A. Rogers, and C. Liang, Journal of Intelligent Material Systems and Structures, Vol. 8, pp. 353-362, 1997.

18. A. D. Johnson, Intersociety Energy Conversion Engineering Conference Record, pp. 530-534, 1975.
19. Z.K. Lu and G. J. Weng, Smart Materials and Structures, Vol. 9, pp. 582-591, 1990.
20. D. E. Hodgson, M. H. Wu and R. J. Biermann, "Shape Memory Alloys,", pp. 1-9.
21. R. J. Wassilewski, Shape Memory Effects in Alloys, Plenum Press, pp.245, 1975.
22. T. A. Schroeder and C. M. Wayman, Scripta Metall., vol 11, pp. 225, 1977 .
23. C. M. Wayman and T. W. Duerig, Engineering Aspects of Shape Memory Alloys Edited By T. W. Duerig, K.N. Melton, D. Stockel and C. M. Wayman, Butterworth-Heinemann Ltd., pp.3-15, 1990.
24. J.W Christian, Theory of Transformations in Metals and Alloys, Pergamon Press, pp.896, 1965.
25. C. M. Wayman and T. W. Duerig, Engineering Aspects of Shape Memory Alloys Edited By T. W. Duerig, K.N. Melton, D. Stockel and C. M. Wayman, Butterworth-Heinemann Ltd., pp.3, 1990.
26. R. Stalmans, J.Van Humbeeck and L. Delaey, Training and the Two Way Effect in Cu-Based SMA alloys, Journal of Physics, Vol. 1, C4-403, 1991.
27. K. Otsuka and X.B. Ren, Intermettallics, vol. 7, pp.511, 1999.
28. J. Haasters, G. Salis-Solio, G. Bensmann, in: T.W. Deurig, K.N Melton, D. Stöckel, C.M. Wayman (Eds.), Engineering Aspects of Shape Memory Alloys, Butterworth-Heinemann Ltd., London, pp. 426–444, 1990.
29. C. Trépanier, M. Tabrizian, L.H. Yahia, L. Bilodeau, D.L. Piron, Mater. Res. Symp. Proc. 459 363–368, 1997.
30. R.C.L. Sachdeva, S. Miyazaki, in: T.W. Deurig, K.N. Melton, D. Stöckel, C.M. Wayman (Eds.), Engineering Aspects of Shape Memory Alloys, Butterworth-Heinemann Ltd., London, pp. 452–469, 1990.
31. J. Van Humbeeck, R. Stalmans, in: K. Otsuka, C.M. Wayman (Eds.), Shape Memory Materials, Cambridge University Press, pp. 149–183, 1998.
32. P.P. Jenkins, Materials Science and Engineering, 51, pp.181-192, 1981.

33. C.M Wayman and T.W Duerig, Engineering Aspects of Shape Memory Alloys Edited By T.W Duerig, K.N. Melton, D. Stockel and C.M Wayman, Butterworth-Heinemann Ltd., pp.3, 1990.
34. E. Hornbogen and B Velten, Progress in Shape Memory Alloys edited by S.Eucken, Informationgesselschaft, Verlag, pp.24, 1992.
35. C.M Wayman and T.W Duerig, Engineering Aspects of Shape Memory Alloys Edited By T.W Duerig, K.N. Melton, D. Stockel and C.M Wayman, Butterworth-Heinemann Ltd., pp.119-123, 1990.
36. P. G. McCormick. Y. Liu. and S. Miyazaki. "Intrinsic Thermo-Mechanical Behavior Associated with the Stress-Induced Martensitic Transformation in NiTi." Material Science and Engineering A. vol. 167. pp. 5 1-56. 1993.
37. H.C Lin., S.K. Wu, Acta Metall. Mater. 42 1623, 1994.
38. K. Gall, H. Sehitoglu, Y.I. Chumlykov, I.V. Kireeva, H.J. Maier, J Eng. Mater-T. ASME. 121 19, 1994.
39. S. Miyazaki, K. Otsuka, ISIJ International. 29 389, 1989.

APPENDIX A

STRESS STRAIN TEMPERATURE GRAPHS

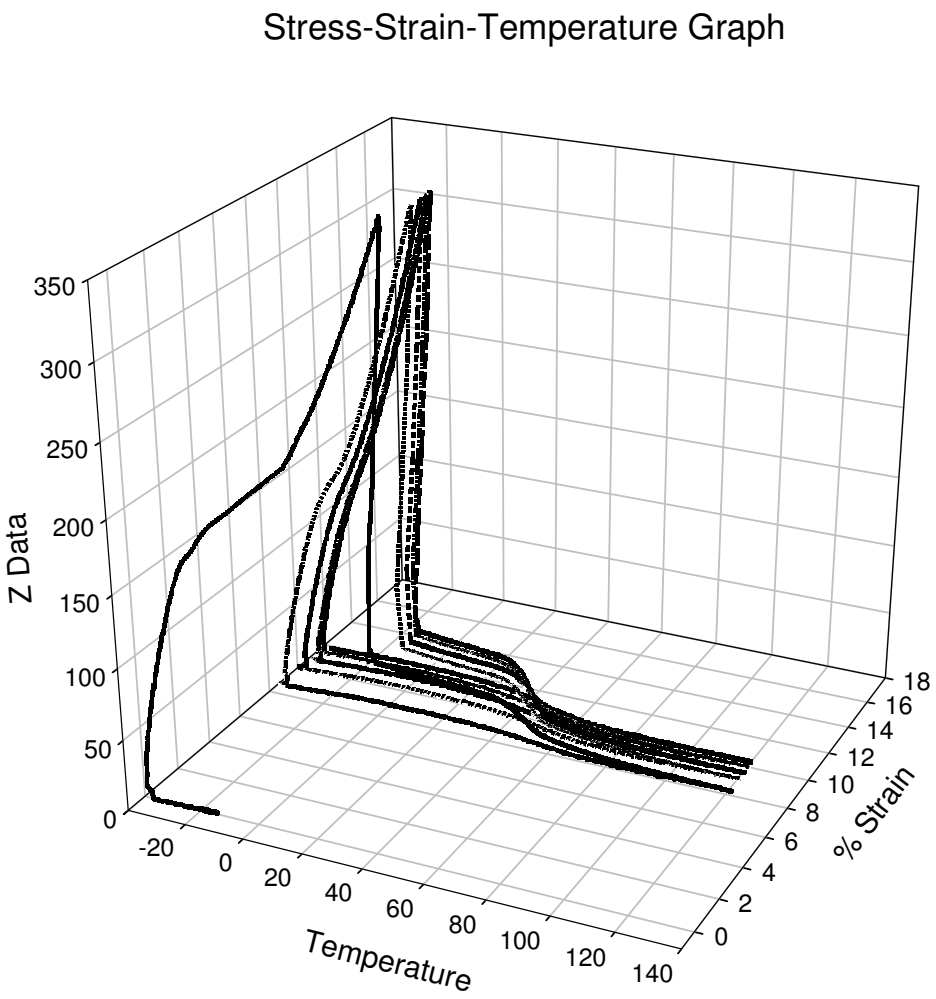

Figure A.1 Process I Type I Test Stress-Strain-Temperature Graph

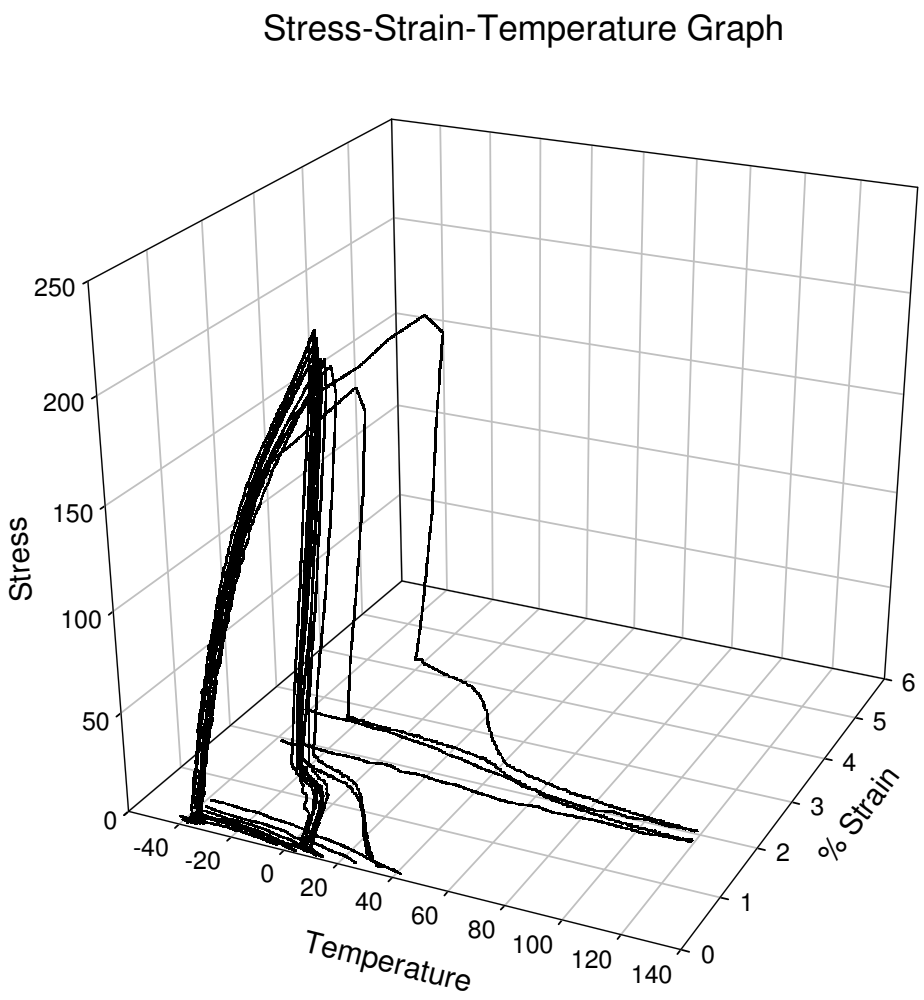

Figure A.2 Process I Type II (2% Strain) Stress-Strain-Temperature Graph

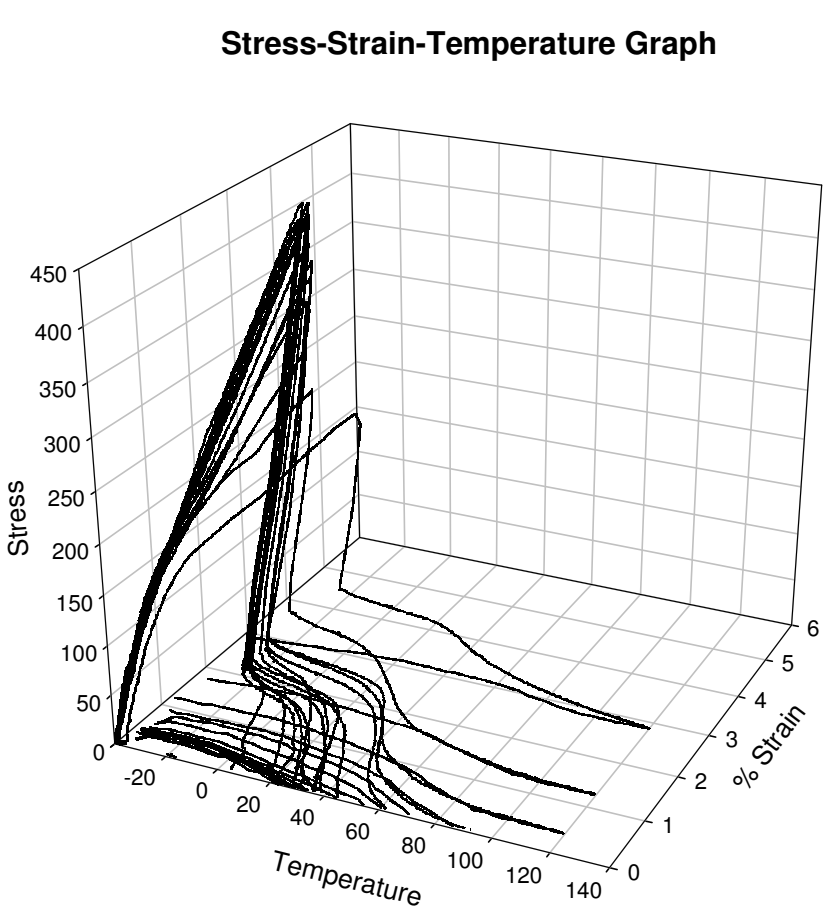

Figure A.3 Process I Type II (4% Strain) Stress-Strain-Temperature Graph

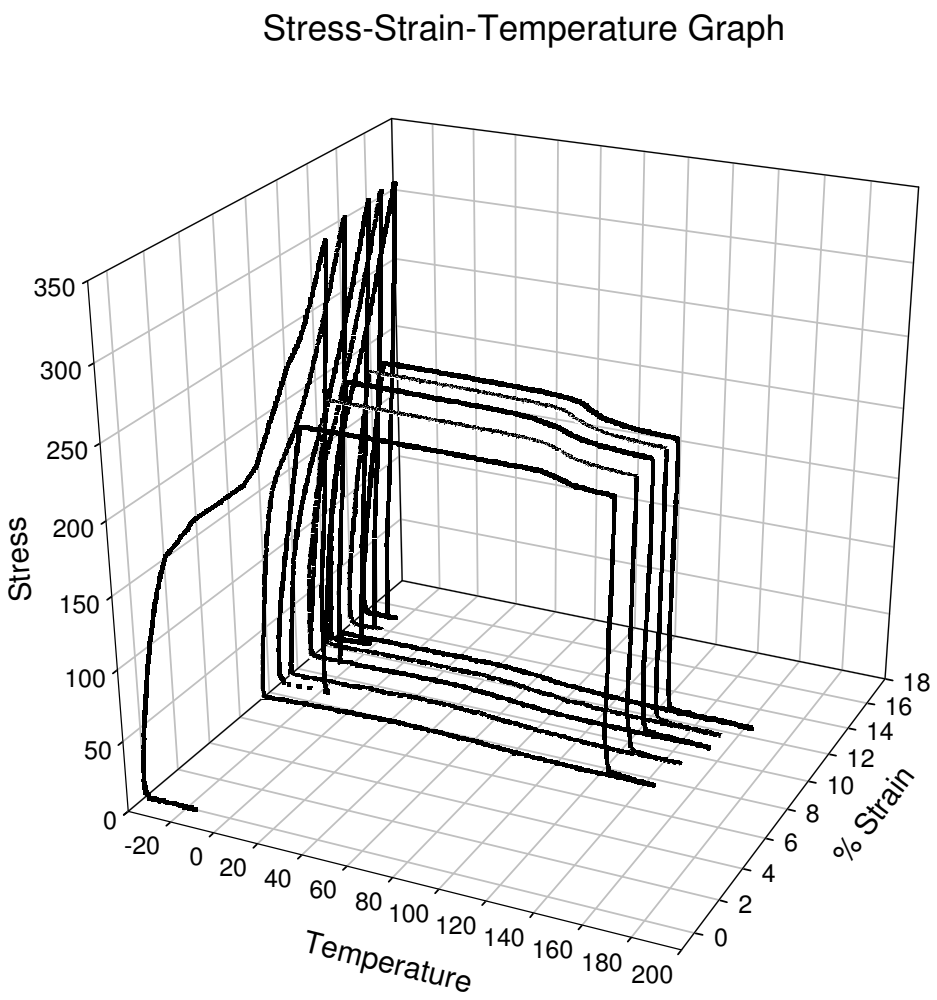

Figure A.4 Process I Type IV Stress-Strain-Temperature Graph

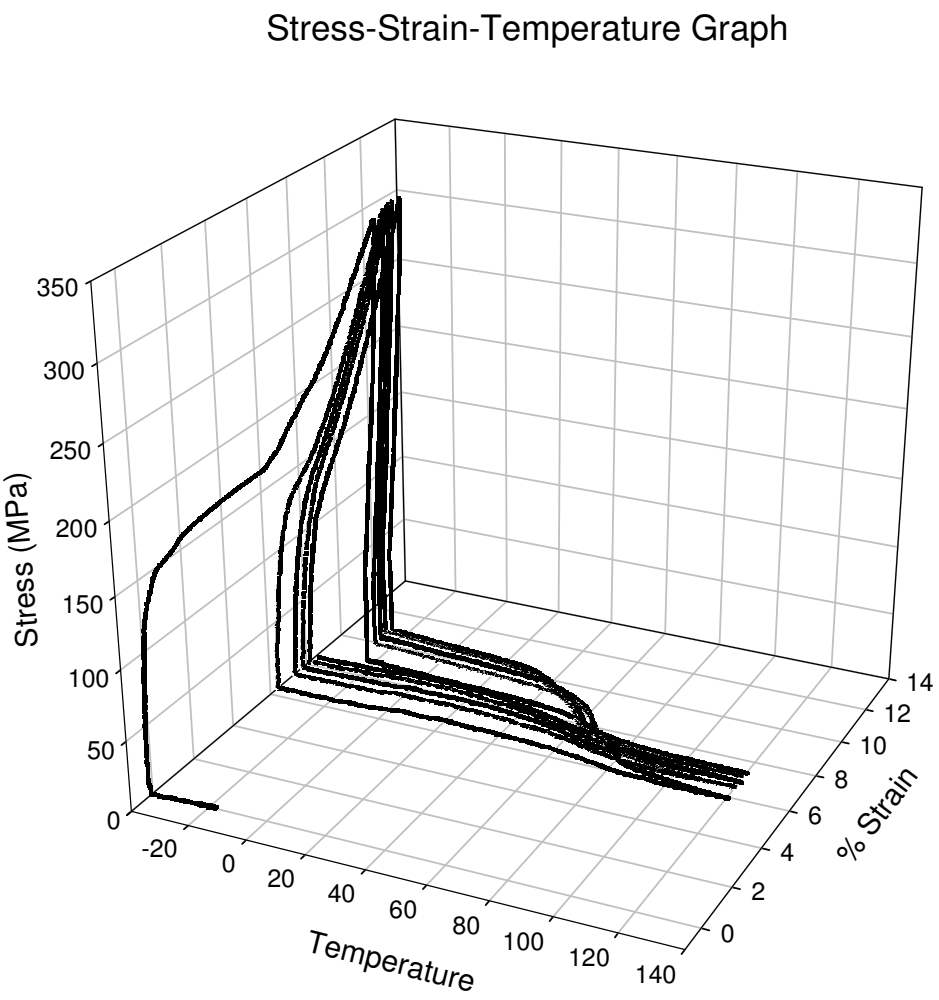

Figure A.5 Process II Type I Stress-Strain-Temperature Graph

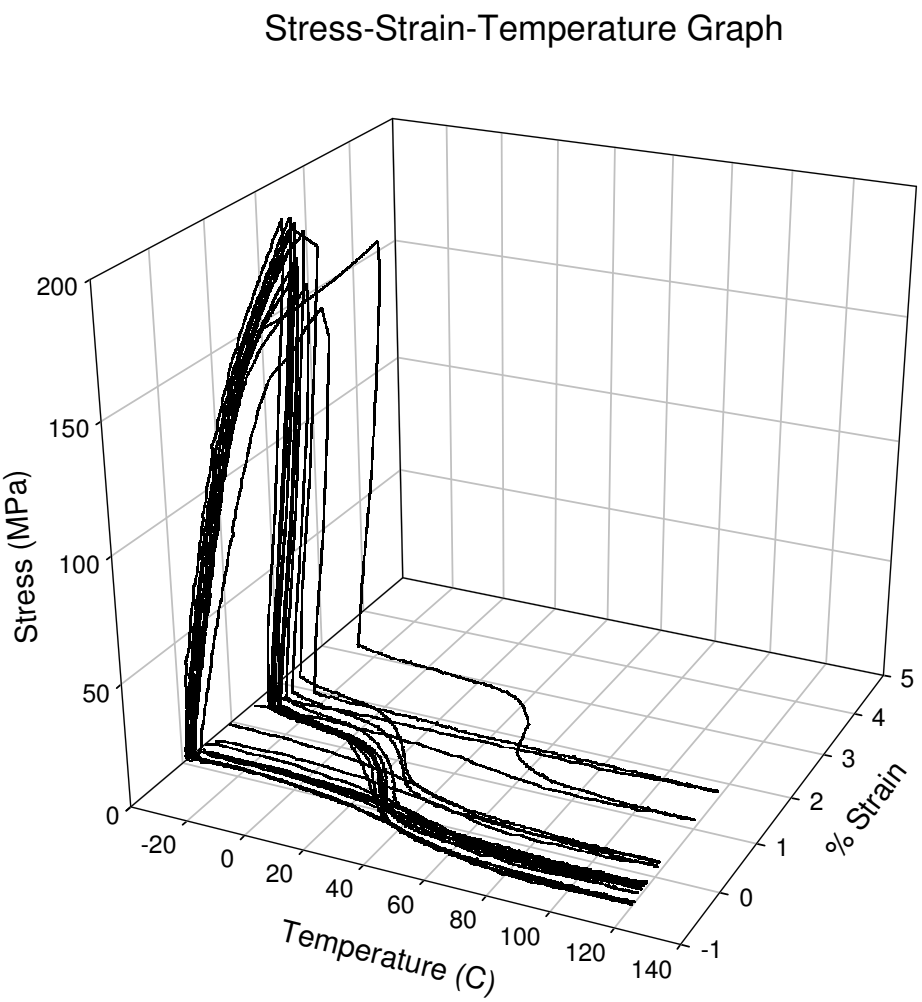

Figure A.6 Process II Type II (2% Strain) Stress-Strain-Temperature Graph

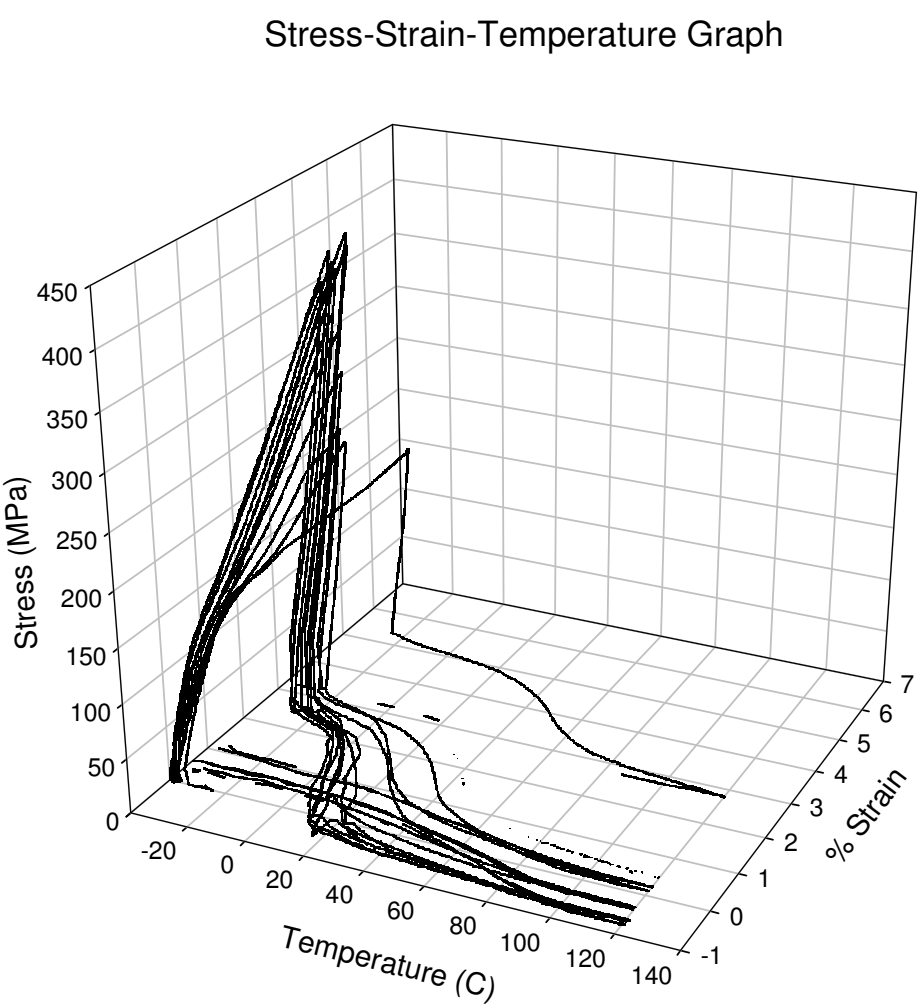

Figure A.7 Process II Type II (4% Strain) Stress-Strain-Temperature Graph

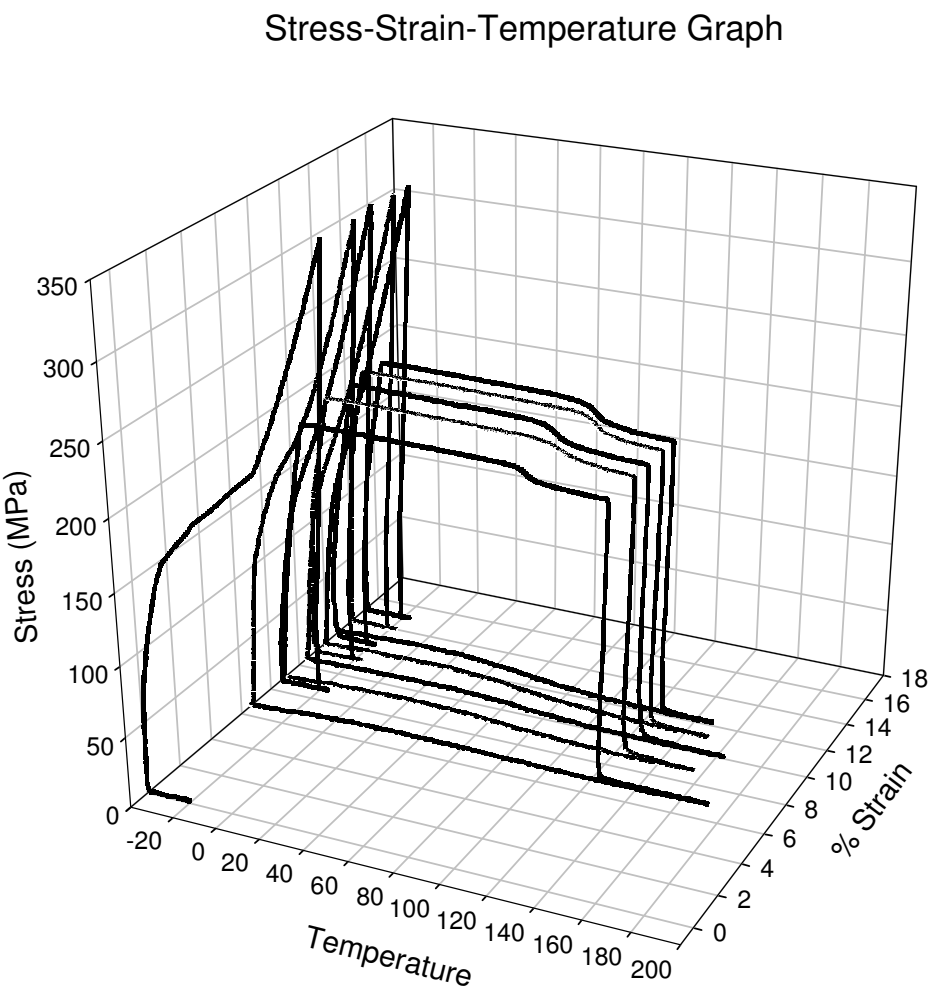

Figure A.8 Process II Type IV Stress-Strain-Temperature Graph

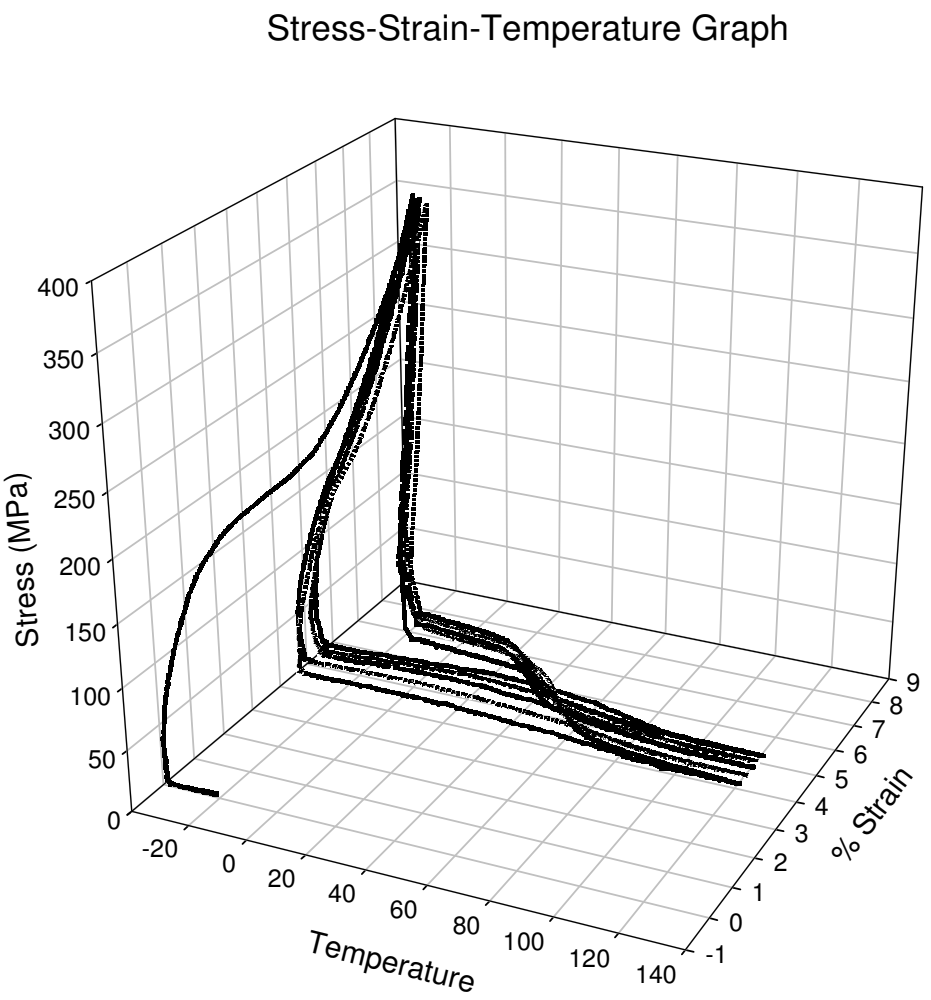

Figure A.9 Process III Type I Stress-Strain-Temperature Graph.

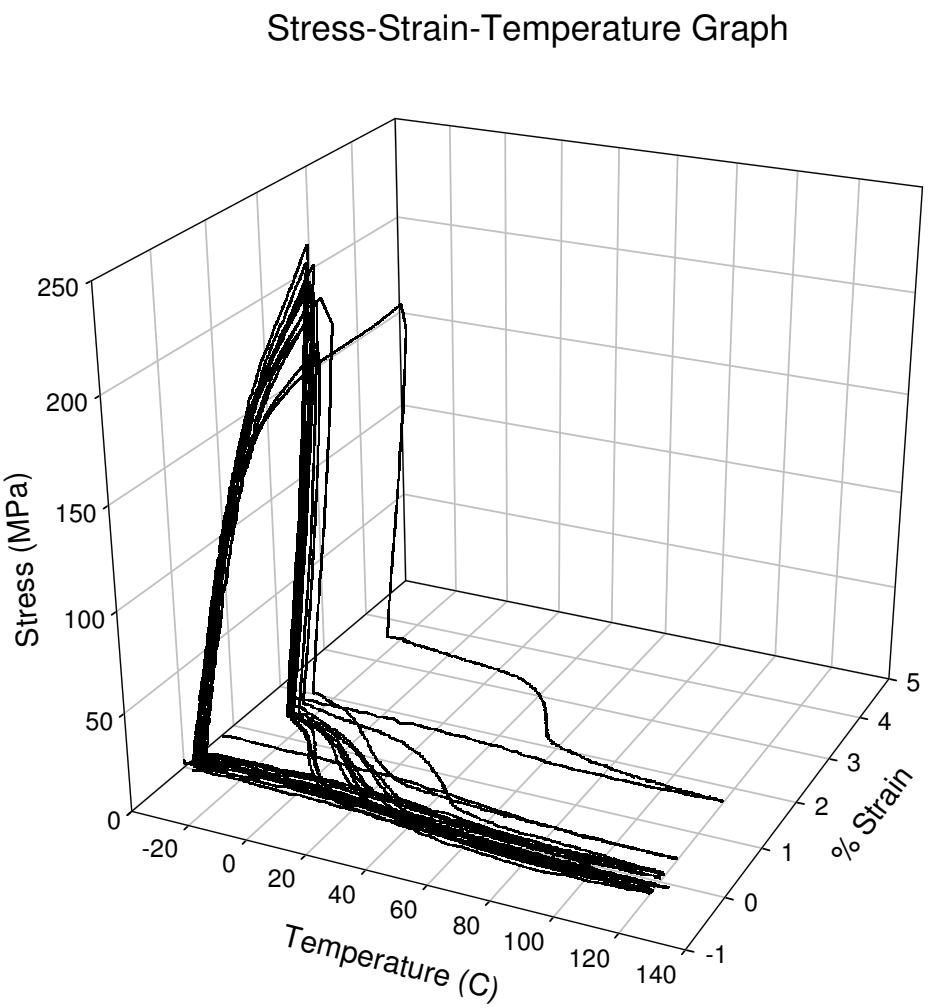

Figure A.10 Process III Type II (2% Strain) Stress-Strain-Temperature Graph

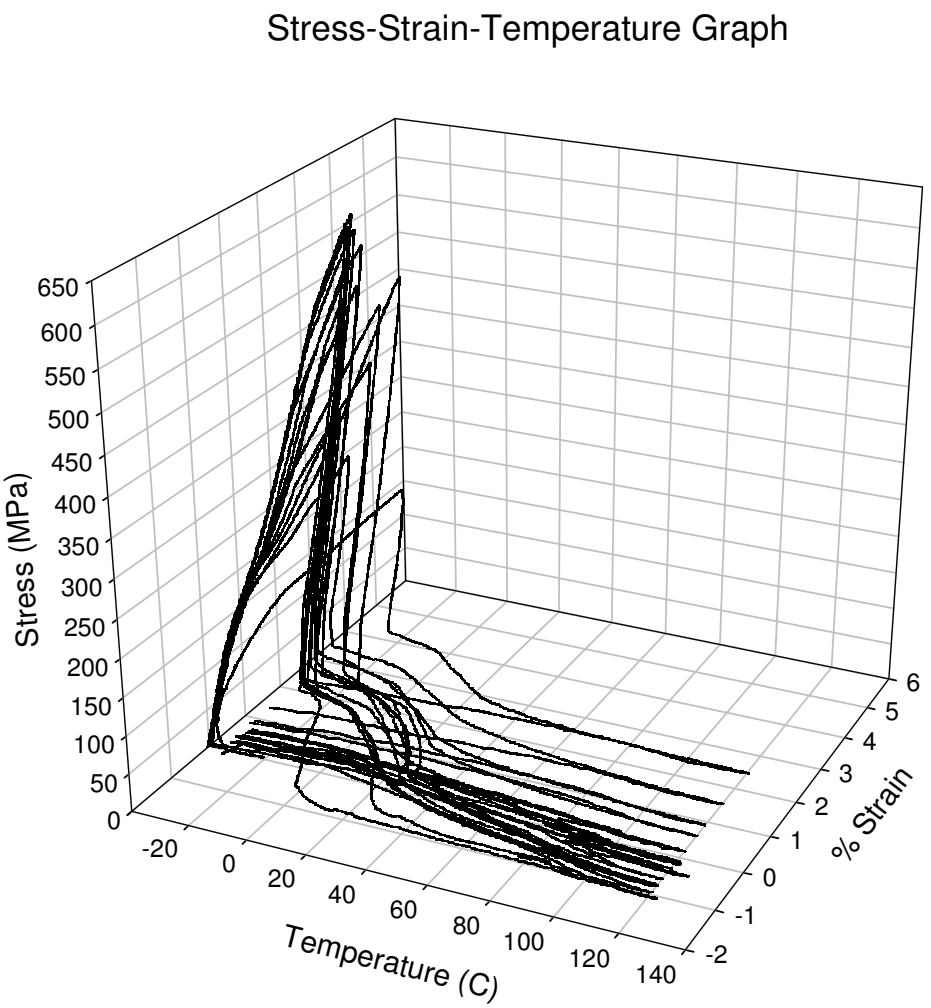

Figure A.11 Process III Type II (4% Strain) Stress-Strain-Temperature Graph

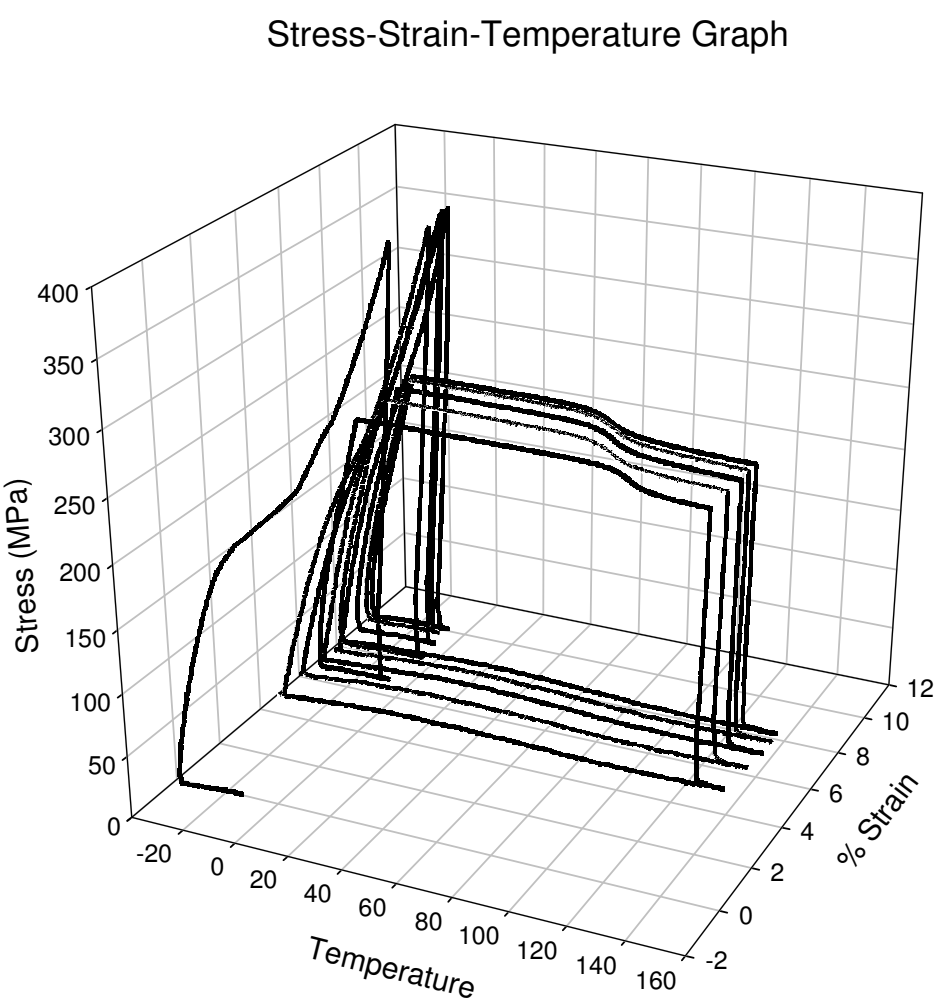

Figure A.12 Process III Type IV Stress-Strain-Temperature Graph

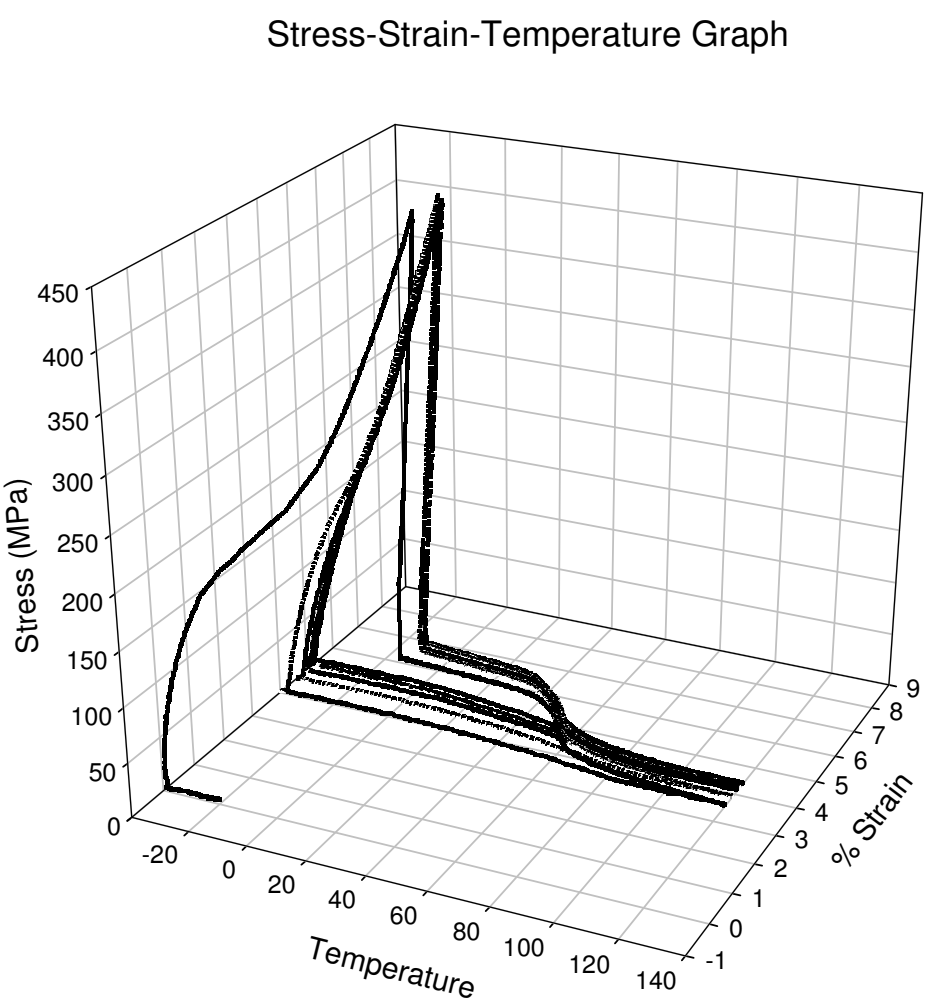

Figure A.13 Process IV Type I Stress-Strain-Temperature Graph

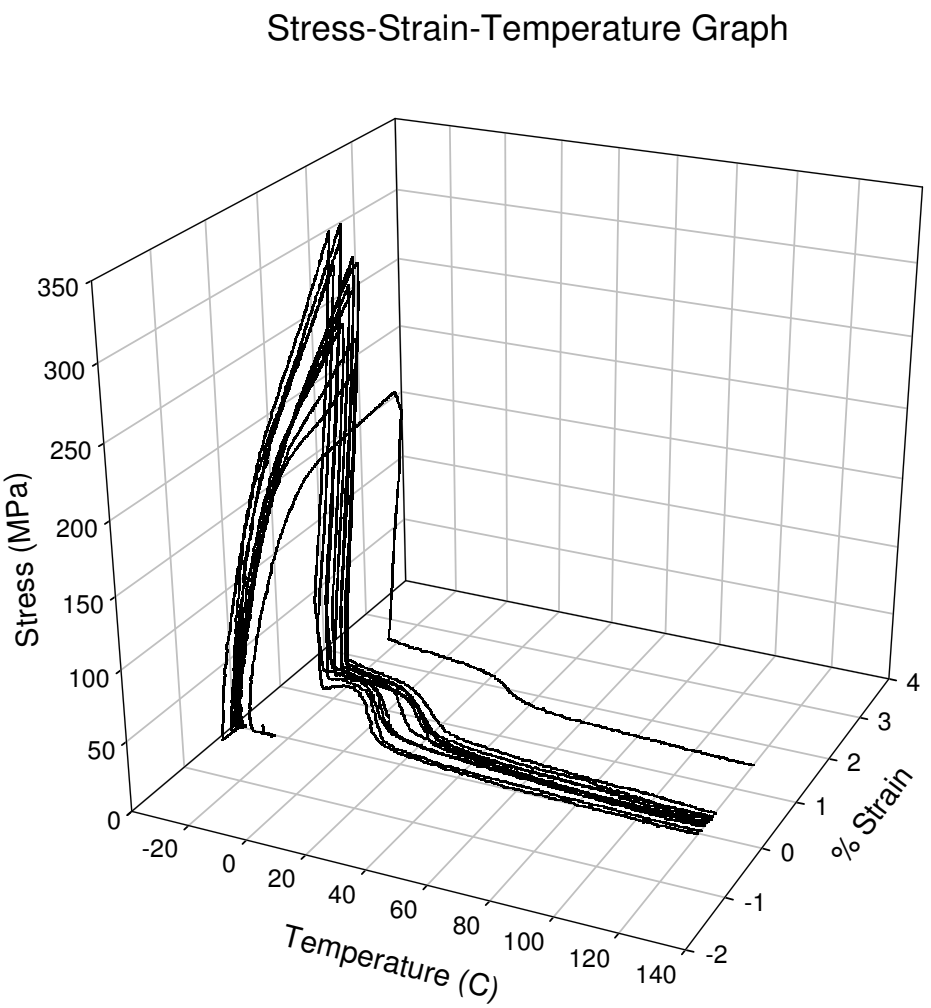

Figure A.14 Process IV Type II (2% Strain) Stress-Strain-Temperature Graph

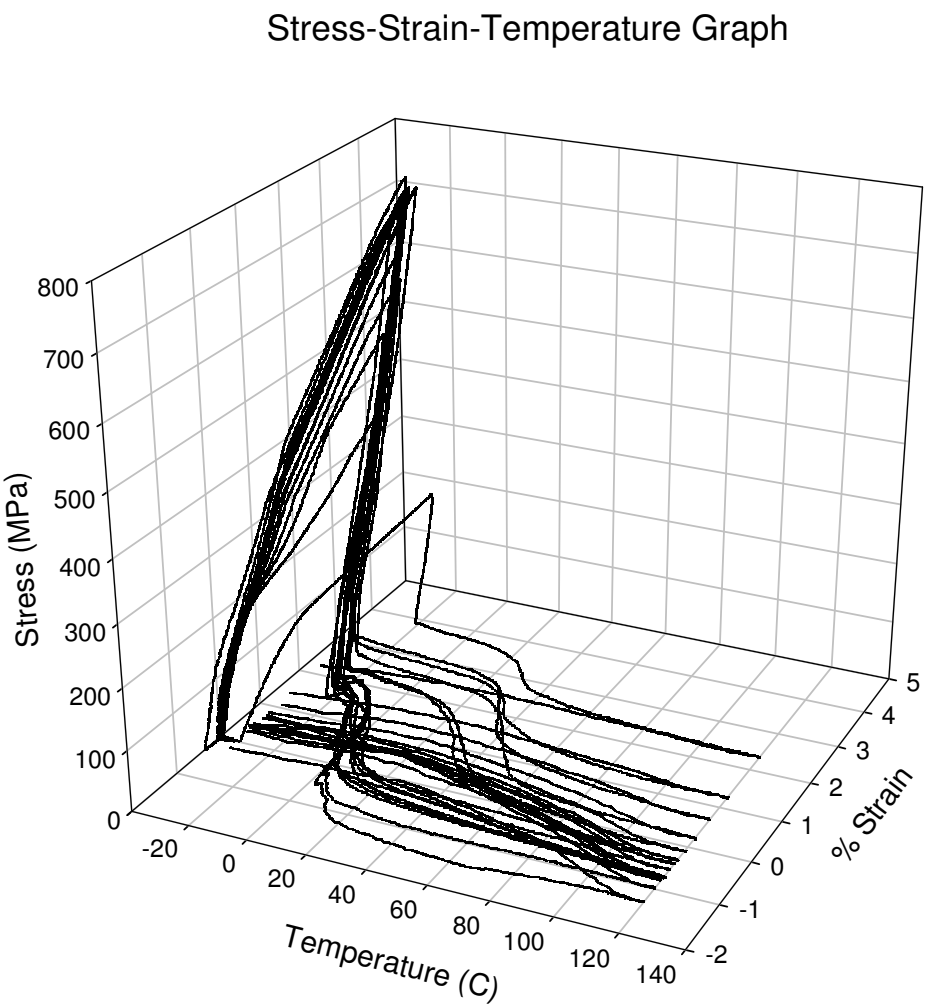

Figure A.15 Process IV Type II (4% Strain) Stress-Strain-Temperature Graph

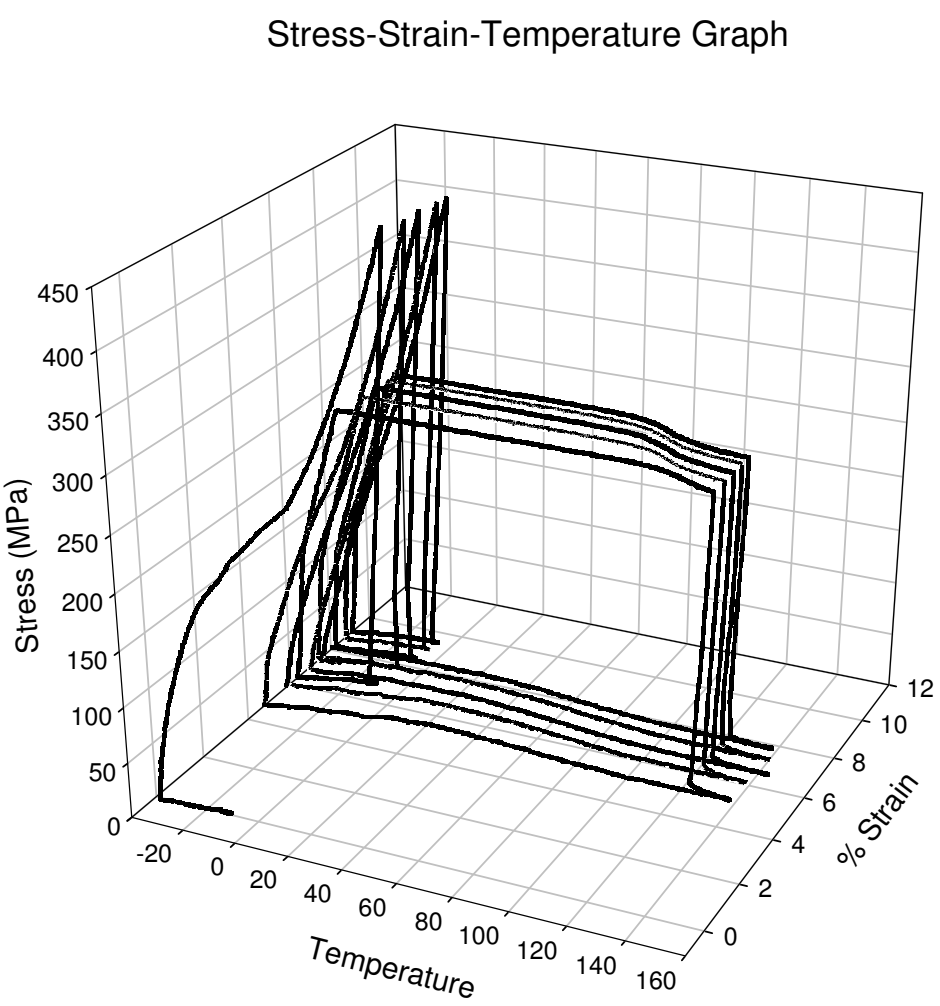

Figure A.16 Process IV Type IV Stress-Strain-Temperature Graph